OPTICAL MEASUREMENTS OF MAGNETICALLY-ALIGNED ASBESTOS FIBERS

by

© Peter Riis, B.Sc.

A Thesis

Submitted to the School of Graduate Studies

in Partial Fulfillment of the Requirements

for the Degree

Doctor of Philosophy

McMaster University

September 1989

ISBN 0-315-52157-0

OPTICAL MEASUREMENTS OF MAGNETICALLY-ALIGNED ASBESTOS FIBERS

DOCTOR OF PHILOSOPHY — McMASTER UNIVERSITY

(1989) — Hamilton, Ontario

(Physics)

TITLE: Optical Measurements of Magnetically-Aligned Asbestos Fibers

AUTHOR: Peter Riis, B.Sc. (University of Waterloo)

SUPERVISOR: Professor E.A. Ballik

NUMBER OF PAGES: xi, 114

LEAF IV and VI OMITTED IN PAGE NUMBERING

Abstract

The magnetic-alignment behaviour of asbestos fibers suspended in water was studied. As the magnetic field rotates, the fibers rotate about their centre. Due to viscous drag, the fibers tend to lag the field, with the lag increasing as the rotation rate increases. A theoretical model describing fiber behaviour was developed. Experiments measuring the phase lag of individual fibers, experiencing torques of the order of 10^{-18} Newton-meters were in excellent agreement with the model. For an unknown fiber the phase lag measurement will give the ratio of the length to radius of the fiber. For a known fiber, the cross-sectional size and shape can be determined.

This research was undertaken with the intention of laying down the groundwork from which an automatic instrument for monitoring asbestos exposure could be made. Initial investigations involved filtering a liquid dispersion in a one Tesla magnetic-field. The filter contained permanently aligned fibers. The filter was made transparent and scattered-light measurements were made relative to the initial magnetic field direction were made. Subsequent research focussed on measuring light scattered by fibers suspended in water while the fibers followed a rotating magnetic-field. The latter technique proved far more sensitive, being able to detect fiber concentrations of the order of one million fibers per liter with relatively simple equipment. On a mass basis, this sensitivity corresponds to one part in 10^{10}. The method did not have the problems associated with the filter itself. Equally important, there is the potential to obtain fiber size information.

Résumé

Le comportement de l'alignement magnétique de fibres d'asbestos en suspension dans l'eau est étudié. Lorsque le champs magnétique tourne, les fibres effectuent une rotation autour de leur centre. Dû au frottement visceux, les fibres tendent à être en retard par rapport au champ; le retard augmente à mesure que la vitesse de rotation augmente. Un modèle théorique décrivant le comportement des fibres individuelles a été développé. Les résultats d'expériences, durant lesquelles ces fibres furent soumises à des torques de l'ordre de 10^{-18} Newton-mètre, confirment le modèle. L'étude du retard de phase d'une fibre inconnue donne le rapport longueur-rayon de la fibre. L'étude d'une fibre connue donne la grandeur ainsi que la forme de la coupe transversale.

Cette recherche fut conduite à fin d'établir les bases nécessaires pour développer un instrument automatique qui pourrait mesurer l'exposition à l'asbestos. Les premières enquêtes ont consistées à filtrer une dispersion liquide dans un champ magnétique de un Tesla. Le filtre contenait des fibres alignées en permanence. Ce filtre était transparent et des mesures de la lumière diffractée relative au champs magnétique initial ont été prises. La recherche subséquente a mesuré la lumière diffractée par des fibres en suspension dans l'eau alors que ces fibres tournant suivaient un champ magnétique rotatif. Cette dernière technique se trouva plus sensible pouvant détecter des concentrations de fibres de l'ordre de 1 million par litre en utilisant de l'équipement relativement simple. Quand à la mesure de masse, cette sensibilité correspond à une part dans 10^{10}. Cette méthode n'a pas les problèmes associés au filtre lui-même. Il est aussi important de noter que cette méthode a le potentiel d'obtenir de l'information concernant la grosseur de la fibre.

Dedicated to the memory of my uncle,

Viggo Andreas Riis

(October 13, 1908 - January 13, 1989).

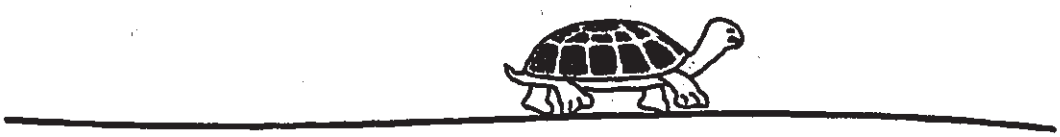

Not that I have already obtained this, or have already been made perfect, but I press on to take hold of that for which Christ Jesus took hold of me. Brothers, I do not consider myself yet to have taken hold of it. But one thing I do: Forgetting what is behind and straining toward what is ahead, I press on toward the goal to win the prize for which God has called me heavenward in Christ Jesus.

Philippians 3: 12-14

Acknowledgements

Time has seen me wander down many unrelated paths since first undertaking this project. Initially it proceeded full steam ahead but circumstances put it on the back burner and kept it there for several years. Finally the time came to finish what has been started.

Having prepared this manuscript, I now appreciate those acknowledgements, that I used to ignore, at the beginning of written works. The efforts of a number of people have enabled me to achieve my goal and I sincerely thank each of them.

Firstly, I want to thank my supervisors: Eric Chatfield, for getting me started on this project; and Ed Ballik, for his patience during the idle years and his full support down the final stretch.

The first portion of this work was performed, while I was a member of the Electron Optics Lab of the Ontario Research Foundation, with funding provided by the U.S. Environmental Protection Agency (contract no. 68-03-2717). I thank: members of the lab for their electron microscope analysis of asbestos samples; co-op students John Hackett and Tony Scott for developing software and equipment, and performing experiments; Lothar Doelher for his faithful dedication in sample preparation and experimental work; and Frank Bottone for his expert craftsmanship in machining custom parts for experimental apparatus.

The theoretical modelling and experimental verification were done at McMaster University. Funding (albeit rather minimal) was partly provided by the National Sciences and Engineering Research Council. There are many people at Mac that I want to thank, but I will not be able to mention them all by name. In particular, I thank: the members of my supervisory committee, Ed Ballik, Jack Kirkaldy and Terry Kennett for their support; Dave Verma for supplying samples of asbestos; Roger Mak for software development; Andy Chik for machining; Andy Duft for his enthusiastic support in tracking down sources for unusual components and machining of special parts; and Scott Hassal for prompt proof-reading of the manuscript. In addition, I thank

all the members of the Physics and Engineering Physics departments (including those secretaries that prodded me to get my thesis finished) who made my time at McMaster one of the most enjoyable periods of my life.

I appreciated using the machine shop facilities at Mohawk College. I am indebted to Pat Hartman of Peterson Electronics for lending me a video overlay circuit-board that allowed computer-generated images to be superimposed on video-camera images. When it came to the design of interface electronics, the assistance of Joerg Adolph was invaluable. I would like to thank photographers Roger Chapman and Jack Whorwood for helping out, especially when timing was critical. I am grateful to Manon Ames and Norm Frenette for translating the abstract into French.

There are two people in particular that deserve special mention. They are Tony Scott and John Savage. I thank Tony for keeping in touch over the years, lighting the firecrackers under my seat to get me rolling, and always being willing to help. I thank John for his constant support, be it late night discussions at Tim Horton's, or computer software for modelling and experiments – a truer friend one could never have.

Peter Riis

September 1989

Table of Contents

Table of Figures

Table of Tables

Chapter 1
Introduction

Asbestos is a known carcinogen, which when inhaled can lodge in the lungs and lead to disease several years later. There is no simple technique for accurately measuring asbestos in order to monitor human exposure to it and hence prevent disease. To date, all regulations on exposure have relied on manual counting using either an optical or an electron microscope. Although, only the electron microscope has proven to give reliable results, phase-contrast optical counting persists for routine asbestos measurements.

The research presented in this thesis explores the prospect of using scattered-light measurements from asbestos particulates aligned in a magnetic field as a means of simplifying and automating the laboratory measuring-process. Should the research be successful, it would pave the way to develop an instrument which would supercede optical counting and would complement electron microscopy. Fiber concentrations could be routinely and accurately monitored with such instrumentation, leaving the use of the electron microscope for the examination of questionable samples and for periodic checking of the instrumentation.

Two experimental techniques were developed. The first involved the filtration of liquid dispersions in a strong magnetic field. This produced filters with permanently aligned fibers and therefore was called the fixed-particle technique. The filter was processed to be made transparent. Light scattered from the resulting sample was then analyzed as a function of the initial magnetic-field direction.

The second technique required the construction of an assembly that had a rotating magnetic-field. Fibers, kept in liquid suspension, would rotate about their center of mass as

they maintained their alignment with the field (dynamic-particle technique). The liquid sample was illuminated with a collimated light-source, and the scattered light was measured as the magnetic field rotated. This produced data containing the scattered-light intensity as a function of magnetic field direction.

Background material essential for this research is presented in Ch. 2 through 4. Chapter 2 gives the properties of asbestos that are pertinent to the research. The magnetic properties of asbestos are dealt with separately in Ch. 3. Modelling of the viscous drag of asbestos fibers is given in Ch. 4.

Initially, efforts focused on the fixed-particle technique. The apparatus was simple, with the most sophisticated component being a commercially available electromagnet. The sample-preparation procedure followed closely that of current optical- or electron-microscopy techniques. While this was a favorable starting point which led to a refined technique, it was limited in its sensitivity to low fiber concentrations. Several attempts were made to improve the sensitivity of this technique, but these met with limited success. A description of the technique and experimental results are given in Ch. 5.

The dynamic-particle technique and the results obtained with it are reported in Ch. 6. It proved to be far superior for detecting low particle concentrations. This was especially true for chrysotile, where it was possible to detect 5 million fibers-per-liter (mfl) with rather simple apparatus as opposed to 750 mfl with the fixed-particle technique. The limitations of the fixed-particle technique were due primarily to the residual structure of the filter causing erroneous scattered-light signals and to fibers becoming embedded in the filter.

Obtaining asbestos-fiber information with the apparatus is not limited to scattered light measurements. The dynamic-particle technique has the ability to provide additional size information by taking advantage of viscous-drag effects as fibers rotate with the magnetic field. The scattered-light peak is observed to increasingly lag the field as the rate of rotation increases. Investigating the behavior of an asbestos fiber suspended in a liquid, as it rotates following a magnetic field became a focal point of the research. A theoretical model was derived which related the phase lag to the dimensions of the fiber. An experimental system was developed

which measured the phase lag of individual fibers at different magnetic-field rotation-rates. The experimental data is in excellent agreement with the theoretical model. The investigation of viscous drag is presented in Ch. 7.

The behavior of other mineral species in magnetic fields is reported in Ch. 8. Results of the research are summarized in Ch. 9.

1.1 Existing Methodology

Most regulations governing exposure to respirable asbestos rely on the use of phase-contrast optical-microscopy. Initially, fibers are collected on membrane filters with air samplers. A known volume of air has passed through the filter in a given period of time. The initial air concentration is then determined by manually counting the number of fibers on a portion of the filter.

Fibers in water tend to be smaller. This has led to transmission electron microscopy (TEM) being the standard method used for analyzing water samples for asbestos content [Anderson and Long 1980]. In addition to providing the resolution required for detecting small fibers, the TEM permits both electron-diffraction and energy-dispersive x-ray analysis for particle identification.

Use of the TEM is considered the only reliable means of measuring asbestos in air or water. High instrument costs, skilled operators and long sample-analysis time make TEM usage expensive. Using the optical microscope is the only affordable technique for routine monitoring and therefore it remains the most commonly used air-sample-analysis technique.

Asbestos measurement by optical- and electron-microscopy has disadvantages. Even with phase-contrast microscopy, optical counting has severe limitations. Fibers with diameters less than 0.25 μm are invisible (taking the resolving power of the microscope to be a half wavelength of a green light source of wavelength 500 nm) and therefore do not get counted. In addition, the technique suffers from the limited ability to discriminate asbestos from other non-asbestos fibers. It is well established that optical counting results are unreliable, with replicate results often being statistically incompatible [NBS 1977, Chatfield 1979].

Use of the TEM is considered the only reliable means of measuring asbestos. The drawbacks are primarily financial --the instrument is very expensive, the measurement time is long, and a highly skilled operator is required.

Trudeau [1979] presents various methods, in addition to microscopy, for monitoring asbestos. Of particular interest is the Fibrous Aerosol Monitor, FAM [GCA 1977], which is intended for on site air analysis. The FAM counts fibers by detecting scattered light pulses from particles in an oscillating electric field. Lilienfeld, who pioneered this work, has since refined the technique to provide partial information on fiber size [Lilienfeld 1987].

Another instrument, the M88 Rapid Fiber Counter by Vickers Instruments [1979, 1980], used magnetic fields to prepare samples containing permanently aligned fibers. It did not directly determine the asbestos fiber content but relied upon optical-microscopy for calibration of each sample type. This has limited the acceptance of the instrument. In addition, it would have suffered limitations similar to that of the fixed-particle technique described in Ch. 5.

Chapter 2

Properties of Asbestos

While there is much information concerning asbestos (fire resistance, etc.), only those properties that relate to this research will be presented. Specifically, these are size and shape, refractive index, and magnetic susceptibility. The properties are summarized in Table 2.1 below and discussed in the following subsections. Values given in Table 2.1b are typical of the samples used in investigating the dynamic-particle technique described in Chapter 6.

Table 2.1. Summary of Pertinent Asbestos Properties

a) Respirable-Fiber Dimensions

diameter	$0.03-3.0\mu m$
length	$>5.0\mu m$

b) Prepared Water-Sample Characteristics (based on TEM count)

	Chrysotile (Ampoule #10)	Crocidolite (Ampoule #9)
estimated mass concentration	$1.89\mu g/l$	$94.0\mu g/l$
mean fiber concentration	$1.99\times10^{6} fib./l$	$1.48\times10^{6} fib./l$
mean length	$1.42\mu m$	$1.43\mu m$
range of lengths	$0.4 to 8\mu m$	$0.5 to 20\mu m$
mean diameter	$0.0518\mu m$	$0.169\mu m$
range of diameters	$0.042 to 1.67\mu m$	$0.048 to 0.476\mu m$

c) Mean Refractive Indices
(of UICC[1] Asbestos Samples, [Heidermanns, 1979])

Chrysotile	1.560
Crocidolite	1.691
Amosite	1.691

d) Density

Chrysotile	$2.55 g/cm^3$
Crocidolite	$3.20 g/cm^3$
Amosite	$3.20 g/cm^3$

e) Magnetic Susceptibility

Chrysotile	$1.5 to 12 \times 10^{-8} m^3/kg$
UICC Crocidolite	$90 \times 10^{-8} m^3/kg$
UICC Amosite	$88 \times 10^{-8} m^3/kg$

2.1 Size and Shape

Particle size and shape are of primary importance in light scattering. Asbestos is fibrous. It is the long, silk-like fibrous nature of asbestos that result in many useful properties. For the purposes of regulation, a fiber is arbitrarily defined as having an aspect ratio of greater than three-to-one (e.g. see NIOSH [1979] or AIA [1979]). The fact that asbestos is fibrous immediately allows one to use light scattering to distinguish it from non-fibrous particulate.

Fibers must be respirable in order to cause damage. This limits fiber size to a diameter of 3.0 μm or less [Trudeau 1979]. As there is no absolute cut-off diameter; this value should

1 Union Internationale Contre le Cancer

only be taken as a guide. The minimum fiber diameter encountered is 30 nm, which corresponds to individual fibrils of chrysotile asbestos [Wicks 1979]. However, chrysotile fibers more often occur as clusters of fibrils rather than as individual fibrils.

Regulations based on optical counting have established a minimum fiber length of 5.0 μm. This arbitrary choice is based more on convenience for optical counting than on epidemiological merits. Fibers shorter than this were included in the present research investigations.

The particle-size parameters are well suited for measurements employing optical-scattering techniques. A general rule (for the applicability of Mie scattering) is that the particle size be greater than one tenth of the wavelength of the incident radiation. Most asbestos particulate meets this criteria; only individual chrysotile fibrils will be difficult to detect.

In addition to respirable fibers, there has been concern over the years on ingested fibers. This has led to investigations of asbestos in drinking water. Fibers found in water are generally smaller than respirable fibers and therefore represent a more difficult measurement problem. For this reason, research has focussed primarily on representative water samples. Typical transmission electron microscope (TEM) calibration of such samples are presented in Table 2.2. These sample ampoules were prepared from the same stock dispersions as the ampoules used in the investigation of the dynamic-particle technique described in Chapter 6.

Table 2.2. Prepared Water Sample Characteristics (based on TEM count)

	Chrysotile (Ampoule #10)	Crocidolite (Ampoule #9)
mean fiber concentration	$1.99\times10^{6} fib./l$	$1.48\times10^{6} fib./l$
95% confidence limits	1.49×10^{6} to $2.48\times10^{6} fib./l$	1.12×10^{6} to $1.83\times10^{6} fib./l$
one fiber corresponds to	$1.35\times10^{6} fib./l$	$6.77\times10^{5} fib./l$
est. mass concentration	$1.89\mu g/l$	$94.0\mu g/l$
number of fibers measured	147	218
mean length	$1.42\mu m$	$1.43\mu m$
mean diameter	$0.0518\mu m$	$0.169\mu m$
range of diameters	0.042 to 01.67 μm	0.048 to 0.476 μm
range of lengths	0.4 to 8 μm	0.5 to 20 μm

2.2 Types

Asbestos is by definition a mineral that is composed of long silky fibers which, when broken, produce smaller fibers instead of randomly shaped fragments. Asbestos can be divided into the two mineral amphibole and serpentine. There are several types of amphibole asbestos, but there is only one type of serpentine asbestos, namely chrysotile. Chrysotile represents over 90% of commercially-used asbestos. The most common varieties of asbestos are shown in Table 2.2. Chrysotile, amosite and crocidolite were used for detailed investigations in this research. Studies of amosite and crocidolite used UICC samples exclusively. Chrysotile investigations used UICC Canadian and a purified form from Union Carbide.

All type of asbestos are silicate-based minerals, having a monoclinic crystal structure. Chrysotile has the interesting property of consisting of cylindrical layers. Their chemical compositions, a summary of which is given in Table 2.3 [Gibbs 1979], may vary within the length of single fiber. Whittaker [1979] and Wicks [1979] give excellent reviews of the chemistry and crystallography of amphibole and chrysotile asbestos.

Table 2.3. Composition of Some Common types of Asbestos

Serpentine Group	
Chrysotile	$3MgO,2SiO_2,2H_2O$
Amphibole Group	
Tremolite	$2CaO,5MgO,FeO,8SiO_2,H_2O$
Crocidolite	$Na_2O,Fe_2O_3,3FeO,8SiO_2,H_2O$
Amosite	$5.5FeO,1.5MgO,8SiO_2,H_2O$
Anthophyllite	$7MgO,8SiO_2,H_2O$

2.3 Optical Properties

Investigating light scattering from asbestos requires the knowledge of the refractive index of a fiber. Asbestos fibers are not homogeneous in this regard. The variations in refractive index are presented in Table 2.4, where n_α is the minimum value and n_γ is the maximum value [Heidermanns, 1979]. With the exception of crocidolite, the n_γ is for the optical electric-field parallel to the length of the fiber.

Table 2.4. Refractive Indices of Common Asbestos Types

	n_α	n_γ
Chrysotile	1.532 - 1.552	1.545 - 1.561
Amosite	1.644 - 1.685	1.674 - 1.728
Crocidolite	1.685 - 1.695	1.689 - 1.699
Anthophyllite	1.598 - 1.647	1.623 - 1.644
Tremolite Actinolite	1.608 - 1.647	1.630 - 1.667

The above variations are very important when identifying asbestos types with the optical microscope. When calculating scattered light intensities, fibers are usually taken to be homogeneous cylinders with refractive indices as given earlier in Table 2.1 [Bohren and Huffman 1984].

2.4 Magnetic Properties

The magnetic properties of asbestos are discussed separately in Chapter 3.

Chapter 3

Magnetic Alignment of Asbestos

Prior to the investigations by Timbrell [1972, 1975], the magnetic properties of asbestos had only been examined using bulk samples [Nagata 1961, Winer and Karpoff 1970]. Timbrell looked at the behaviour of microscopic particles of asbestos in magnetic fields. He found that the fibers align in magnetic fields. Depending on the type of asbestos, the fibers will align parallel to, normal to, or at a constant angle to the magnetic-field direction. Timbrell referred to these alignment modes as P-type, N-type, and T-type (transverse), respectively, as illustrated in Fig. 3.1. This naming convention will be followed in the thesis.

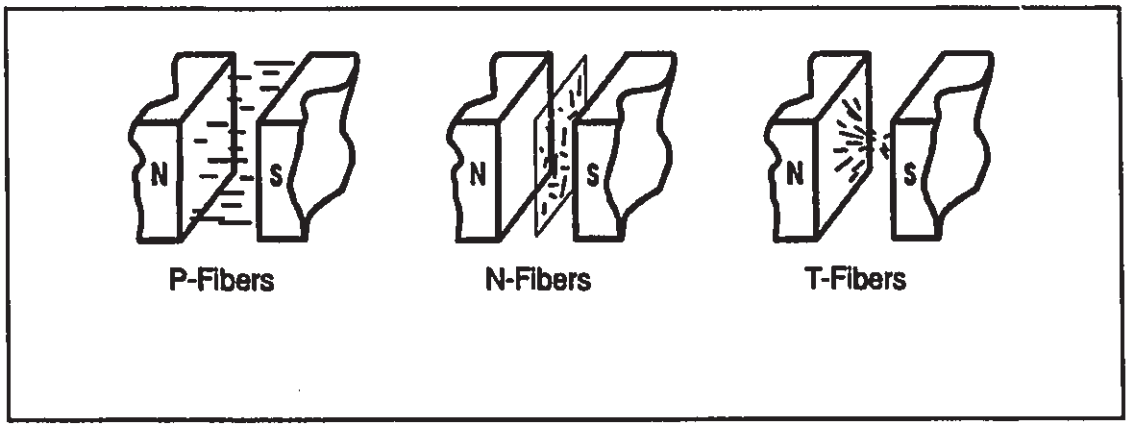

Figure 3. 1. Magnetic alignment modes of asbestos particulate

3.1 Demonstration of Alignment

Permanent samples of magnetically-aligned fibers on microscope slides can be prepared using the Agar technique described in section 3.1.1 below. The alignment behaviour can be examined with the optical microscope, or by looking at the forward light-scattering pattern

when illuminating the bottom of the slide with a laser. Figures 3.2 to 3.6 show optical micrographs, and the corresponding light-scattering pattern for different samples of asbestos.

With no magnetic field applied the orientation of the fibers is random (Fig. 3.2). However, when the same dispersion of UICC crocidolite is used to prepare a sample in a magnetic field, the alignment is very well defined, (Fig. 3.3) with fibers either parallel to or perpendicular to the magnetic-field. The majority of the fibers are parallel to the field (P-type). UICC amosite contains comparable proportions of both P-type and N-type fibers (Fig. 3.4). Chrysotile fibers align parallel to the field, but they maintain a curved shape (Fig. 3.5). New Zealand Cummingtonite, which is T-type, only contains fibers of low aspect-ratio (Fig. 3.6).

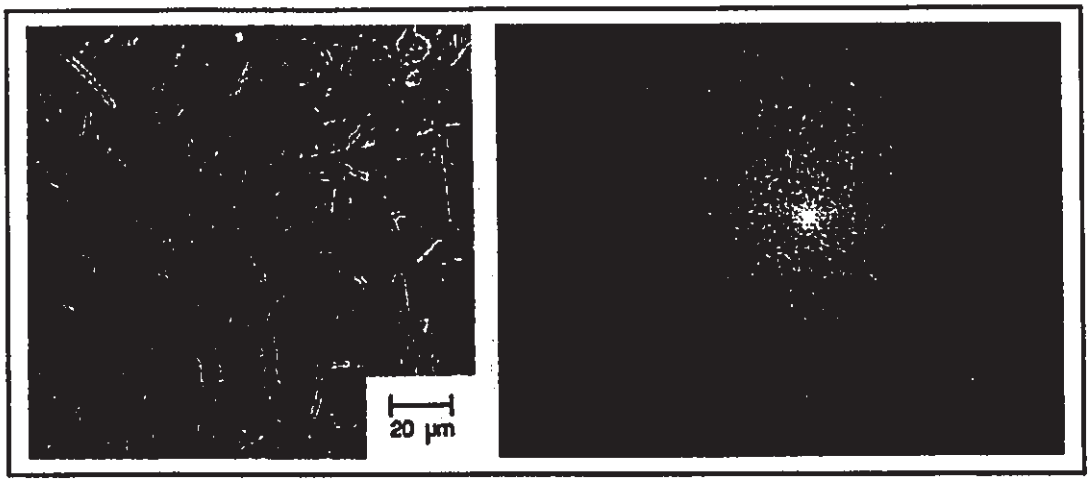

Figure 3.2. Phase-contrast optical micrograph and corresponding forward light-scattering pattern of unaligned UICC crocidolite.

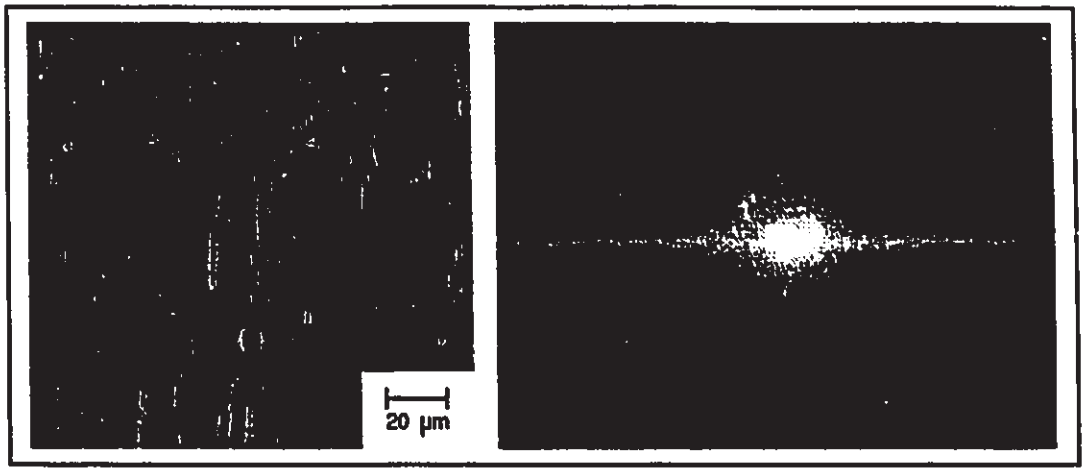

Figure 3.3. Phase-contrast optical micrograph and corresponding forward light-scattering pattern of magnetically-aligned UICC crocidolite.

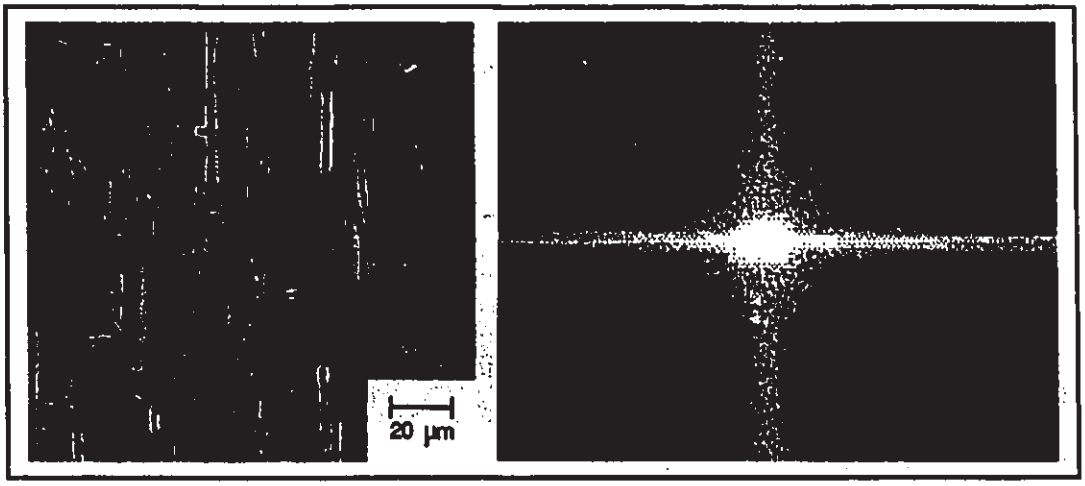

Figure 3.4. Phase-contrast optical micrograph and corresponding forward light-scattering pattern of magnetically-aligned UICC amosite.

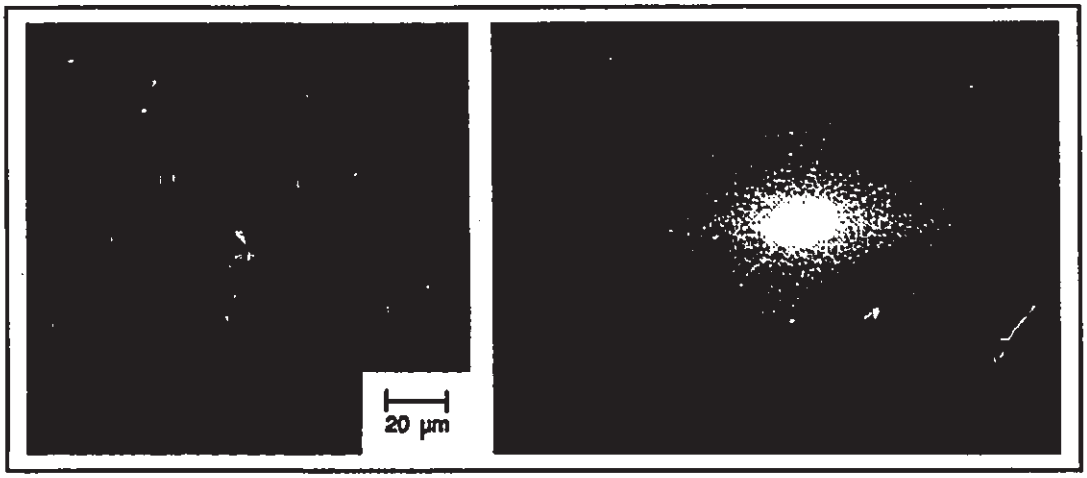

Figure 3.5. Phase-contrast optical micrograph and corresponding forward light-scattering pattern of magnetically-aligned UICC Canadian chrysotile.

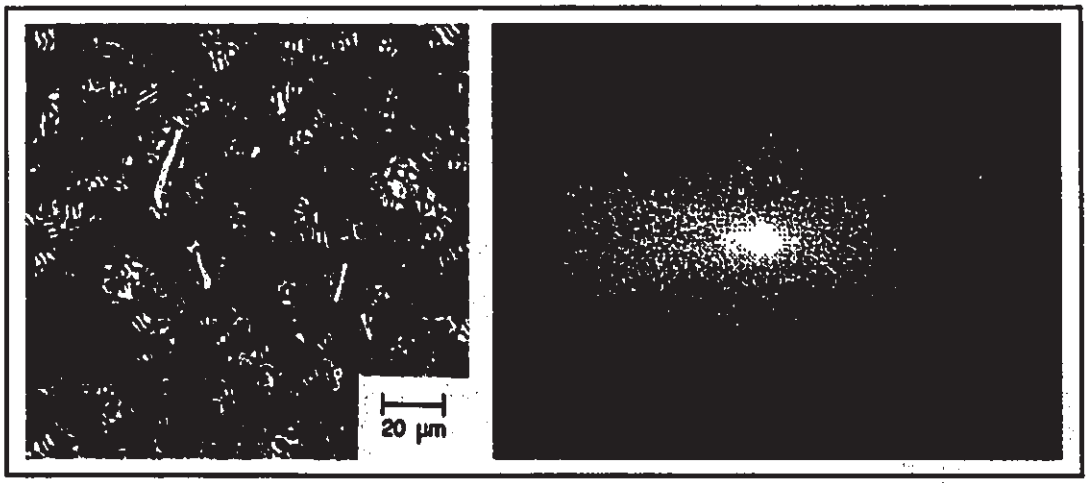

Figure 3.6. Phase-contrast optical micrograph and corresponding forward light-scattering pattern of magnetically-aligned New Zealand cummingtonite.

3.1.1 Sample preparation

For permanently-aligned samples, a 1% aqueous agar solution may be used for the dispersion. A droplet is placed on a microscope slide and the slide then placed in a magnetic field of approximately 0.5 Tesla and allowed to dry. The result is a film containing permanently-aligned fibers (alternatively, a dispersion medium of 0.5% celloidin in amylacetate may be used).

3.2 Cause of Alignment

The most extensive investigations into the causes of asbestos fiber alignment in magnetic fields has been performed by Stroink [1980, 1981]. He discusses three possible mechanisms resulting in fiber alignment:

a) isotropic paramagnetism

b) anisotropic paramagnetism

c) ferromagnetic impurities.

These mechanisms are discussed in more detail in sections 3.2.1 to 3.2.3, respectively. A fiber that is isotropically paramagnetic would experience a torque in a magnetic field that would reach stable equilibrium when aligned parallel to the magnetic field. The alignment direction of anisotropically paramagnetic fibers depends on the relative values of the magnetic susceptibility in different directions in the fiber. Anisotropy can account for all three modes of alignment. The inclusion of "impurities" (primarily magnetite) can result in an orientation based on the shape of the impurities. For example, if the impurities are needle-like in shape and perpendicular to the length of the fiber, then the fiber would align perpendicular to the field. Consequently, magnetic impurities can also cause the three alignment modes.

Stroink [1980] attributes the alignment behaviour of crocidolite and chrysotile to the inclusions of magnetite. The cause for amosite alignment is less definitive but may be due to needle like inclusions of magnetite. Detailed investigations of individual fibers would be required to gain a better understanding of amosite alignment.

Cressey [1980] examined aligned amphibole fibers using selected-area electron-diffraction. She found that the crystallographic y-axis, of N-type UICC amosite fibers, was oriented within 20 degrees of the initial magnetic-field direction. This implies that the direction of

the maximum magnetic-susceptibility is along the y-axis. The samples were prepared using a filtration technique similar to that described in Chapter 5. Misalignment, as individual fibers contact the filter surface, would account for the 20° variation.

Timbrell [1975] observed that when a "parent" fiber is broken into smaller fibers, the resulting fibers are both P-type and N-type. Asbestos species containing both types of fibers have the same chemical composition in each fiber. An explanation for the presence of both P- and N-fibers within a single asbestos species has not been found.

3.2.1 Isotropic Paramagnetism

In order to determine the behaviour of a fiber in a magnetic field, one first needs to know the magnetic moment of the fiber. Consider a cylindrical fiber of length L and radius R located with its length along the z-axis, as depicted in Fig. 3.3.

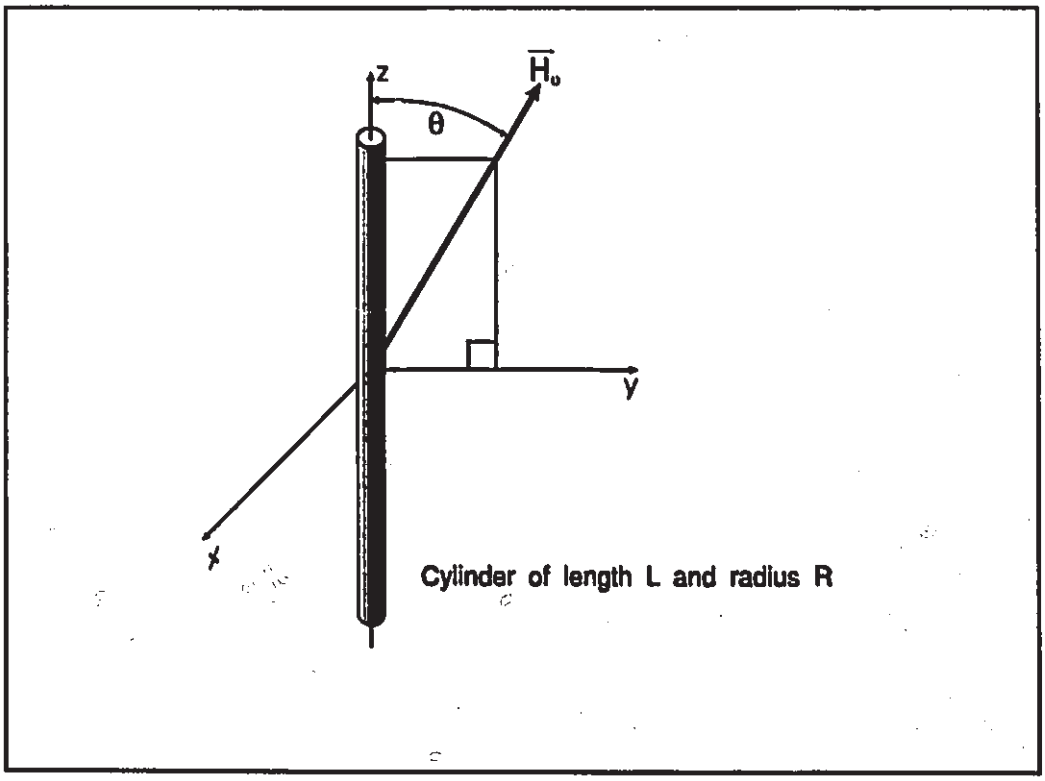

Figure 3.7. Cylinder in a magnetic field

The external magnetic field, H_O, is parallel to the y-z plane and inclined at an angle θ to the z-axis. The field inside the fiber is given by

$$\vec{H}_{internal} = (H_0 \sin\theta - D_y M_y)\hat{y} + (H_0 \cos\theta - D_z M_z)\hat{z} \quad , \qquad 3.1$$

where D_y and D_z are field demagnetizing factors, and M_y and M_z are the components of the magnetization $\vec{M}$ [Brown 1962]. For an infinite cylinder the demagnetizing factors are $D_x = D_y = 1/2$ and $D_z = 0$. These values will introduce only a small error in calculations of fibers having a large aspect-ratio (e.g. $L = 20R$ gives $D_z = 0.02$ [Stroink 1980]). The magnetization inside the fiber is given by

$$\vec{M} = X_m \vec{H}_{internal} \quad ,$$

where X_m is the magnetic susceptibility. Solving for $\vec{M}$ gives

$$\vec{M} = X_m H_0 \left(\frac{\sin\theta}{1 + X_m/2}\hat{y} + \cos\theta\hat{z} \right) \quad . \qquad 3.2$$

Since the magnetization is constant inside the fiber (cylinder), the total magnetic moment is simply

$$\vec{m} = V\vec{M} \quad , \qquad 3.3$$

where V is the volume of the fiber ($\pi R^2 L$). The torque on a magnetic moment in a magnetic field is given by

$$\vec{T} = \vec{m} \times \vec{B} \quad , \qquad 3.3$$

and therefore the torque on the fiber is

$$\vec{T} = V\vec{M} \times \vec{B} = -\frac{V X_m^2 H_0 B_0}{2 + X_m} \sin 2\theta \hat{x} \quad . \qquad 3.4$$

The negative sign indicates that the torque causes the fiber to align parallel to the field. It is important to note that the torque is proportional to the square of the magnetic susceptibility; therefore fibers with a smaller susceptibility will experience a much smaller magnetic-torque.

To verify that in fact this torque is adequate to overcome thermal energies, Stroink [1980] calculated the energy difference between parallel and perpendicular fiber alignment. The results of his energy calculations for a 1 μm diameter and 50 μm long fiber are presented in Table 3.1.

Table 3.1. Alignment Energy [Stroink 1980]

Type	δE ergs
UICC crocidolite	1.15×10^{-9}
UICC amosite	1.09×10^{-9}
UICC chrysotile	1.31×10^{-11}
chrysotile: Baie Verte, Nfld.	1.95×10^{-12}

Typical room-temperature thermal-energies are of the order 10^{-14} ergs which is considerably less than the alignment energies presented in the table. These calculations demonstrate that isotropic fibers align with the magnetic field.

3.2.2 Anisotropic Paramagnetism

In the most general case, the components of the susceptibility can all be different. Since asbestos fibers are being modelled as cylinders, a different value for X_z only will be considered, i.e., let $X_{mx} = X_\mu = AX_{mz} = AX_m$ In this case the torque on the fiber is

$$\vec{T} = \frac{X_m V H_0 B_0 \sin 2\theta}{1 + AX_m/2}\left(A\left(1-\frac{X_m}{2}\right)-1\right)\hat{x} \quad . \qquad 3.5$$

The torque depends on the value of the parameter A and can lead to either parallel or perpendicular alignment. The alignment is parallel when

$$A < \frac{1}{1 - X_m/2} \quad ,$$

and perpendicular when

$$A > \frac{1}{1 - X_m/2} \quad .$$

When the above relationship for A approaches unity, then the torque on a fiber is greater than that of an isotropic fiber.

3.2.3 Ferromagnetic Impurities

The inclusions of impurities such as magnetite in a fiber can lead to fiber alignment such that the average magnetic moment of the various domains are aligned with the field. For parallel alignment, this indicates that the permanent moment of each magnetite inclusion is parallel to the length of the fiber. Similar arguments apply for N-type and T-type fibers.

3.3 Values of the Magnetic Susceptibility

Experimentally-measured values of magnetic susceptibility at room temperature are presented in Table 3.2 [Stroink 1984]. The samples consisted of randomly oriented fibers, and therefore no crystal-axis-specific information was obtained.

Table 3.2. High Field Magnetic Susceptibility of Asbestos [Stroink 1984]

Type	$X_m \times 10^{-8} m^3/kg$
UICC crocidolite	90 ± 4
UICC amosite	88 ± 3
UICC Canadian chrysotile	12 ± 2
chrysotile: Clinton Creek, Yukon	2.9 ± 0.2
chrysotile: Cassiar, B.C.	9.7 ± 1
chrysotile: Thetford, Que.	1.5 ± 0.4
chrysotile: Baie Verte, Nfld.	4.4 ± 0.4

Stroink [1980, 1981] calculated the magnetic susceptibility using the Curie-Weiss law

$$X_m = \frac{n\mu^2 N_o}{3kM(T - T_c)} \quad , \qquad 3.6$$

where, n is the concentration of the magnetic ions,
M is its atomic weight,
μ is the effective magnetic moment,
N_O is Avogadro's number,
k is Boltzman's constant, and
T_C is the Curie temperature.

The Curie temperature is small and was assumed to be zero, and the magnetic-moment was taken to be 5.5 μ_B [Earnshaw 1968]. The magnetic behaviour was attributed to the presence of iron in the asbestos fibers. Stroink found good agreement with experimental values, except for UICC Canadian chrysotile, which had a calculated value approximately 1/4 that of the measured value.

Measurements specific to each fiber axis have not been made. Consequently, magnetic-torque calculations are limited to the assumption that the fibers are isotropic.

3.4 Magnetic Field Requirements for Fiber Alignment

Initial work by the author had shown that crocidolite and amosite align very precisely with magnetic fields. It was found that even the residual magnetic field (present when the magnet was not energized) was adequate to produce some alignment of these fibers. In contrast, the alignment of chrysotile fibers required much stronger fields. Therefore, chrysotile was used to investigate the minimum magnetic field required for efficient alignment.

The technique used for this investigation was the fixed-particle method described in Chapter 5. Aliquots of 10 ml volume from a 250 ng/l chrysotile dispersion were filtered at magnetic-field strengths ranging from 0.2 T up to 1.0 T in increments of 0.2 T. The resulting filter samples were prepared and the scattered light distributions then measured. The areas of the scattered light peaks were measured as a function of magnetic-field as illustrated in Fig. 3.4. Maximum alignment was achieved for field strengths greater than 0.4 T. These results demonstrate good repeatability for strong fields, and that 0.4 T is the minimum field-strength for the fixed-particle technique. Field strengths used in the subsequent experimental investigations were 1.0 T for the fixed-particle method and 0.92 T for the dynamic-particle method. These values ensured reliable alignment of the particulate.

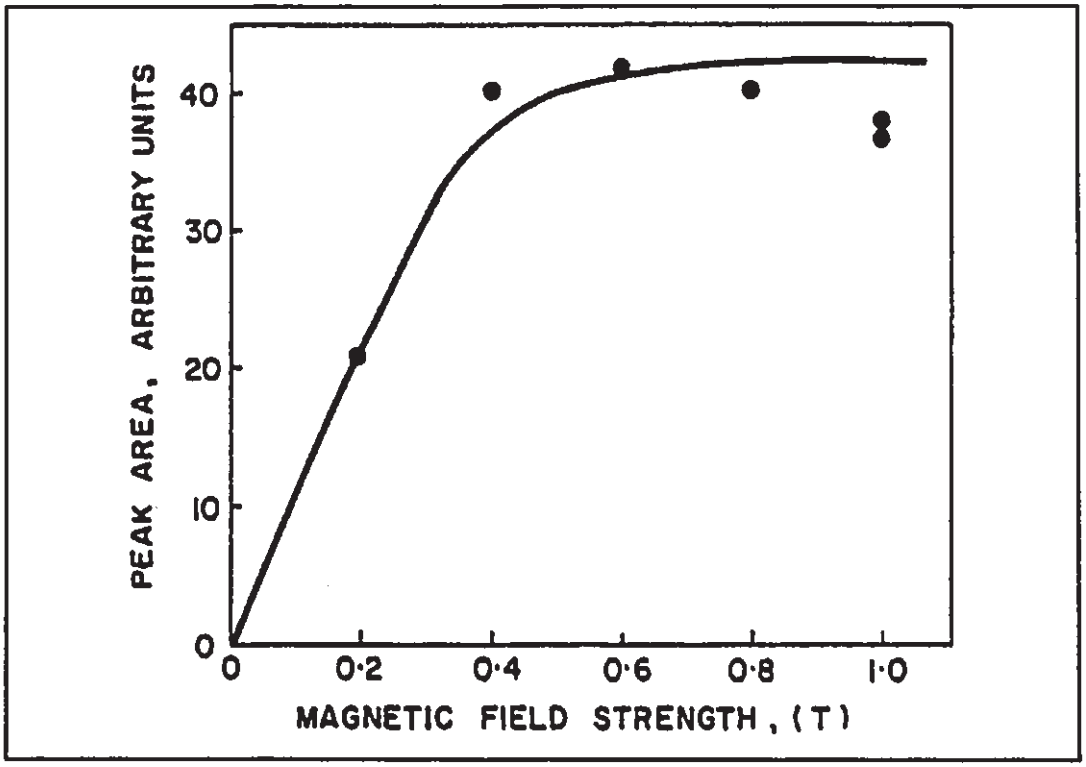

Figure 3.8. Variation of peak area with magnetic-field strength for Union Carbide chrysotile

3.5 Behaviour in Electric Fields

The behaviour of asbestos fibers in electric fields was observed with a simple set of experiments. The results presented here are not thorough but give an indication of the behaviour. Chrysotile has a strong attraction to the electrodes, while amosite demonstrated almost no effect.

3.5.1 The Experiment

Two parallel aluminum electrodes, 2.0 mm apart, were vacuum deposited on glass microscope slides. Plastic gaskets, 0.023 mm thick, were glued to the slides creating a shallow well in which to place liquid dispersions. A few droplets of the sample dispersion would fill the well and then a coverslip was placed over it. The behaviour of the asbestos fibers was observed while a field up to 1500 volts DC was applied to the electrodes.

3.5.2 Results

Dispersions of amosite and chrysotile in a number of suspension liquids were tried. The results are summarized in Table 3.3.

Table 3.3. Observations of the Behaviour of Asbestos Fibers in Electric Fields

Suspension liquid	UICC Amosite	Chrysotile (John Mansville)
light paraffin oil	(1) -align parallel with field but effect is weak and slow -observable only at electrode surface	(2) -parallel to field; fibers aligned quickly -observable throughout the area between the electrodes; fibers move towards the electrodes
ethanol	-weak, similar to (1)	
cyclohexane	-weaker than (1)	-similar to (2) (fibers did not disperse well)
deionized water	-electrical conduction is too high causing electrodes to decompose	

3.5.3 Discussion

Chrysotile shows a much stronger behaviour in electric fields than amosite (and presumably other amphiboles). The behaviour of chrysotile is thought to be due to its strong zeta potential. Other investigations have used electric fields for asbestos analysis. Melton, of Battelle Labs, [Melton et al 1978] used electrophoresis as one step in a procedure that was developed to separate asbestos from the rest of a sample for later optical counting. The ability of x-ray diffraction to detect chrysotile was improved by using an AC field, applied to two interlaced finger-like electrodes, to align chrysotile fibers [Birks et al, 1975]. The behaviour of chrysotile in electric fields could be a useful complement to magnetic alignment in designing an automated instrument for measuring asbestos.

Chapter 4

Torque due to Viscous Drag

Asbestos fibers suspended in liquid, rotate about their center, maintaining alignment with a rotating magnetic-field. The alignment is caused by the magnetic torque discussed in Chapter 3. Experimental results (discussed in section 6.3.4) suggested that the fibers lag the magnetic field. As the rotation rate increases, the phase lag increases. This led to an investigation of the fluid dynamics of a cylinder rotating about its center. A theoretical model for the torque caused by viscous drag is developed in this chapter. An experiment that specifically tested the model for asbestos fibers is given in Chapter 7.

4.1 Modelling Viscous Drag

The viscous-drag torque experienced by a rotating cylinder consists of two components, that due to the cylinder wall, and that due to the cylinder ends. Both contributions are of comparable magnitude.

4.1.1 Drag of the Cylinder Wall

The starting point in determining the torque due to viscous-drag of the cylinder wall, is to consider the flow past an infinite cylinder with the direction of flow at normal incidence to the length of the cylinder. For a cylinder of radius R, the drag per unit length is given by [Landau and Lifshitz 1959]

$$F = \frac{4\pi\eta u}{1/2 - \gamma - \ln(uR/4\nu)} \quad , \qquad 4.1$$

where η = dynamic viscosity,

γ = Euler's constant (0.5772156649...),

u = fluid velocity,

R = fiber radius, and

υ = kinematic viscosity.

As a fiber suspended in a fluid follows a magnetic- field, it rotates about its center. This means that the fluid velocity is zero at the center of the fiber and increases linearly along the length of the fiber. At a distance l from the center of the fiber, the fluid velocity is $u = \omega l$, where ω is the angular velocity of the fiber. The viscous-drag force at the point l, on the cross-sectional slice dl, is

$$dF = \frac{4\pi\eta\omega l}{1/2 - \gamma - \ln(\omega l R/4\nu)} dl \quad . \tag{4.2}$$

This is illustrated in Fig. 4.1. The torque exerted by the fluid at the point is simply the distance from the center times the force at that point. That is,

$$dT = \frac{4\pi\eta\omega l^2}{1/2 - \gamma - \ln(\omega l R/4\nu)} dl \quad . \tag{4.3}$$

Integrating this equation over the length of the fiber gives the total torque due to viscous drag of the cylinder wall,

$$T = 2\int_0^{L/2} \frac{4\pi\eta\omega l^2}{1/2 - \gamma - \ln(\omega l R/4\nu)} dl \quad . \tag{4.4}$$

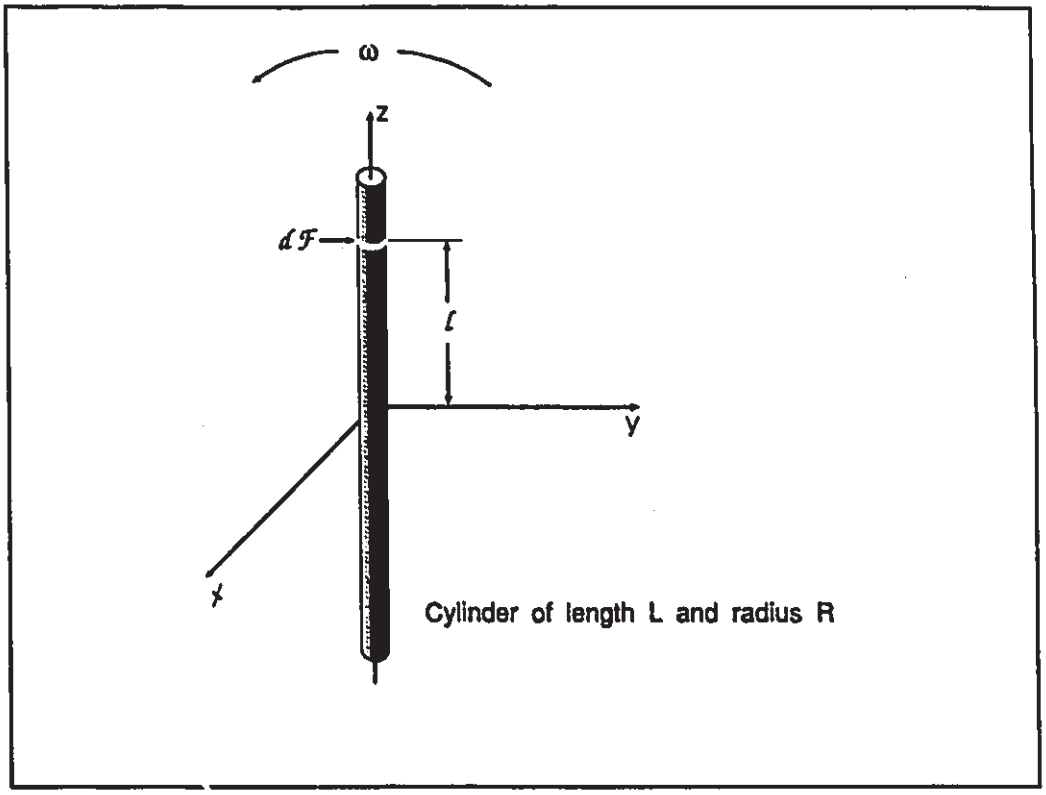

Figure 4.1. Viscous drag on a rotating cylinder

This integral is of the form

$$T = a_o \int_0^{L/2} \frac{l^2}{b_0 - \ln l} dl \quad , \tag{4.5}$$

where

$$a_o = 8\pi\eta\omega \quad , \tag{4.6a}$$

and

$$b_o = \frac{1}{2} - \gamma - \ln\left(\frac{\omega R}{4\nu}\right) \quad . \tag{4.6b}$$

Carrying out a series of variable substitutions leads to

$$T = a_o e^{3b_o} \int_{3(b_o \ln(L/2))}^{\infty} \frac{e^{-l}}{l} dl \quad . \tag{4.7}$$

The solution to the integral is the exponential integral E_1 [Abramowitz and Stegun 1970], and therefore

$$T = \alpha_o e^{3b_o} E_1(z) \quad . \tag{4.8}$$

where z, in terms of the original parameters is,

$$z = 3\left(\frac{1}{2} - \gamma - \ln\left(\frac{\omega R L}{8\nu}\right)\right) \quad . \tag{4.9}$$

In turn, the exact expression for the torque is

$$T_{wall} = 8\pi\eta\omega E_1\left[3\left(\frac{1}{2} - \gamma - \ln(\omega R L/8\nu)\right)\right] e^{3\left(\frac{1}{2} - \gamma - \ln(\omega R/4\nu)\right)} \tag{4.10}$$

The asymptotic expansion for the exponential integral is [Abramowitz and Stegun 1970]

$$E_1(z) \sim \frac{e^{-z}}{z}\left(1 - \frac{1}{z} + \frac{2}{z^2} - \frac{6}{z^3} + (-1)^n \frac{n!}{z^n} - \ldots\right) \quad . \tag{4.11}$$

Evaluating this series approximation against the exact value of E_1 over the range of values of interest showed that the series converges rapidly. In fact, the first term comes within 5% of the correct value. (Confirmation of the integration, evaluation of the exponential integral, and graphical analysis were done with the assistance of T. Scott, of the Maple Group at the University of Waterloo, using Maple Symbolic Computation System Ver. 4.2 [Char et al 1988].)

Therefore, the torque due to the viscous drag of the cylinder wall can be calculated from

$$T_{wall} \sim \frac{\pi\eta\omega L^3}{3(1/2 - \gamma - \ln(\omega R L/8\nu))}\left(1 - \frac{1}{z} + \frac{2}{z^2} - \ldots\right) \quad . \tag{4.12}$$

4.1.2 Drag of Cylinder Ends

The shape of the ends of the cylinder must be taken into consideration. If they are taken as hemispheres of radius R, then one has two symmetric hemispheres moving at the

velocity of the end of the fiber. Stoke's formula for the force on a sphere, moving at a velocity u, is

$$F = 6\pi R\eta u \quad . \tag{4.13}$$

The ends are equivalent to a sphere moving at a velocity of $\omega L/2$. The torque is the distance ($L/2$) from the center of the fiber times the force. Therefore, the torque due to hemispherical ends is

$$T_{ends} = \frac{3}{2}\pi\eta\omega R L^2 \quad . \tag{4.14}$$

Another approach is to consider the ends of the cylinder as a flat disk. The equation for the force on a disk of radius R, moving at a velocity u, parallel to the plane of the disk is [Landau and Lifshitz 1959]

$$F = 32\eta R u/3 \quad . \tag{4.15}$$

This value is 0.566 times that of the sphere. In reality, the ends of asbestos fibers are somewhere between the two in shape. The approximation of a hemispherical model will be used.

4.1.3 Total Drag

Combining the results of the previous two sections allows the total torque, due to viscous-drag of a rotating cylinder, to be determined using

$$T_{drag} = T_{wall} + T_{ends} \quad . \tag{4.16}$$

This torque is shown in Figs. 4.2 to 4.4 for three different cylinders with sizes as given in the figure captions. The calculations were done for cylinders suspended in room temperature water, using the viscosities given in Table 4.1.

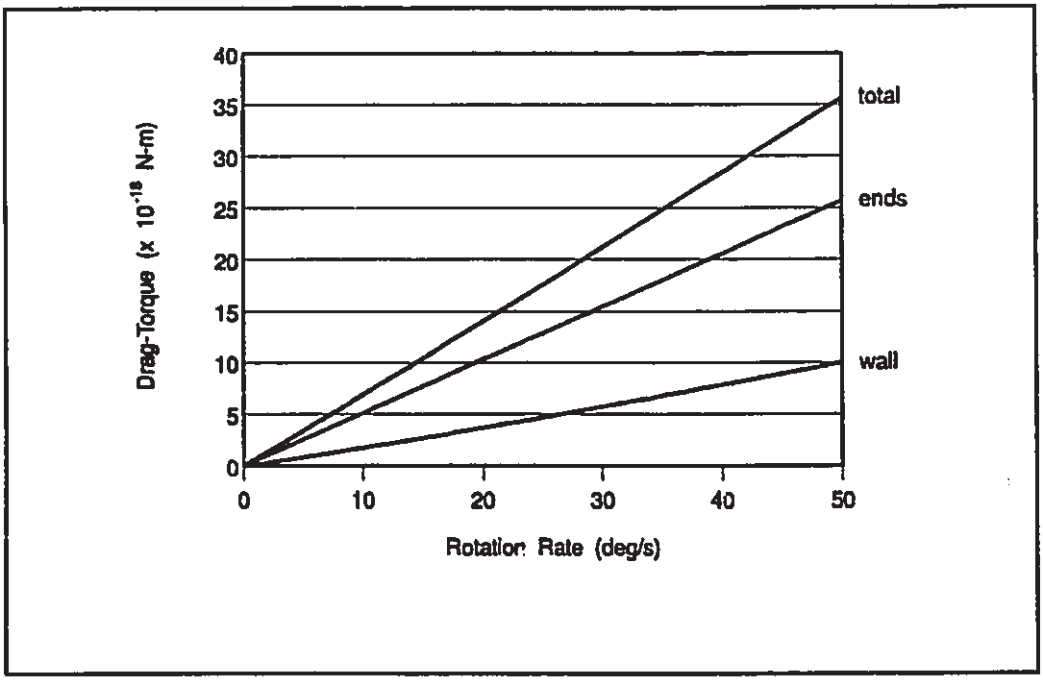

Figure 4.2. Torque due to viscous-drag for a cylinder of length 50 μm and diameter 5.0 μm

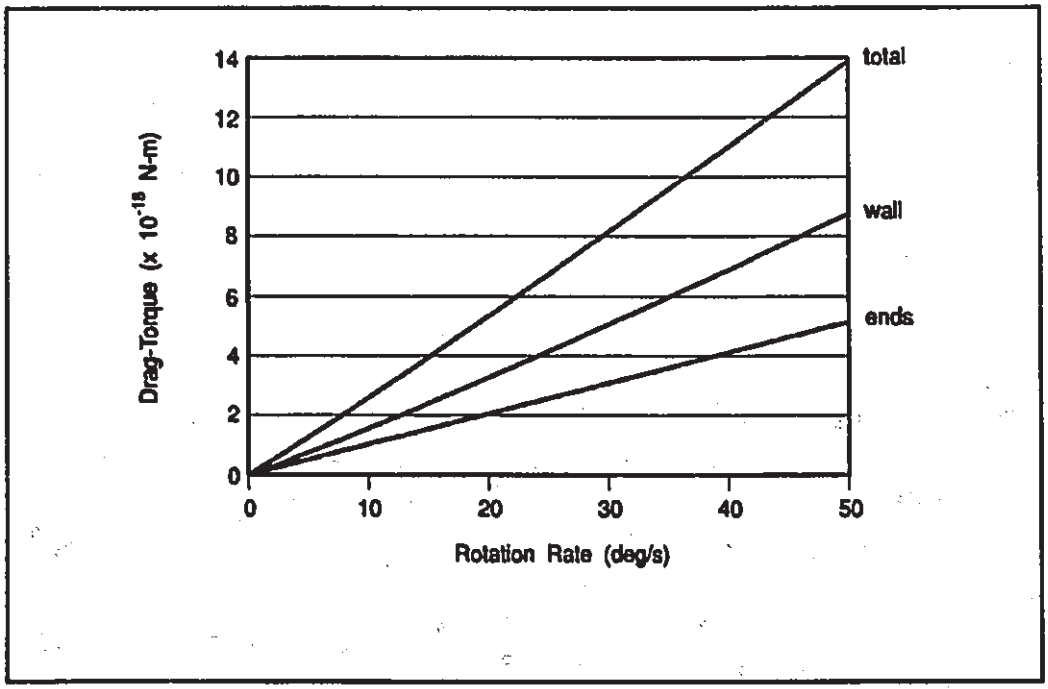

Figure 4.3. Torque due to viscous-drag for a cylinder of length 50 μm and diameter 1.0 μm

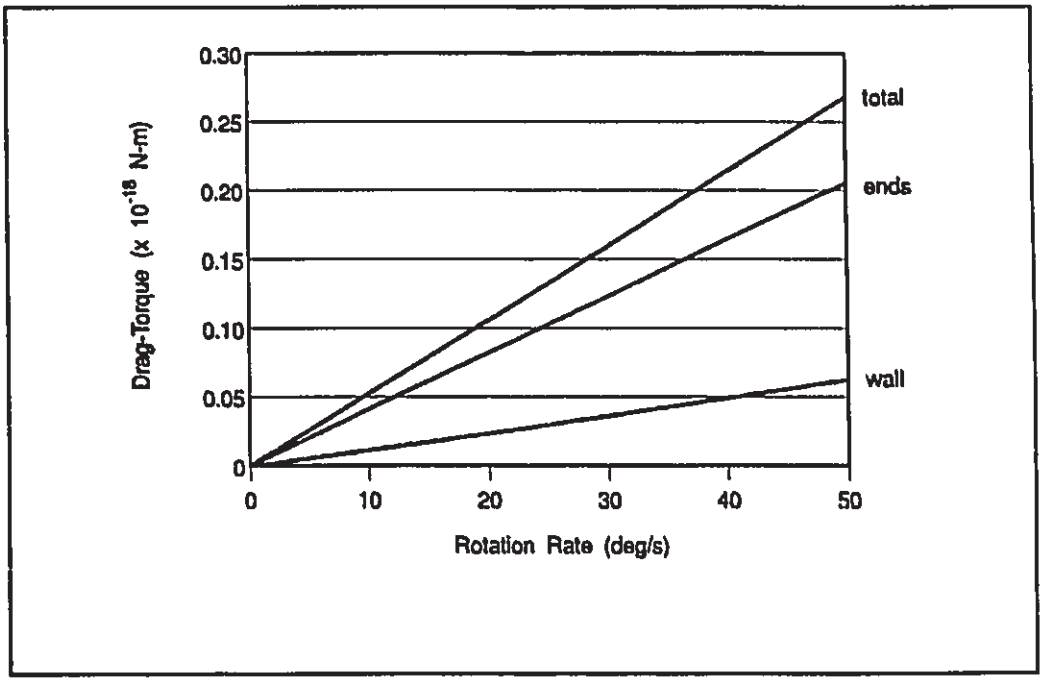

Figure 4.4. Torque due to viscous-drag for a cylinder of length 10 μm and diameter 1.0 μm

Table 4.1. Viscosity of Water at Room Temperature (20^{0}C)

	Symbol	Value
dynamic viscosity	η	0.0100 g/cm-sec
kinematic viscosity	ν	0.0100 cm^2/sec

The graphs demonstrate some general properties of the viscous-drag torque of rotating cylinders. The contribution from the ends of the cylinder and the cylinder wall are of comparable magnitude. At first this may seem unreasonable, but the series expansion (Eq. 4.12) shows that the wall's component is roughly proportional to the cube of the length. Consequently, most of the drag-torque occurs at the ends of the cylinder. The figures demonstrate that as the ratio of the length to diameter decreases, the ends of the cylinder contribute a larger fraction of the total drag.

In summary, the torque due to viscous drag is primarily dependent upon the length of the fiber. The drag-torque from the ends are proportional to the square of length, and the drag-torque from the wall is approximately proportional to length cubed. The

dependence of radius is much less significant since the drag-torque from the ends are proportional to the radius, and the drag-torque from the wall is almost independent of the radius.

An earlier attempt to model the viscous-drag behaviour of rotating asbestos-fibers was made by Chatfield [1984] who suggested an empirical relationship of $L^2R^{1/3}$. Unfortunately, Chatfield did not provide calibration information in his paper, and therefore his results cannot be compared against the model.

4.2 Drag versus Magnetic Torque

Asbestos fibers experience two competing forces, the magnetic torque causing the fiber to align with the field, and the frictional drag force as the fiber rotates about its center through the fluid. It is the balance between these that leads to a particular phase lag at a given rotation-rate, namely

$$T_{magnetic} = T_{drag} \quad . \tag{4.17}$$

The equation for the magnetic torque on an isotropic cylinder is

$$T_{magnetic} = \frac{\pi R^2 L X_m^2 H_0 B_0}{2+X_m} \sin 2\theta \quad . \tag{4.18}$$

where the volume V, of Eq. 3.4 has been replaced by $\pi R^2 L$. Expressing the magnetic torque as $T_{mag} \sin(2\theta)$, where the coefficient T_{mag} is determined from the above equation, allows the expression for the phase lag of a rotating cylinder to be written as

$$\theta = \frac{1}{2} \sin^{-1}\left[\frac{T_{drag}}{T_{mag}}\right] \quad . \tag{4.19}$$

Figures 4.5 to 4.7 show the phase-lag versus rotation rate for the cylinders of Figs. 4.2 to 4.4 respectively. The cylinders are taken to have a magnetic susceptibility equal to that of crocidolite, and to be in a magnetic field of 0.47 T. The difference in phase lag between the two 50 μm long fibers is drastic. Magnetic-torque is proportional to fiber volume whereas

the viscous drag is dominated by length. The 5.0 μm diameter cylinder experiences 25 times more magnetic torque than the 1.0 μm cylinder of the same length, whereas the drag-torque differs only by a factor of 3. This model demonstrates that fibers of low aspect ratio (short thick fibers) will remain essentially aligned with the field, while long thin fibers will experience a significant phase lag. Comparing Figs. 4.5 and 4.7 shows that fibers of the same aspect ratio will have similar phase lags. This means that measured phase-lags of an unknown fiber allow one to determine the aspect ratio, but specific cylinder dimensions would require very precise measurements.

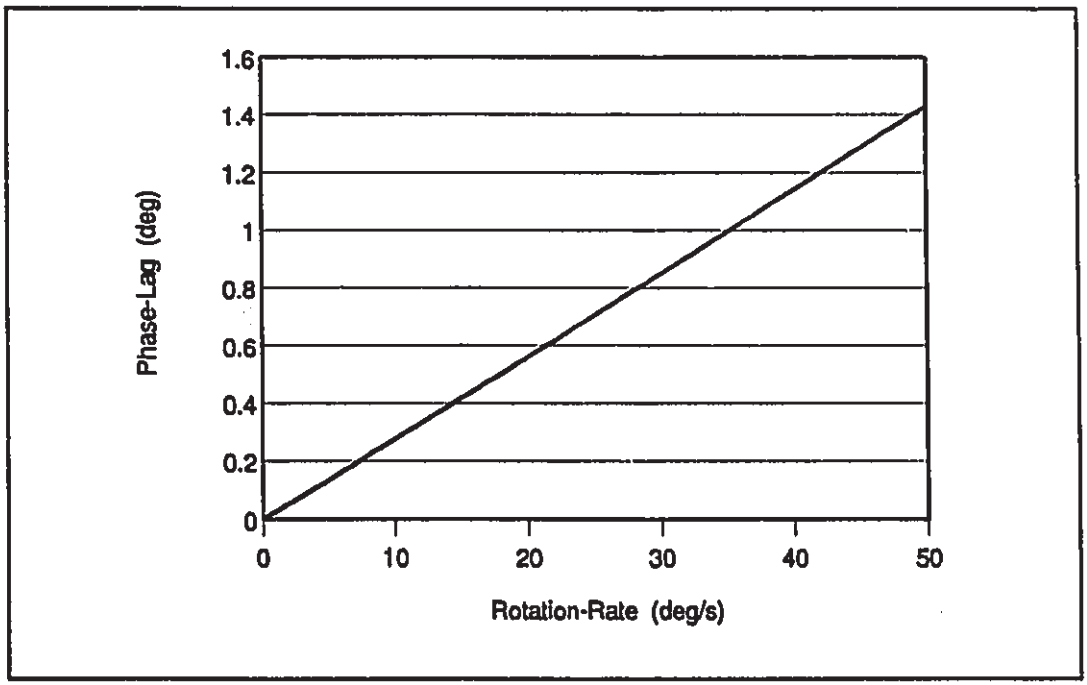

Figure 4.5. Phase-lag versus rotation-rate for a cylinder of length 50 μm and diameter 5.0 μm

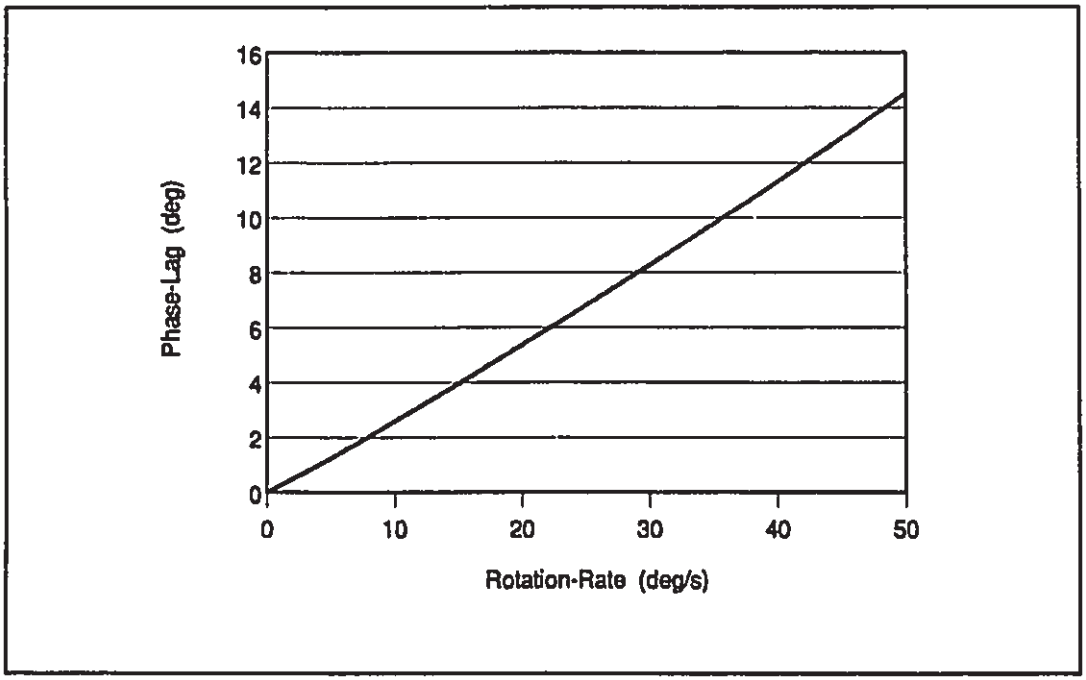

Figure 4.6. Phase lag versus rotation-rate for a cylinder of length 50 μm and diameter 1.0 μm

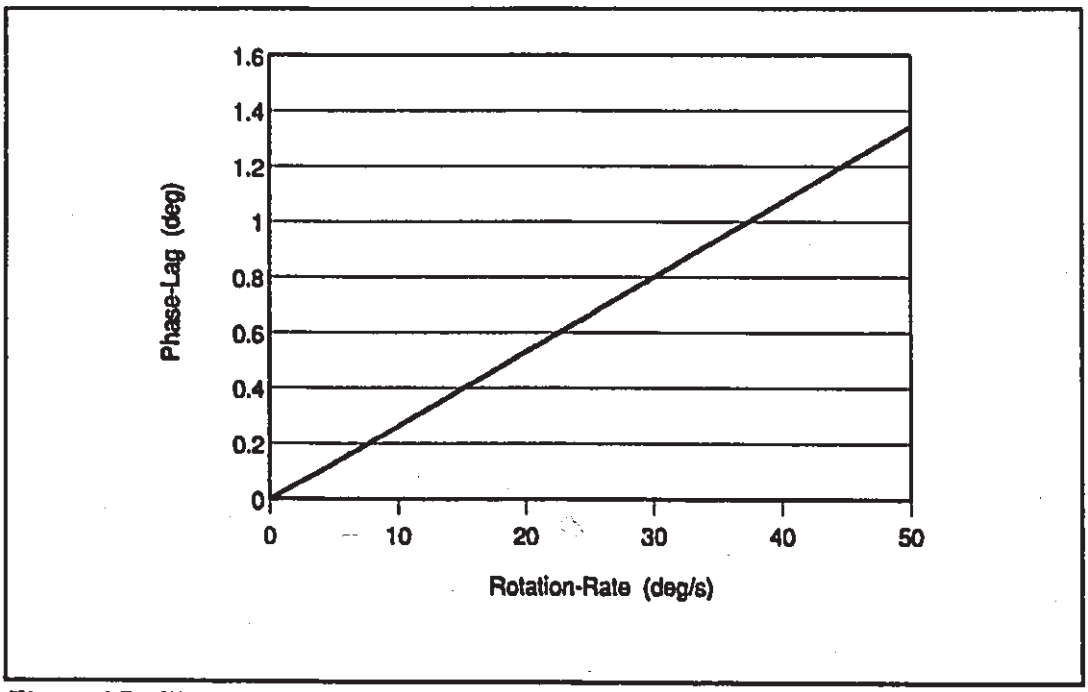

Figure 4.7. Phase lag versus rotation-rate for a cylinder of Length 10 μm and diameter 1.0 μm

Chapter 5
The Fixed-Particle Method

Current methodology for water-analysis involves the filtration of a known volume of water, followed by filter preparation and subsequent analysis with the transmission electron microscope (TEM) [Anderson,1980]. A logical extension of this technique is to filter water samples in a magnetic field. The fibers become aligned by the field prior to contacting the filter, and maintain their alignment while settling on the filter surface. Instead of preparing the filter for TEM analysis, preparation is made for light-scattering analysis. The result of such preparation is a clear plastic membrane containing permanently aligned-fibers, which forms the basis of the "Fixed-Particle Technique".

The technique is described in detail in the following sections. (See also Riis and Chatfield [1982, 1983].) Although initial results were very encouraging, later work showed that the method was of limited use in detecting low concentrations of asbestos. Attempts made to improve the sensitivity (see section 5.4) all involved the introduction of additional steps during filter preparation, but yielded minimal improvements in sensitivity. The fixed-particle technique was eventually abandoned in favour of the dynamic-particle technique described in Chapter 6.

5.1 Experimental Setup

The principle of the scattered-light analysis technique is illustrated schematically in Fig. 5.1. The sample is a transparent plastic film, prepared from a filter containing permanently-aligned fibers. The procedure for preparing the samples is discussed in section 5.2.2. A beam of laser light illuminates the aligned-fiber sample, which is rotated about an axis coincident with the center of the beam. A photomultiplier detector is mounted so that

its axis intersects the incident beam at the center of the sample. The angle of intersection ϕ, can be varied. As the sample is rotated, the detected scattered-light is measured as a function of the original magnetic-field direction.

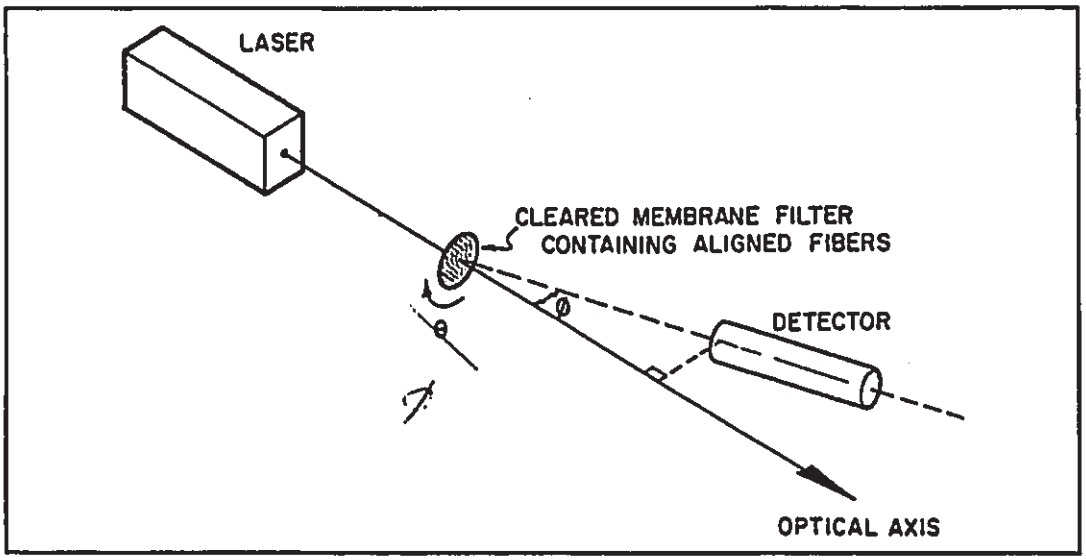

Figure 5.1 Schematic of system used for the analysis of light scattered from permanently-aligned asbestos fibers

The actual instrumentation used, shown in Figure 5.2, is oriented the same as in Fig. 5.1. Light from an expanded argon ion laser, ($\lambda = 514.5nm$) passes through the aperture at the far left, and then illuminates uniformly a 1.5 cm diameter area of the transparent membrane-filter sample located at the center of the vertical turntable. The opening in the turntable is 2.5 cm in diameter. Essentially all of the fibers on the filter contribute to the scattered-light, which is detected by a photomultiplier assembly mounted on an arm. This arm can be rotated about the center of the sample to vary the angle ϕ. The output signal from the photomultiplier is fed to an oscilloscope for visual observation or to an x-y recorder for permanent records. The signal consists of intensity peaks from the fibers superimposed on a background signal caused by scattering from the substrate and non-asbestos particulate. A variable offset unit, consisting of a potentiometer and a battery, was in series with the signal in order to apply a reverse potential to cancel the background signal. This is illustrated in Fig. 5.3.

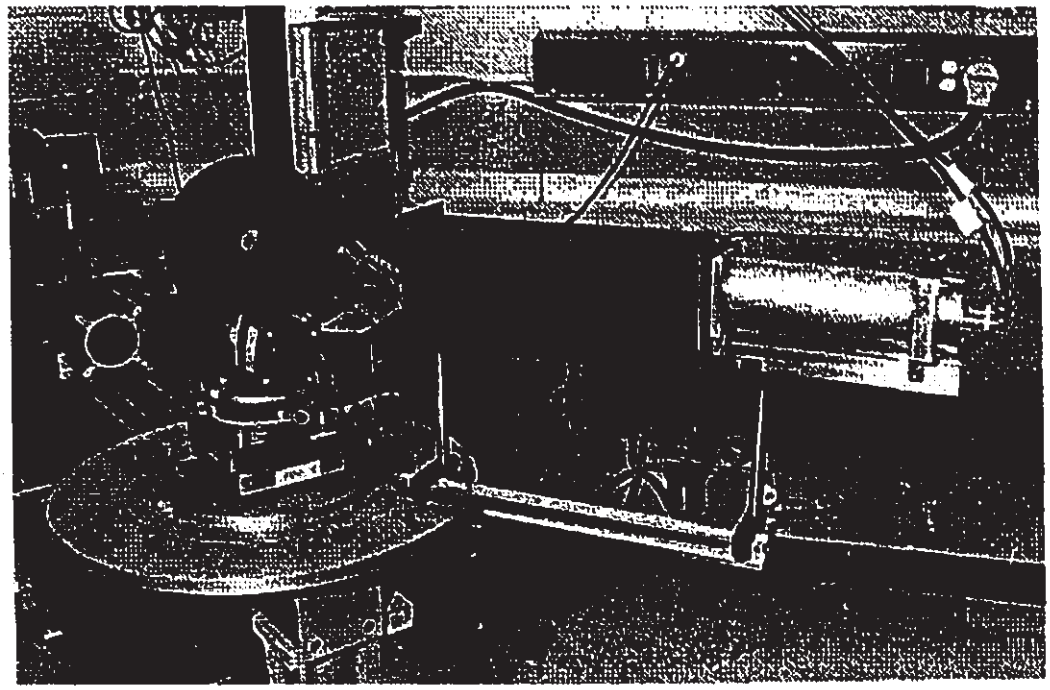

Figure 5.2 Experimental System

Typical scattered-light profiles obtained with the system are shown in Figs. 5.4 to 5.7. These are for UICC crocidolite, UICC amosite and Union Carbide chrysotile, respectively. The profiles should be compared against the optical micrographs and the scattered-light patterns of Figs. 3.3 to 3.5. Chrysotile has very broad peaks, making it easily distinguishable from the scattered-light profiles of amphiboles. In addition, the relative quantities of P- and N-type fibers differ in crocidolite and amosite, resulting in different scattered-light profiles. This demonstrates that the technique provides a means of discriminating between types of amphibole asbestos.

The above profiles were recorded under identical experimental conditions. That is, the detection angle ϕ, the photomultiplier aperture, the illuminated sample area, and the laser power were kept constant. All of the samples had a comparable mass-loading on the filters. Note that chrysotile has a considerably-smaller signal amplitude. The reason for this is discussed in Chapter 6 section 4.

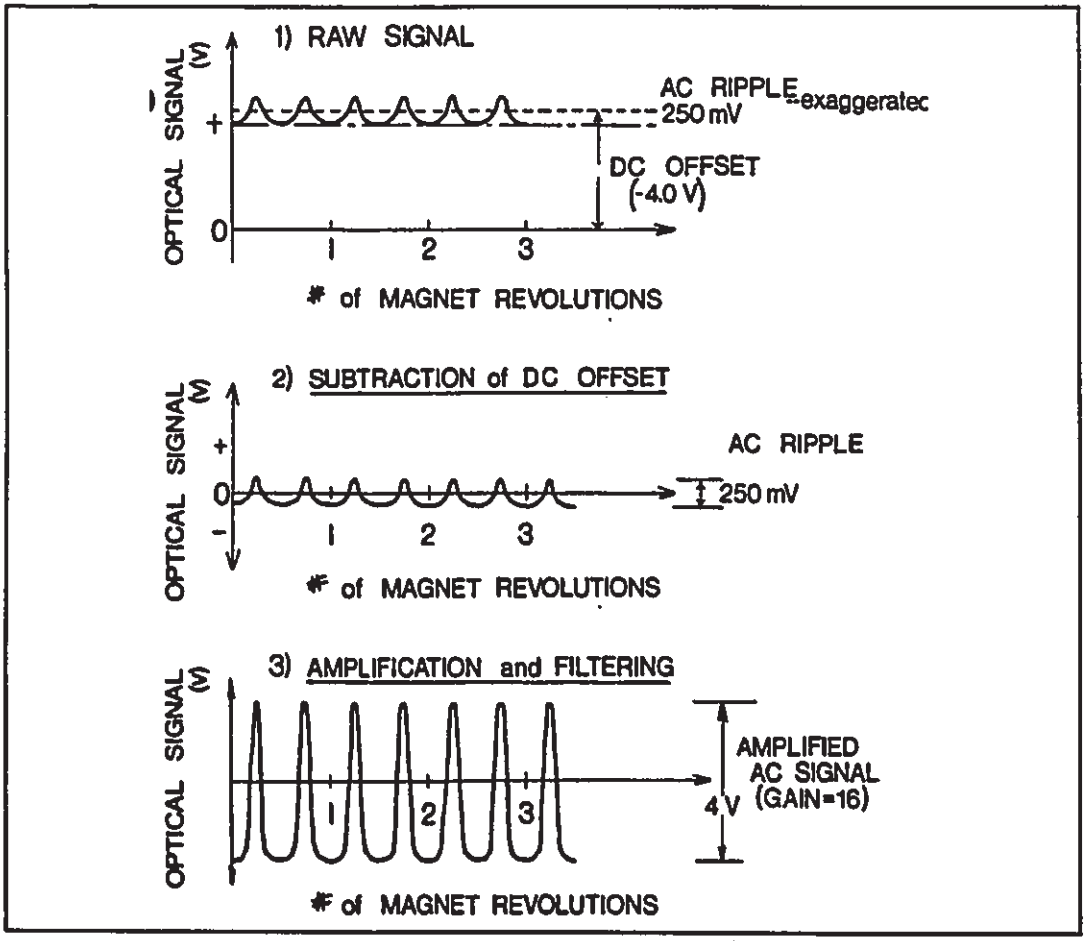

Figure 5.3 **Schematic showing a typical signal and the use of a reverse potential to cancel the background signal. The magnitude of the desired ac ripple is greatly exaggerated. [Scott 1984]**

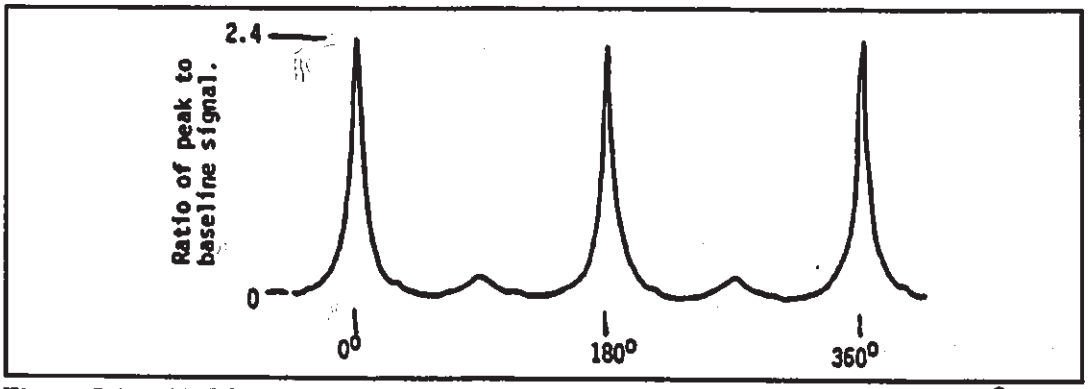

Figure 5.4 **UICC crocidolite scattered-light profile (filter loading = 15 ng/mm^2).**

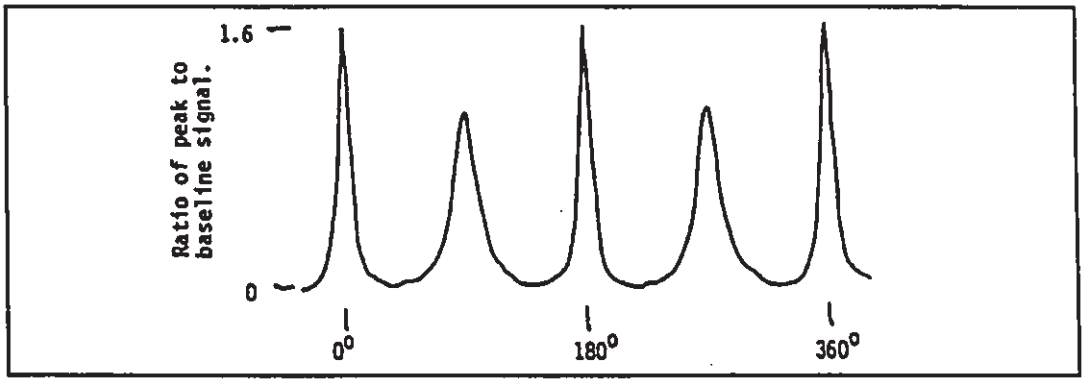

Figure 5.5 **UICC Amosite scattered-light profile (filter loading = 16 ng/mm^2).**

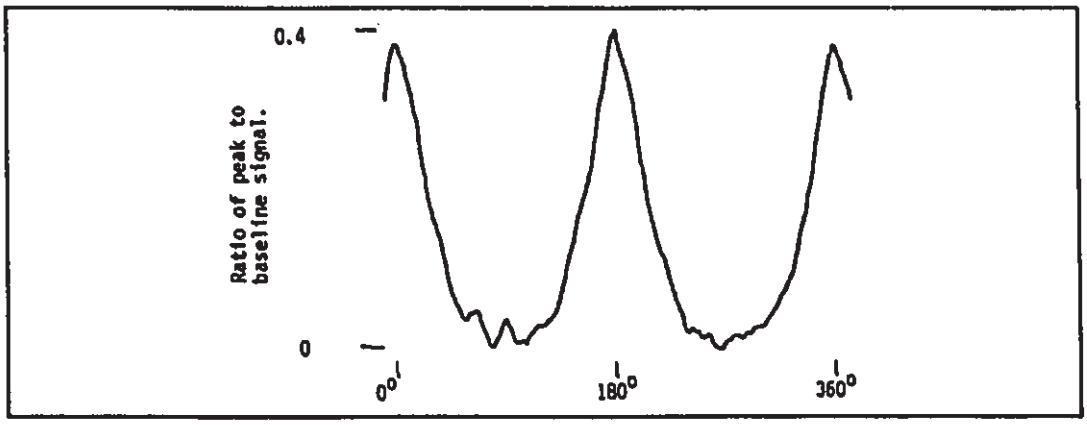

Figure 5.6 **Union Carbide Chrysotile scattered-light profile (filter loading = 12 ng/mm^2).**

5.2 Sample Preparation

5.2.1 Filtration of Aqueous Fiber Dispersions

The sample preparation technique was designed to produce a membrane filter which contained aligned fibers. The fibers aligned by a magnetic-field applied during the filtration procedure (sometimes referred to as magnetic filtration). The filtration apparatus, shown in Fig. 5.7, was located between the poles of an electromagnet. A filter reservoir was attached to a 25 mm diameter glass filtration-assembly (Millipore Corporation XXIO 025 00) with a nonmagnetic clamp. Suction for the filtration was

provided by a water-jet pump (aspirator). Fibers become aligned as the liquid passes through the magnetic field, and retain their orientation when collected on the filter surface. This technique has the advantage of concentrating fibers from a known volume of liquid onto the active area of the filter. The complete procedure is specified by steps (a) to (e).

(a) With a 0.22 μm pore-size type GS MilliporeR filter mounted in the filtration assembly, the aspirator is turned on and the magnetic field is adjusted to the desired value (about 1.0 T).

(b) The desired volume of liquid is filtered through the assembly. The filtration rate is restricted to ensure that the fibers have adequate time to become aligned before contacting the filter surface. The filtration rate can be adjusted by changing the applied vacuum. A filtration rate of about 10 ml/minute has been found to be satisfactory.

(c) The magnetic field is then turned off.

(d) A mark is made on the edge of the filter nearest to one pole of the magnet. This provides a permanent record of the field direction during filtration.

(e) The filter is removed and dried for approximately 15 minutes at 70 °C.

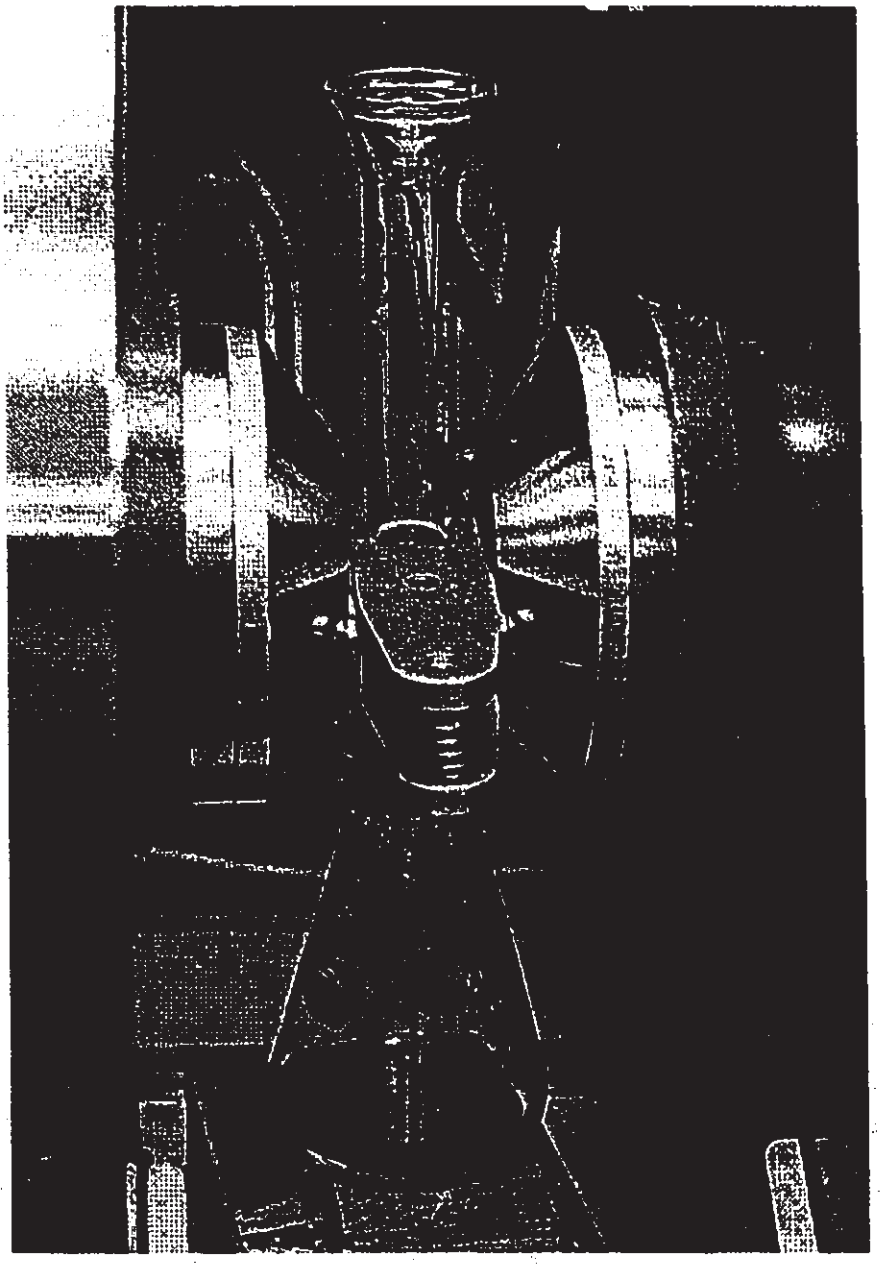

Figure 5.7 The filtration assembly located between the poles of an electromagnet.

5.2.2 Clearing of Membrane Filters

The filter on which the aligned fibers have been deposited must be rendered transparent before being examined using the light-scattering equipment. It was found that the

detection level for the presence of fibers was dependent on the degree of filter transparency which could be obtained. Therefore, several different preparation-techniques were investigated, and these are discussed in subsection 5.2.2.1. All of the filter-clearing techniques involve the collapse of the membrane-filter sponge-structure by exposure to acetone vapor. During this procedure the filter must not become distorted and the fibers must retain their orientations. Furthermore, the filter must be held in position on a flat substrate. The best preparation technique, and the one that ultimately was used routinely, is as follows.

(a) A small amount of dichloroethane is placed on a 5 cm by 7.5 cm microscope slide. The filter is wetted in the dichloroethane and transferred immediately onto another microscope slide.

(b) The edges of the filter are immediately attached to the slide using an acetone based adhesive (nail polish). This step must be performed quickly, since the filter lifts from the slide as the dichloroethane evaporates.

(c) The filter is exposed to a stream of acetone vapor by holding the slide in front of the vapor nozzle of an acetone vapor generator, as illustrated in Fig. 5.8.

(d) The slide is mounted on the turntable of the light-scattering apparatus and is ready for measurements.

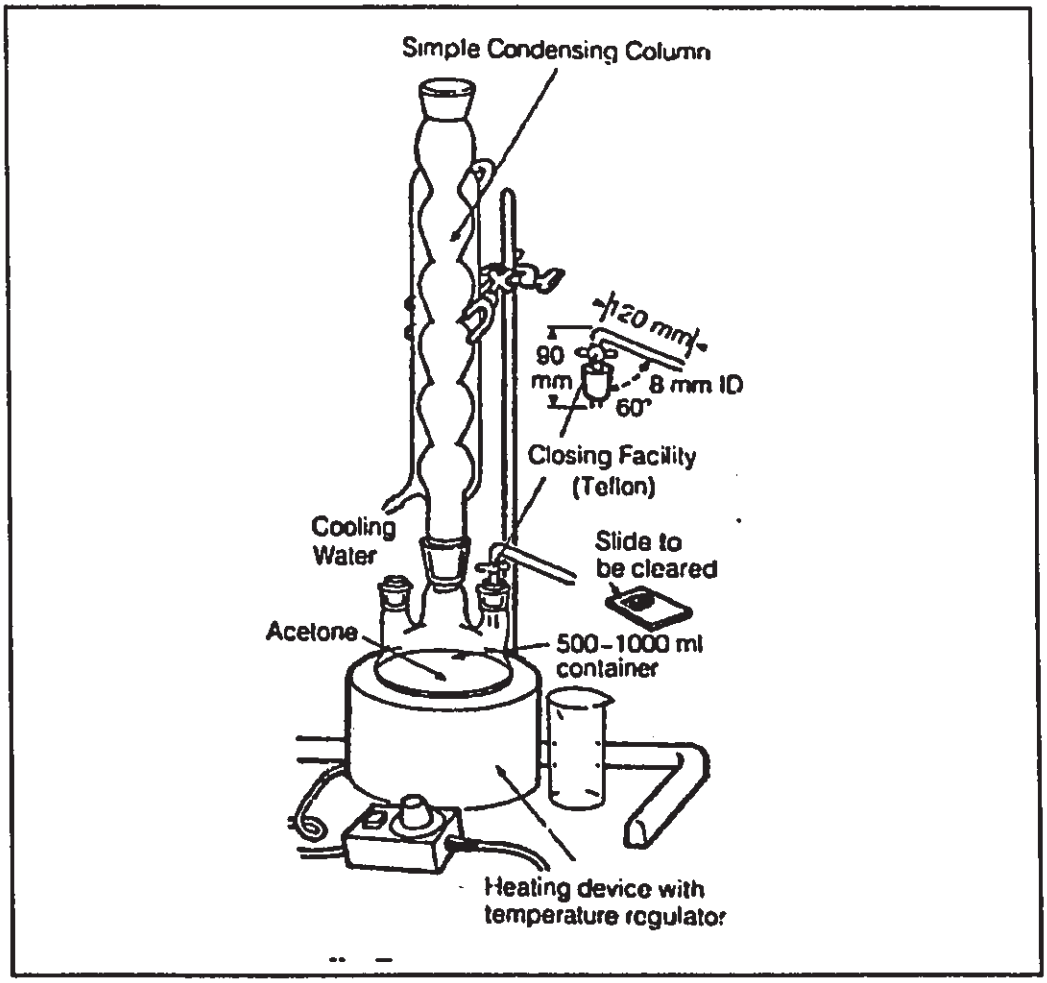

Figure 5.8 Acetone vapor generator used to collapse membrane filters [Asbestos International Association 1979].

5.2.2.1 Investigations into Filter Preparation

In the original technique, a clean glass microscope-slide was used as a substrate for the filter. The slide was first dipped in a solution of 20% collodion in ethanol and subsequently allowed to stand for about 30 s. This produced an adhesive film on the surface of the slide. The filter was then placed onto this surface film, using a rolling action to inhibit formation of air bubbles between the glass slide and the filter. Next, the filter was collapsed by exposing its surface to acetone vapor. This was done by inverting the slide over a beaker containing acetone [Ortiz and Izom, 1974]. When

the filter had become transparent, it was removed from the acetone vapor and allowed to stand for a few minutes, during which the filter plastic solidified. The final result was a clear plastic membrane containing permanently aligned fibers.

For scattered-light analysis, the filter was carefully removed from the glass slide after cutting one edge to release it. It was then placed in a holder, which in turn was mounted at the center of the vertical turntable. Although the sample could be removed from the glass slide immediately after clearing, it usually peeled from the surface more easily if stored for approximately 24 h after removal from the acetone vapor.

Cleared filter samples, prepared from unused filters, were examined using the equipment described in section 5.1. The transparency of such a sample is found by measuring the forward scattered-light intensity in the same way that asbestos-containing samples are measured. The detection limit for asbestos fibers is ultimately determined by the variation in the scattered light intensity from a blank sample as it is rotated. It is therefore desirable that intensity and intensity-variation with sample-rotation be minimized. This will ensure that the scattered light intensity from filtered particulate will form as large a proportion of the total signal as possible. Accordingly, measurements were made on a series of blank samples prepared using various techniques, and these measurements were compared with values obtained from cleaned microscope-slides, cover-slips and thin collodion membranes.

Initial measurements indicated that the collodion used to attach the membrane-filter to the microscope slide was itself a source of scattered light, and therefore alternative means of attachment were investigated. It was found that the buckling and distortion of a membrane filter during the acetone clearing-procedure could be prevented if the pores of the filter were filled with a compatible, but acetone-miscible, solvent. The solvent used was 1,2-dichloro- ethane, and an optimum procedure was developed for clearing of 0.22 μm pore-size type GS Millipore filters without disturbing the fiber alignment. In this procedure, a small amount of dichloroethane was first placed on a 5 cm by 7.5 cm microscope-slide. The filter was placed on the dichloroethane and

immediately transferred to another similar microscope-slide. The wetting of the filter causes it to adhere to the slide, but does not leave a permanent adhesive film which would be a source of unwanted scattering. The edges of the filter were then rapidly attached to the slide using an acetone based adhesive (nail polish). This step must be performed quickly, since the filter lifts from the slide as the dichloroethane evaporates. The method was quick and effective in yielding filters which lay in contact with the slide surfaces. The filter was immediately cleared by exposure to acetone vapor.

In a study of acetone-vapor clearing-methods, it was found that the technique published by the Asbestos International Association [1979] (AIA), yielded clearer filters than those produced by various modifications of the acetone vapor chamber method of Ortiz and Isom [1974]. In the AIA method, the equipment shown in Fig. 5.8 is used to direct a stream of acetone vapor onto the filter surface. Although the AIA clearing process was somewhat variable, and the samples produced were found to yield a wide range of scattered light intensities, the actual values were lower than those given by any other technique tested.

A summary of the measurements is given in Table 5.1. It can be seen that scattered light from the glass microscope-slide did not contribute significantly to the background intensity when compared with the values obtained for cleared membrane-filters. Moreover, collodion, which was previously used to attach the filters to glass slides, scattered light strongly. Therefore, the use of collodion should be avoided in sample preparation.

The sample preparation procedure, which produced the lowest background scattered-light was first to mount the filter using the dichloroethane technique and then to clear the filter using the AIA acetone-vapor method. The variability of the scattered light signal obtained from a group of ten such preparations was measured; these results are shown in Table 5.2. Note that, with one exception, all of the filters yielded two peaks in the scattered-light profile having similar shape to those obtained

Table 5.1 Measurements of scattered light from sample-preparation media.

Medium	Background signal (mV)	Peak-to-peak signal (mV)
cleaned glass microscope slide	90 - 250	15 - 100
cleaned glass cover slip	300 - 900	75 - 150
50 nm thick collodion membrane on slide	400 - 1500	120 - 1000
0.22 μm pore-size type GS Millipore filter, AIA cleared	3000 - 6000	150 - 1000
0.22 μm pore-size type GS Millipore filter, vapor chamber cleared	9000 - 20000	500 - 1000
0.45 μm pore-size PVC Copolymer Gelman filter cleared with a dioxane cyclohexane solution	8000 - 25000	1000 - 2000

for aligned fibers of chrysotile asbestos. When the peaks occurred in the same positions as those expected for chrysotile, they imposed a lower limit for the detection level. It was not possible to obtain a flat response from most of the preparations.

Table 5.2 Measurements of scattered light from blank filter-samples prepared using dichloroethane adhesion followed by clearing in acetone vapor.

Sample number	Background signal, mV	Peak-to-peak signal, mV	Shape of peak-to-peak signal
1	1990	190	two peaks per revolution, similar to chrysotile
2	1760	120	two peaks per revolution, similar to chrysotile
3	1940	180	two peaks per revolution, similar to chrysotile
4	2170	300	two peaks per revolution, similar to chrysotile
5	3960	1000	one peak per revolution approximating a sinusoid
6	2560	330	two peaks per revolution, similar to chrysotile
7	3280	750	two peaks per revolution, similar to chrysotile
8	2160	190	two peaks per revolution, similar to chrysotile
9	1720	310	two peaks per revolution, similar to chrysotile
10	1820	190	two peaks per revolution, similar to chrysotile

5.3 Results

Experiments were performed to determine the sensitivity of the technique for different types of asbestos. Three varieties were investigated, UICC crocidolite, UICC amosite, and purified Union-Carbide chrysotile. Differing volumes from stock dispersions and dilutions thereof were magnetically filtered to produce filter samples with a wide range of asbestos content. The results are presented in section 5.3.1.

The effect of the presence of non-asbestos particulate was examined by mixing a non-asbestos dispersion with an asbestos dispersion. It is reported in section 5.3.2

The technique was not as sensitive as desired for low particle concentrations. Consequently, methods to improve the sensitivity were investigated. These are discussed in section 5.3.3.

5.3.1 Detection Levels for Asbestos Fibers Dispersed in Double-Distilled Water

Samples were prepared by filtration employing a range of volumes of a stock dispersion of UICC crocidolite in double-distilled water. The procedure was repeated for both UICC amosite and Union-Carbide chrysotile. Scattered-light profiles were obtained for all of the samples. Figures 5.4, 5.5 and 5.6 show the scattered-light profiles for a filter-loading of about 15 ng/mm^2 for each of the three materials. It can be seen that, for this filter loading, there was a strong easily-detectable signal from the aligned fibers. When the filter loading was further reduced by a factor of 20 to 100, the profiles shown in Figs. 5.9, 5.10 and 5.11 were obtained. The peaks were still easily detectable at these reduced concentrations. This demonstrates that concentrations five times smaller are still measurable. Therefore, in the absence of major proportions of other particulate material, these results suggest that fiber concentrations of about 0.1 ng/mm^2 are detectable for all of the three varieties.

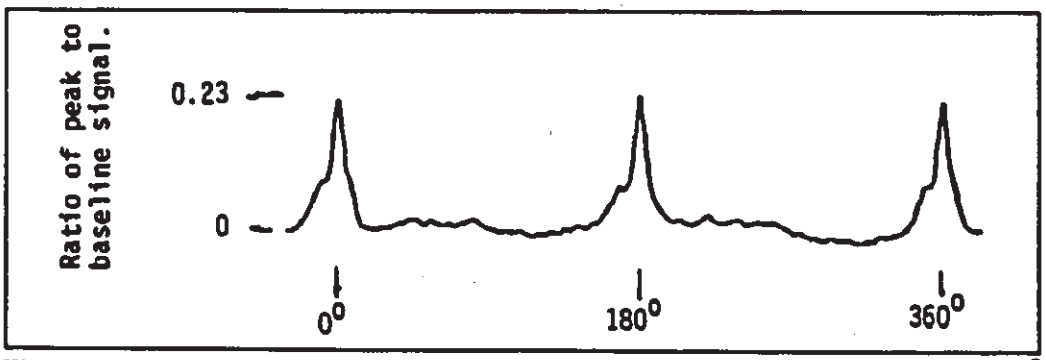

Figure 5.9 **UICC crocidolite scattered-light profile. Filter loading = 0.4 ng/mm^2 (mass loading corresponds to 850 fib/mm^2 of median length 0.6 μm).**

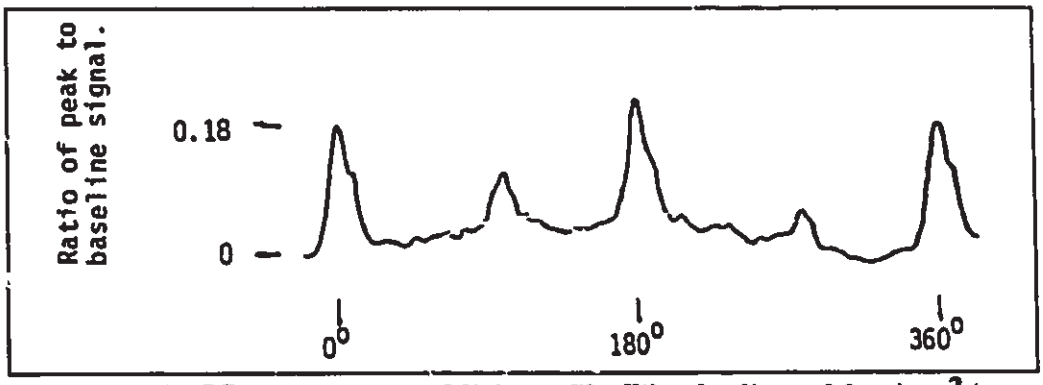

Figure 5.110 UICC amosite scattered-light profile. Filter loading = 0.2 ng/mm^2 (mass loading corresponds to 280 fib/mm^2 of median length 1.0 μm.)

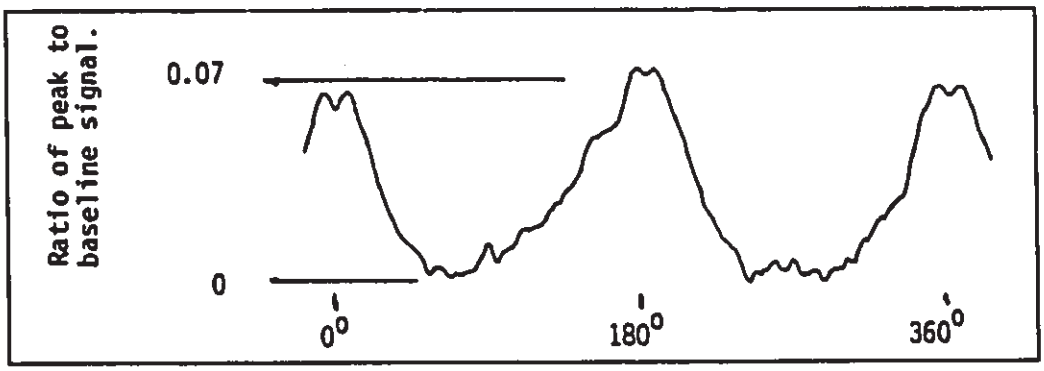

Figure 5.11 Union-Carbide chrysotile scattered-light profile. Filter loading = 0.6 ng/mm^2 (mass loading corresponds to 10^5 fib/mm^2 of median length 1.0 μm).

The peak areas for all of the scattered-light profiles obtained from each material were measured using a planimeter, and the areas expressed in arbitrary units were plotted as functions of mass concentrations and numerical fiber-concentrations. The graphs showing the dependence of the scattered light signal on quantity of fiber (filter loading) are presented in Figs. 5.12 to 5.15.

In the results for crocidolite shown in Fig. 5.12, it can be seen that for mass concentrations below 0.1 ng/mm^2, measurements on different samples with the same filter loading range over a factor of 8. At these concentrations, the peaks from the fibers are sometimes difficult to separate from the noise. Therefore a concentration of 0.1 ng/mm^2 is the minimum detection-level for crocidolite. Detailed detection-level studies were not

performed for amosite, but the patterns shown in Figs. 5.13 and 5.14 are similar to that obtained from crocidolite. The data for chrysotile, shown in Fig. 5.15, indicate that at low concentrations, peaks are present which are unrelated to the presence of chrysotile. Accordingly, chrysotile scattering-peaks, similar to those shown in Fig. 5.11, should be interpreted with considerable caution.

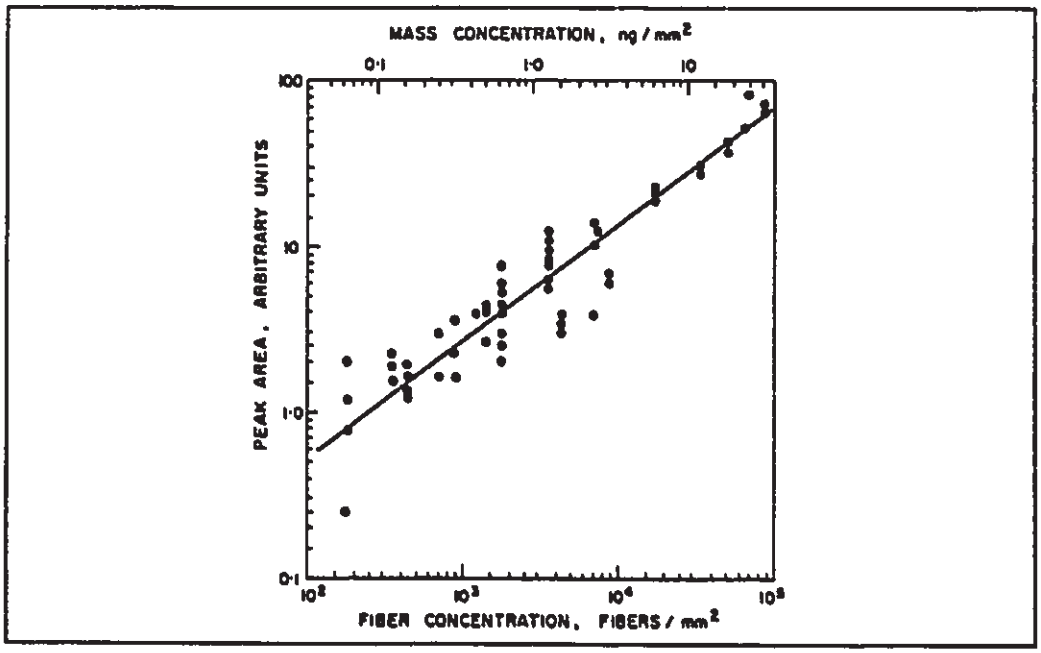

Figure 5.12 UICC crocidolite: area of P-fiber peaks versus mass and fiber concentration on the filter.

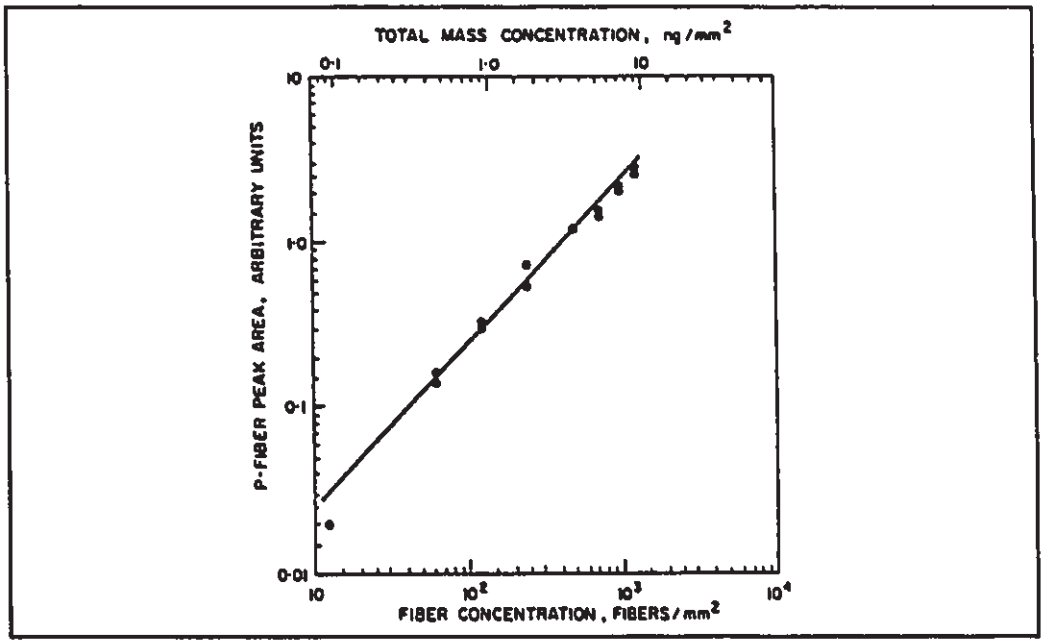

Figure 5.13 UICC amosite: area of P-fiber peaks versus mass and fiber concentration on the filter.

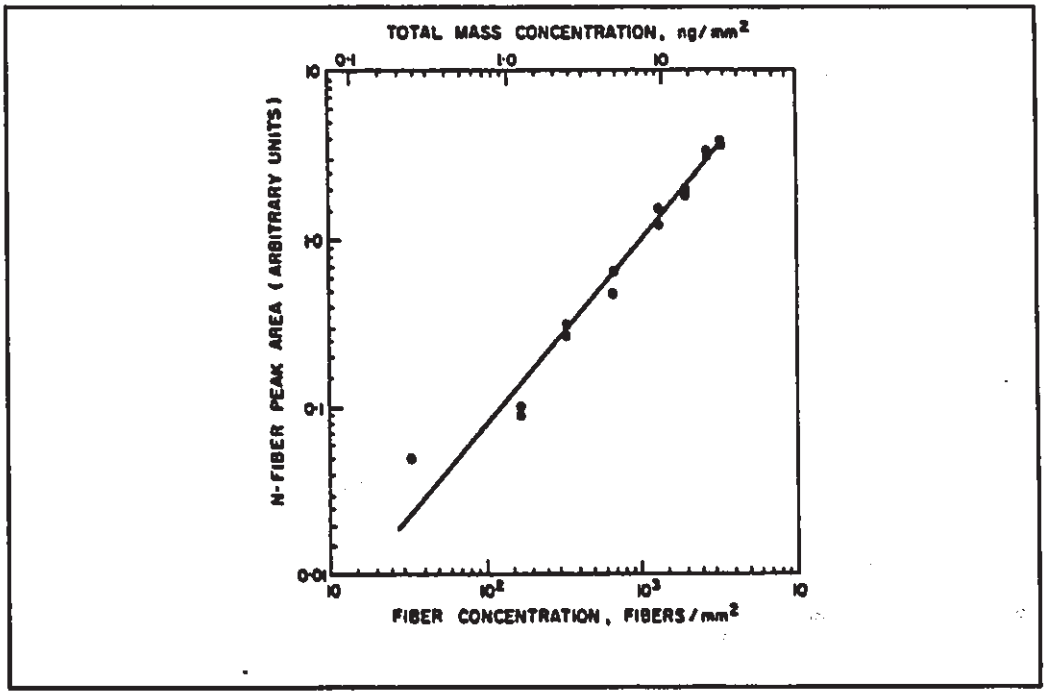

Figure 5.14 UICC amosite: area of N-fiber peaks versus mass and fiber concentration on the filter.

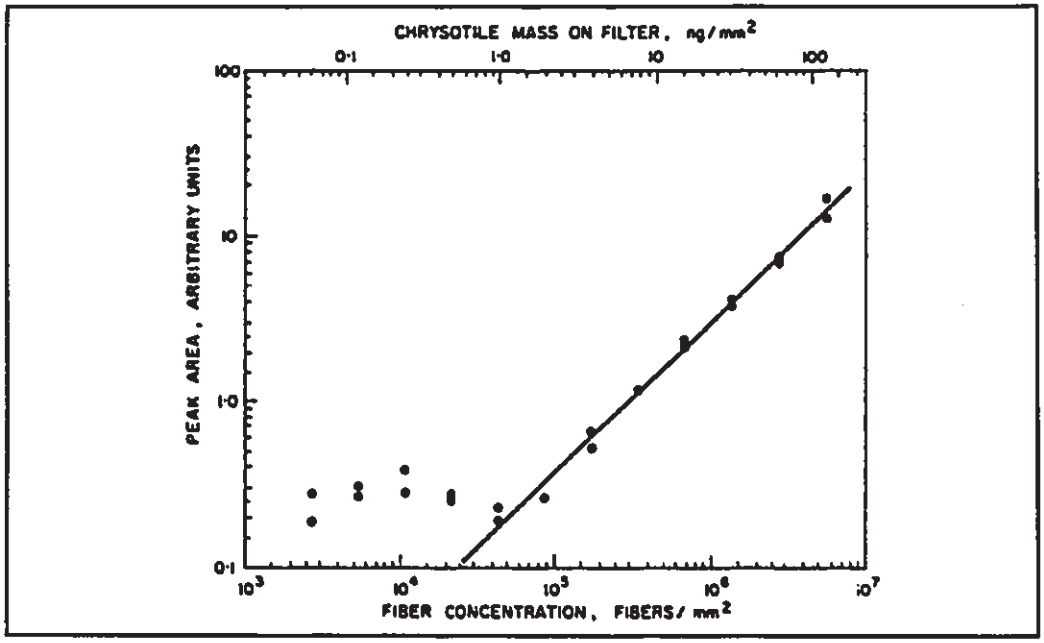

Figure 5.15 Union-Carbide chrysotile: area of P-fiber peaks versus mass and fiber concentration on the filter.

For fiber concentrations greater than approximately 10^5 fib/mm^2 (1.0 ng/mm^2) there appears to be a direct relationship with peak area. At concentrations below these values, the peak areas maintained an approximate constant value similar to that observed at 10^5 fib/mm^2, regardless of fiber concentration. It is thought that these are artifact peaks originating from residual structure in the collapsed filter, and that this residual structure defines a minimum detectable limit for these measurements. These results indicate that the method of filtering in a magnetic field, followed by collapsing of the Millipore filter, gives a detection limit for chrysotile in the order of 10^5 fib/mm^2 (1.0 ng/mm^2). Ten filter-samples prepared with a 10^5 fib/mm^2 loading of chrysotile further supported this value for the detection limit; only three samples yielded easily recognizable fiber-peaks.

5.3.2 Effects of Non-Fibrous Particulate

To investigate the effects of non-fibrous particulate, various volumes of municipal drinking water were mixed with dispersions of amosite. The resulting dispersions were then prepared for scattered-light measurements. Figure 5.16 shows the scattered-light

profile when the filter loading was approximately 50 ng/mm^2 of total insoluble solids and 1 ng/mm^2 of amosite. It was found that the only major effect of the nonfibrous particulate was to increase the value of the background intensity of the scattered light. The results suggest that, even in the presence of nonfibrous particulate, the minimum detection levels remain the same. This conclusion is reasonable in view of the fact that most of the intensity of the background scattered-light originates from the filter itself.

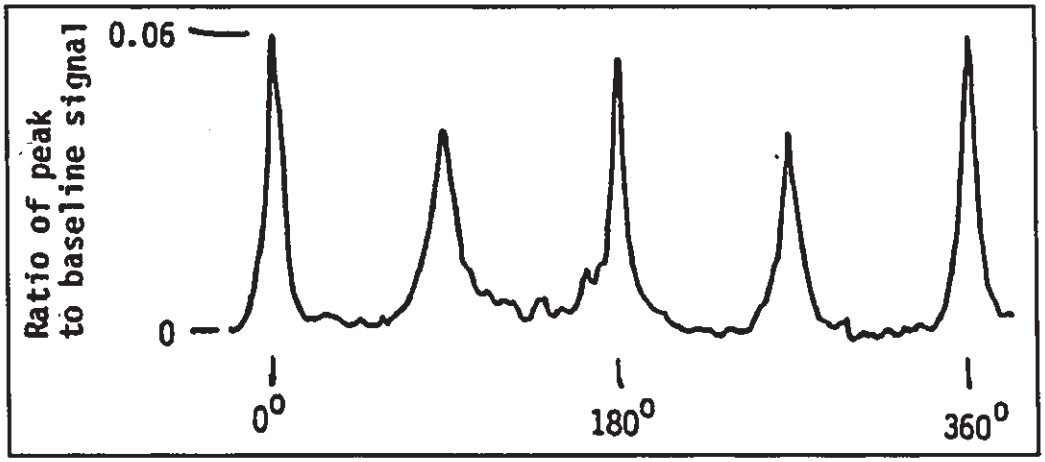

Figure 5.16 Scattered light profile showing peaks from amosite in municipal drinking water. Filter loading was 1 ng/mm^2 amosite and 50 ng/mm^2 total insoluble solids.

5.4 Signal Enhancement

The measurements made using crocidolite and chrysotile fibers indicated that the minimum detectable concentrations on filters were about 0.1 ng/mm^2 and 1.0 ng/mm^2, respectively. The US Environmental Protection Agency [Riis and Chatfield 1982] has suggested that an automated technique should be able to detect levels in the original dispersions as low as 1.0 ng/l. To achieve this low level for chrysotile, would require concentration of the chrysotile from 200 liters of water onto a filter with a 200 mm^2 active area. The presence of other particulate in such a large volume of water would probably degrade the detection-limit still further. Clearly, a significant improvement in the detection level of the fixed particle-technique is required before being used for water sample analysis.

The scattered light from a blank filter cannot be reduced below some minimum level. Therefore, alternative approaches are necessary to increase measurement sensitivity. These include enhancement of the scattered-light signal from the aligned fibers or the removal of the scattering component coming from the filter substrate. Various approaches were taken and are discussed below.

5.4.1 Complete Dissolution of the Filter Medium

The scattered light from the filter background could be eliminated if the fiber orientations could be retained while the filter itself was dissolved or oxidized. A number of different techniques were investigated, all of which were based on extraction replication of the filter surface. A thick layer of silicon monoxide was deposited by vacuum evaporation in order to fix the fiber orientations. The filter was then placed on a glass slide and procedures such as solvent extraction or low-temperature ashing were used to remove the filter medium. All of these techniques failed to yield optically flat samples. Residual cracks and wrinkles in the thin film yielded large peaks in the scattered light unrelated to the presence of fibrous material. Accordingly, this approach was abandoned.

5.4.2 Use of Reflective Scattering Techniques

One way to avoid the limitation of detection-level imposed by the residual internal structure of the cleared membrane filter is to arrange the equipment so that reflective scattering from the filter surface is measured. In the early work on the magnetic-alignment technique, a capillary-pore filter (Nuclepore) was used to filter the fiber dispersion, after which a coating of gold was applied to the filter surface either by vacuum evaporation or by sputtering. The reflected scattered light intensity at an angle of about 30° from the optical axis was measured. Although strong signals from aligned fibers were obtained, reflective scattering was found to be very sensitive to imperfections on the filter surface. In particular, scratches on the filter surface were found to yield very large spurious peaks in the scattered light profiles.

The surface-imperfection problem was reduced by using a Millipore filter and collapsing the structure in the same way as for the forward-scattering technique. However, spurious peaks from many of the samples were still observed and, at that time, the technique was abandoned. At the improved detection levels already achieved by the forward-scattering technique, the spurious peaks associated with reflective scattering would present an even more serious obstacle to reliable measurements.

5.4.3 Radio-Frequency Plasma Etching of Filters

During collapse of the membrane filters by exposure to acetone vapor, many of the fibers are known to become totally embedded in the filter plastic. This reduces their contribution to the scattered-light signal. Fibers embedded in the filter can be brought to the surface by etching the sample in an r.f. plasma asher. In order to evaluate the potential of this procedure for signal enhancement, a set of filter samples, having a 3500 fib/mm^2 loading of aligned crocidolite fibers, was prepared. The scattered-light profile of each sample was measured. The samples were then exposed to different etching times ranging from one to eight minutes at an r.f. power level of 50 W, after which the scattered light profile of each was recorded again. The results are summarized in Table 5.3. For a two-minute etching time the peak height was found to increase by a factor of 2.2, which was the maximum improvement obtained. Further increase of etching time up to about 6 minutes resulted in a gradual reduction of peak height. After this time, there was a sudden drop to about 0.14 of the initial aligned-fiber peak. The background scattered light intensity was also found to increase with etching time. These results suggest that

(a) the optimum etching time was about 2 minutes,

(b) the increase in background intensity was due to development of structure on the filter surface, and

(c) the sudden loss of peak height may be due to detachment, loss or disturbance of fibers when the sample was excessively etched.

Table 5.3 The effect of r.f. plasma etching on aligned crocidolite-fiber samples

ETCHING TIME (min)	BEFORE ETCHING		AFTER ETCHING		CHANGE IN PEAK HEIGHT after/before
	Background signal, (V)	P-fiber peak height, (V)	Background signal, (V)	P-fiber peak height, (V)	
1.0	3.9	1.33	4.3	2.05	1.54
2.0	4.4	2.89	8.8	6.40	2.21
3.0	4.4	3.68	12.5	6.80	1.85
4.0	5.1	5.36	16.1	8.90	1.66
5.0	5.1	5.37	22.4	7.25	1.35
6.0	4.4	4.76	31.3	0.66	0.14
7.0	4.4	5.14	32.3	0.22	0.04
8.0	5.0	4.53	32.4	0.15	0.03

A similar experiment was performed with filters which had loadings of 10^5 fib/mm^2 of aligned chrysotile fibers. For an etching time of 1.5 minutes, the peak height was found to increase by a factor of 3.5, while the background intensity increased by a factor of 2. For longer etching times the peaks at 0° and 180° became unequal in height.

It is clear that some improvement in the scattered-light signal can be obtained using the plasma-etching technique. However, there is not a significant potential to improve the detection level to acceptable values.

5.4.4 Shadowing of Particulate by Vacuum Deposition of Opaque Films

The angular asymmetry of the scattered-light intensity from cleared membrane filters, which often has the appearance of chrysotile scattered-light profiles, is responsible for establishing the minimum detection limit. The contribution from the substrate can be greatly reduced by application of an opaque layer on the filter, except in those areas occupied by particles. An opaque layer (e.g. gold or aluminum) can be applied by vacuum deposition, either normal to the filter surface or at some other angle. If the deposition is applied at normal incidence to the filter surface, the layer will be continuous except at the edges of the particles; if applied at some other angle, uncoated areas will occur on the filter surface where it is shielded from the evaporation source by the particles. It was

thought that large improvements in the detection limit might be achieved by correlating the direction of deposition of the opaque film with the alignment direction expected for the fibers.

Experiments were conducted with opaque evaporated gold coatings. Some filter samples were coated at normal incidence, and others were coated at 45° incidence. The gold evaporation source was arranged so that the P-fibers were oriented with their lengths perpendicular to the evaporation direction. This geometry caused the P-fibers to produce uncoated slits on the filter surface, the dimensions of which were roughly the same as those of the fibers, while the rest of the filter was rendered opaque.

The results obtained from experiments conducted using aligned-fiber samples of crocidolite and chrysotile are shown in Table 5.4. Significant improvements in peak-to-background ratios were obtained, but it was found that signals generated from nonfibrous particulate were similar to those from fibrous material. The technique was abandoned in favor of the dynamic-particle technique described in Chapter 6. However, it is possible that further investigation of the technique, using two evaporation directions and signal processing, could eliminate the signals from the non-fibrous components.

Table 5.4 Improvements in the peak-to-background signal produced by gold coating.

Sample treatment	Peak to background ratio before	after	Ratio of improvement
Crocidolite: gold coated at normal incidence	0.32	2.14	6.7
Crocidolite: gold coated at 45° incidence	0.54	4.00	7.4
Chrysotile: gold coated at normal incidence	0.22	1.76	8.0

5.5 Evaluation

The best sensitivity achieved using the fixed-particle technique was for a filter loading of about 0.1 ng/mm^2 for crocidolite and 1 ng/mm^2 for chrysotile. If a 200 mm^2 active area is used, the minimum total filter loadings detectable are 20 ng and 200 ng, respectively. The EPA has suggested a desired detection level of 1 ng/l of asbestos in water [Riis and Chatfield 1982]. For chrysotile, concentration of the fibers from 200 liters of water would be needed to achieve this. Even assuming a further order-of-magnitude improvement is possible by using the gold coating technique (section 5.4.4), a desirable detection level approaching 1 ng/l cannot be achieved. Although the fixed-particle technique is more sensitive to crocidolite, detection of 1 ng/l initial water concentrations still would require an unreasonable filtration volume.

Chapter 6
The Dynamic-Particle Method

In the dynamic-particle method, asbestos fibers are suspended in a liquid during the measurement. A magnetic-field rotates around the liquid suspension, and the fibers also rotate, maintaining their orientation with the field direction. The forward-scattered light-intensity is measured at a fixed angle to the optical axis while the field is rotating. The variation in scattered light intensity is only from the particulate that follows the magnetic field. This means that the problems associated with variability of the light scattered by the rotating filter (in the fixed-particle technique) are eliminated because only the fibers themselves rotate. Furthermore, the scattering from individual particles, which are not affected by the magnetic field, is random. These move under Brownian motion only and therefore contribute only to the background signal. This technique was found to have a much better sensitivity than the fixed-particle technique and therefore was chosen as the recommended technique for asbestos measurement.

6.1 Equipment Design

The experimental setup is shown schematically in Fig. 6.1. The fiber suspension is contained in a cylindrical fused-silica spectrophotometer-cell (5 ml volume and 2 cm path-length). The magnet has a field strength of 0.9 T across a gap of 2.5 cm, and can be rotated about the optic axis at speeds of approximately one to 60 revolutions per minute. No suitable magnet system was available commercially, therefore, it was necessary to construct the magnet assembly and the rotation mechanism. In this system, the signal from the photomultiplier detector is fed to a microcomputer, and the scattered-light profile is displayed on the computer video screen. The use of a computer allows much more flexibility when measuring the scattered light and analyzing the patterns produced. In particular, scattered-light

intensity-data can be accumulated over a number of revolutions of the magnet, thus permitting averaging out of the effects of random scattering from particulate other than fibers.

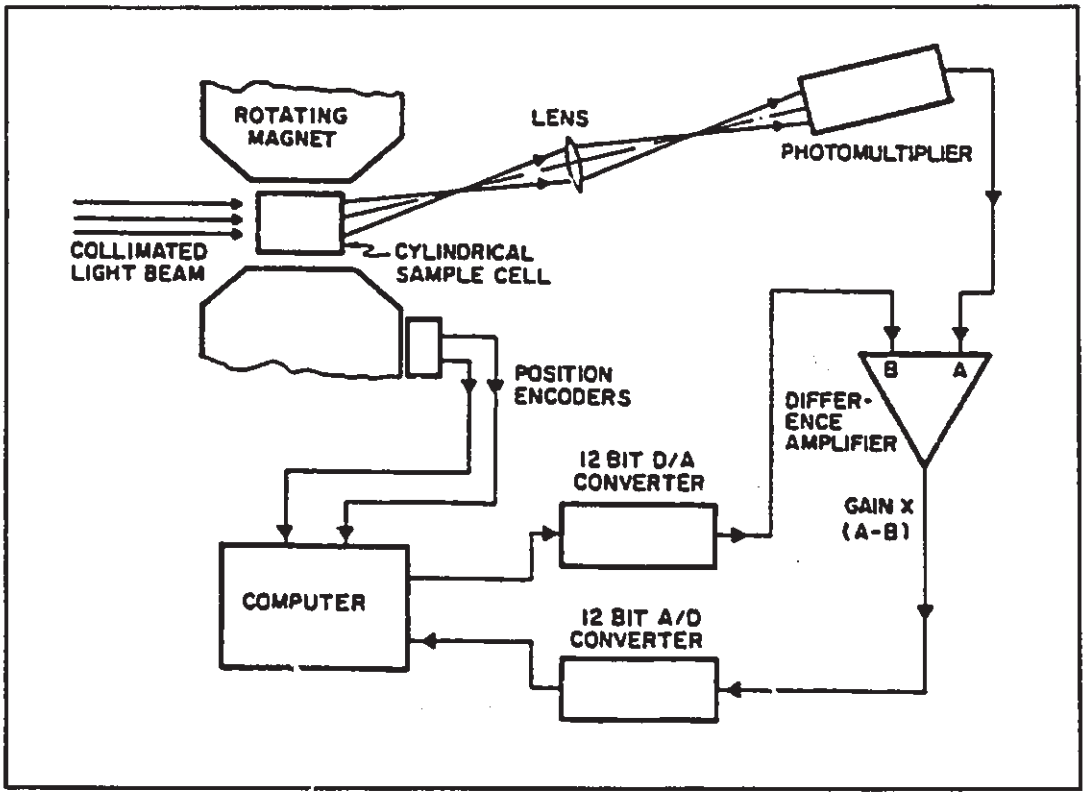

Figure 6.1 Schematic of equipment used for analysis of light scattered from magnetically-aligned fibers in liquid suspension.

The experimental system is shown in Fig. 6.2. The instantaneous position of the magnet is detected by two optical encoders, one to synchronize the data acquisition with the field orientation, and the other to tell the computer the instantaneous position of the magnet. There are 212 divisions within a single revolution of the position encoder and therefore the data is gathered in a 212-element array. The sample-loading mechanism consists of the hollow cannon-shaped device shown in Fig. 6.3, which holds the sample cell on the end. The cannon device slides horizontally on an optical rail allowing the sample to be placed between the poles of the magnet. The incident light beam passes down the axis of the hollow tube.

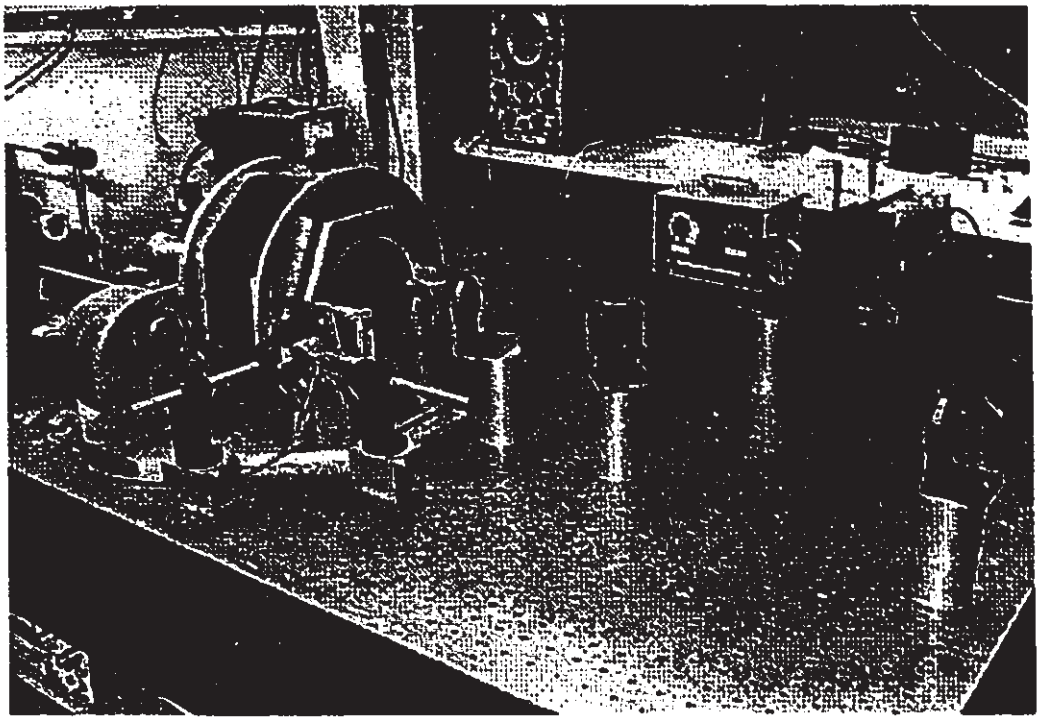

Figure 6.2 Experimental setup for the dynamic-particle system.

The operating procedure for the equipment is very simple. The liquid sample is first loaded in the system and positioned between the poles of the magnet, which is then made to rotate. The computer determines the angular velocity by timing one revolution. The intensity of the scattered light is measured at each of the 212 positions within one revolution. The average value of the signal (for the 212 positions) is used to adjust the gain of a difference amplifier, so that peaks are amplified to between 1 - 5 V. The output of the difference-amplifier, at each of the 212 positions for a single rotation, is then recorded. Data from a specified number of revolutions of the magnet are accumulated and averaged. The scattered light profile can then be displayed on a video terminal or sent to a plotter.

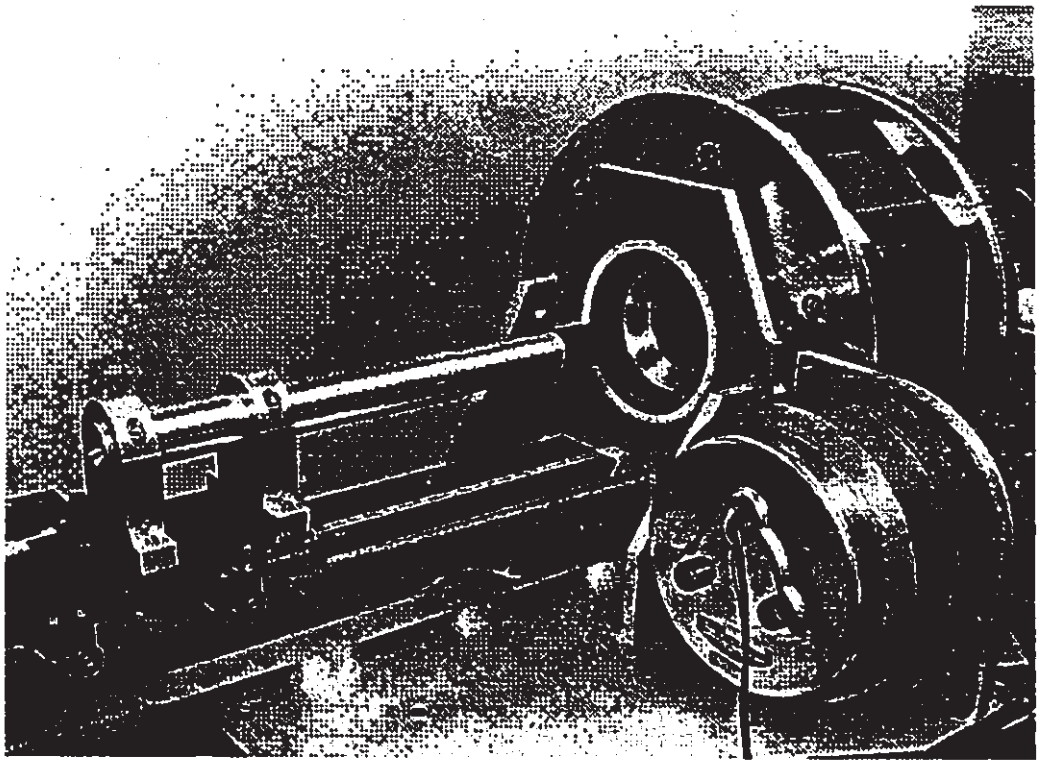

Figure 6.3 Sample loading mechanism.

6.2 Sample Preparation

Usually, the fiber dispersion in water is placed in the spectrophotometer cell and measured directly. However, when fiber concentrations are low, either nonselective or selective preconcentration may be necessary (see Timbrell [1977], and, Riis and Chatfield [1982]).

6.3 Measurements and Results

It was found that there are three types of particulate which are relevant to the measurement technique:

(a) fibers which align with and rotate with the magnetic field,

(b) randomly shaped particles which rotate with the magnetic field, and

(c) particles (fibers or randomly shaped) which do not respond to the magnetic field.

The fibers in category (a) produce scattered-light profiles which have peaks. At high magnet-rotation rates, fibers may lag behind the orientation they would assume in a stationary field. Category (b) particles always produce broad scattered-light peaks corresponding to alignment at 45°. Surprisingly, glass particles fall into this category. Category (c) particles simply contribute to a uniform background scattered-light signal. Some particles of (b) and (c) are usually present in all samples, and certainly are present in environmental water samples.

The scattered-light profiles obtained for three varieties of asbestos were examined to confirm that the dynamic fiber technique would produce data comparable with that from the filtration method. Figures 6.4, 6.5 and 6.6 show the profiles for UICC crocidolite, UICC amosite and Union-Carbide chrysotile respectively. Although the curves for the two amphibole varieties were similar to those obtained from the filtration method, the chrysotile peaks were observed to lag behind the magnetic field by about 10° under the conditions of the measurement.

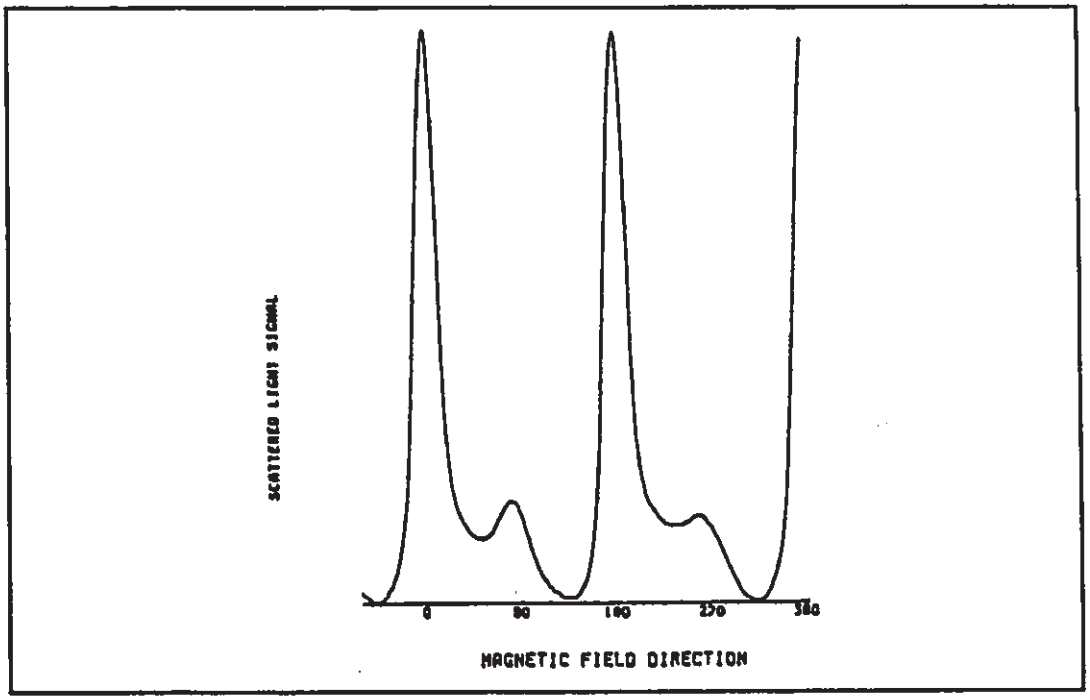

Figure 6.4 UICC crocidolite scattered-light profile.

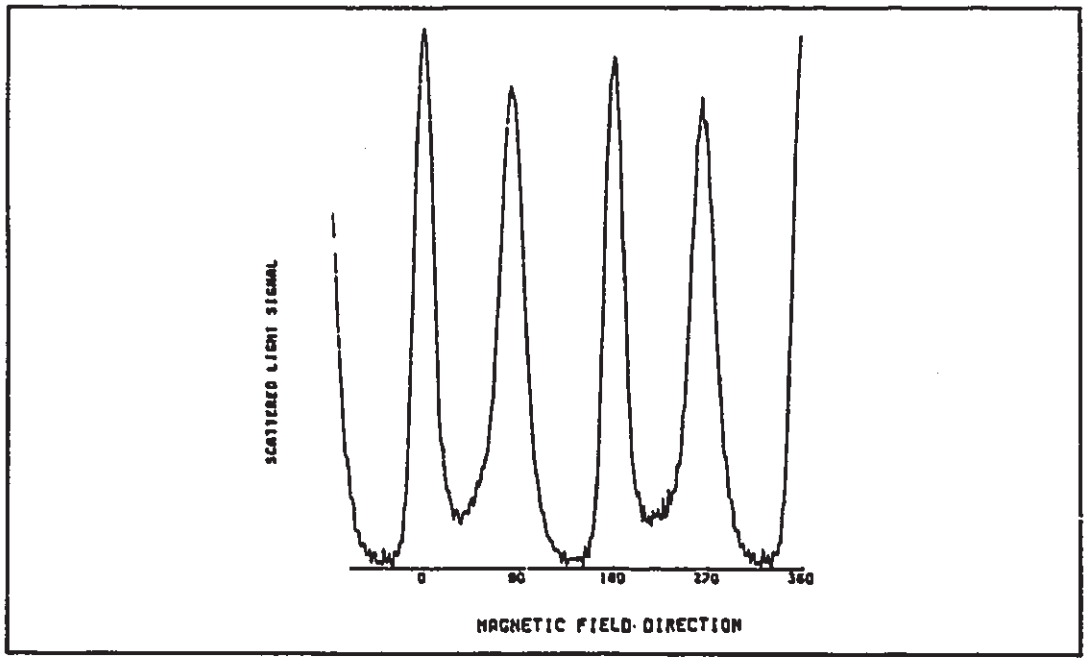

Figure 6.5 UICC amosite scattered-light profile.

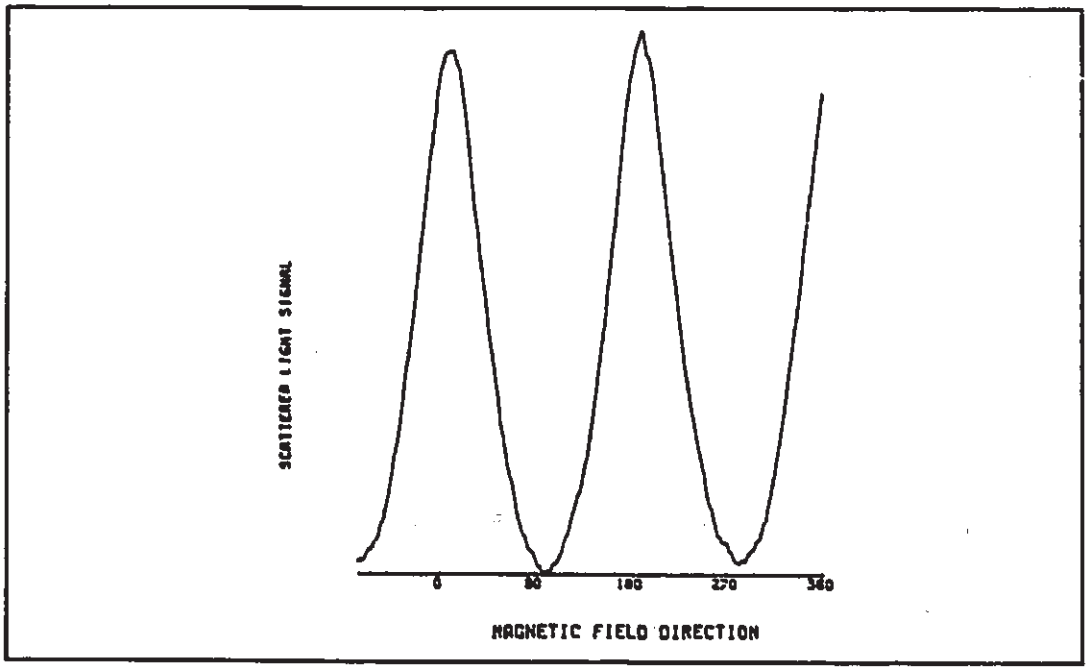

Figure 6.6 Union-Carbide chrysotile scattered-light profile.

6.3.1 Measurement of Blank Samples

One of the most challenging problems in the use of this equipment was to obtain a satisfactory blank profile. The system is extremely sensitive to suspended particulate in the sample, and it was found that two effects initially prevented achievement of a flat profile which did not contain scattered-light peaks.

The first effect was the presence of a sinusoidal signal displaying one cycle per revolution of the magnet. To investigate this effect, a source of scattered light which did not vary with magnet rotation was required. This was conveniently arranged by positioning a thin sheet of polyethylene in place of the spectrophotometer cell. It was found that variations in the stray magnetic-field during rotation of the magnet was altering the gain of the photomultiplier. The effect could not be eliminated, but was minimized by a combination of magnetic shielding and re-positioning of the photomultiplier. At high values of amplifier gain, it was found that the baseline of the signal still displayed a slight sinusoidal variation, which could then be removed by profile subtraction to leave only the relevant signal.

The second effect was a consequence of the inability to produce absolutely particle-free water. The only water suitable for preparation of low background samples was found to be water double-distilled in glass, with precautions being taken not to disturb ground glass joints during the distillation. Filtered water was in no way satisfactory, since in the context of these measurements filtration merely replaces one kind of particulate with another which originates from the downstream surfaces of both the filter and the filtration equipment. For the low-background work, double-distilled water (using a Corning Mega-Pure^{R} still) has been found satisfactory. However, the distillate must be collected directly in borosilicate-glass bottles having plastic screw-caps with Teflon liners.

To obtain a blank scattered-light profile, the "particle-free" double-distilled water must be handled only in a laminar flow hood. As many as ten successive washings of the cell may be necessary before a sufficiently low level of particulate contamination is achieved. Ultrasonic treatment should be avoided, since this tends to generate particulate.

The background effects can be subtracted from the initial scattered-light profiles to determine the contribution from the asbestos fibers alone.

6.3.2 Measurement of Detection Levels

The variation of the scattered-light signal with fiber concentration, and the detection limits of the apparatus, were investigated using dispersions of UICC crocidolite and Union-Carbide chrysotile. The experiments were performed by preparing a series of fiber dispersions from serum bottles of standard fiber suspensions. The serum bottles had concentrations of 140 mfl (million fibers per liter) for crocidolite and 200 mfl for chrysotile. Dispersions of lower concentrations were prepared by successive dilution of portions of the initial dispersion with "particle-free" water. The concentrations were spaced "logarithmically" using intervals of a factor of 3, from the serum bottle concentration down to approximately 0.2 mfl. The spectrophotometer cell was loaded with each dispersion in turn, starting with the lowest concentration and working upwards to avoid cross-contamination. The scattered light profile of each dispersion was measured for 10 to 20 revolutions at a magnet speed of 10 RPM for crocidolite, and for 5 revolutions at 1 RPM for chrysotile. Figures 6.7 and 6.8 illustrate the variation in scattered light signal with fiber concentration.

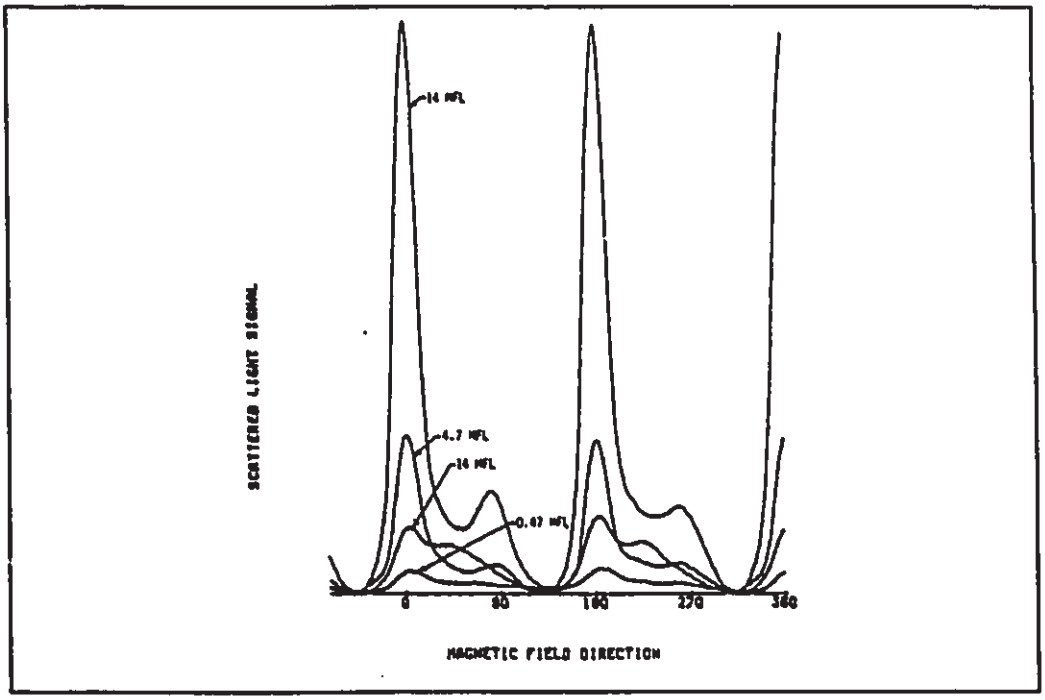

Figure 6.7 **UICC crocidolite scattered-light profiles for decreasing fiber-concentrations.**

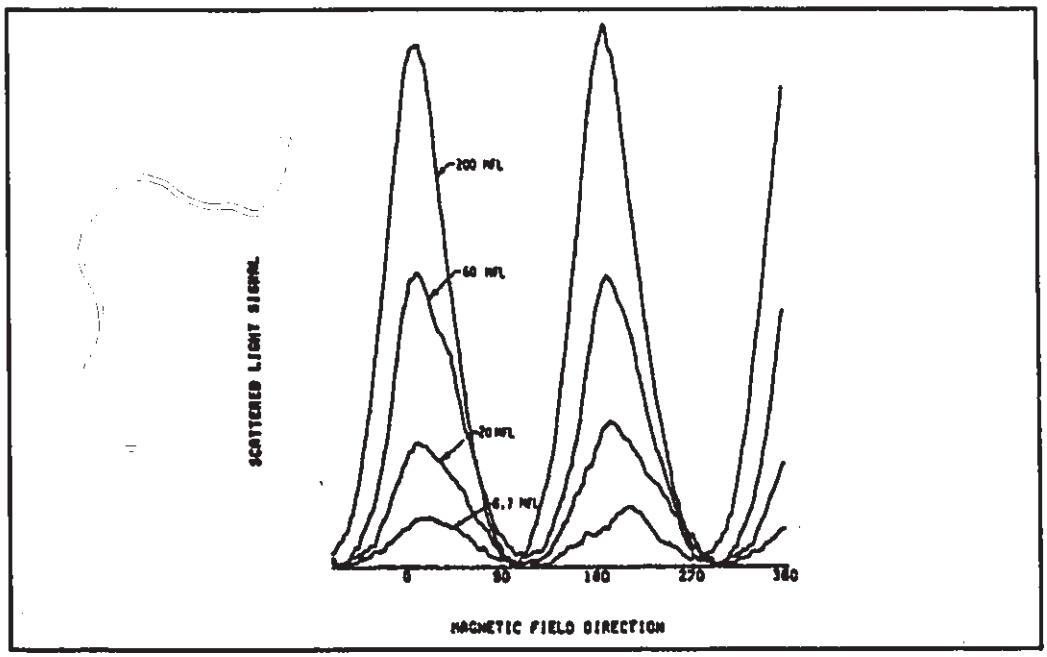

Figure 6.8 **Union-Carbide chrysotile scattered-light profiles for decreasing fiber concentrations.**

The variation of peak area with fiber concentration is shown in Fig. 6.9 for crocidolite and in Fig. 6.10 for chrysotile. (Background effects were subtracted.) The detection level was found to be about 0.5 mfl for crocidolite, and about 5 mfl for chrysotile. These detection levels, which apply to the fiber dispersion in the spectrophotometer cell, correspond to mass-concentration detection-levels of about 180 ng/l and 30 ng/l for crocidolite and chrysotile, respectively.

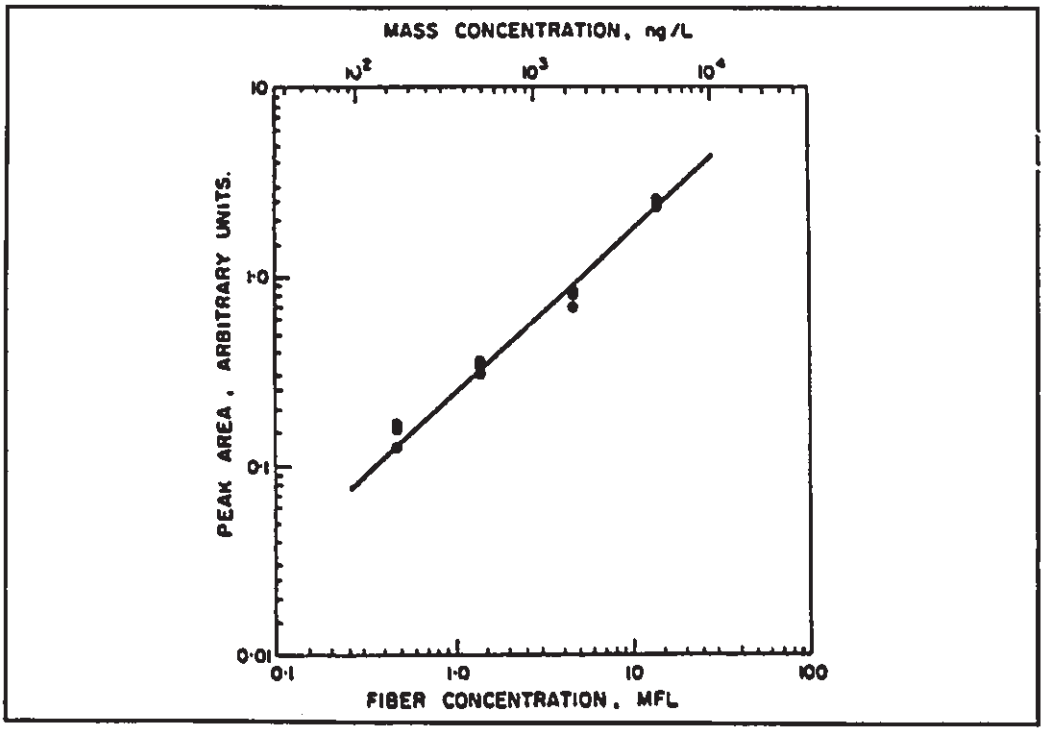

Figure 6.9 Variation of peak area with fiber concentration for UICC crocidolite.

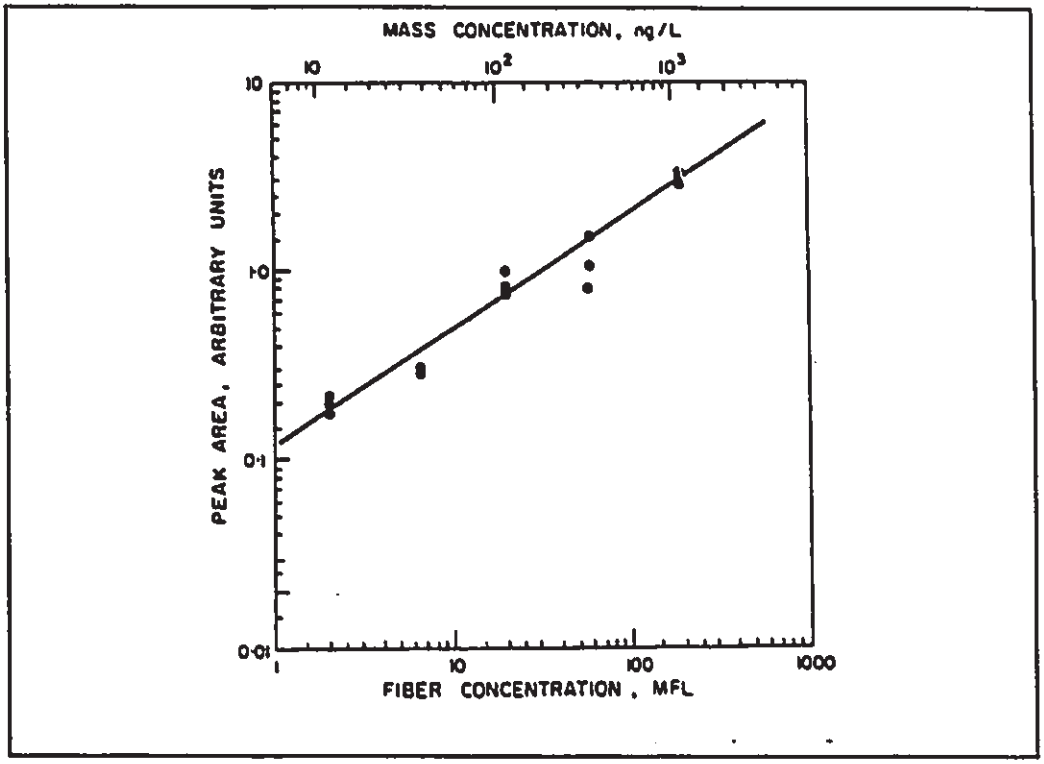

Figure 6.10 Variation of peak area with fiber concentration for Union-Carbide chrysotile.

6.3.3 Effects of Nonfibrous Particulate

Nonfibrous particulate which does not respond to the magnetic field contributes only to the constant component of the background scattered-light signal. Other particulate which does respond can produce interesting effects as was demonstrated by borosilicate glass.

Figure 6.11 shows the profile obtained from borosilicate-glass particulate in water. This material rotates with the magnetic field and gives rise to broad peaks at 45° and 225°. This effect was not noticed when using the fixed-particle alignment-technique, probably because it was below the detection level of the method, and perhaps also because any preferred orientations of particles having random shapes would be disturbed when they contacted the filter.

The origin of the peaks has not been fully investigated, but can be explained if the particles adopt orientations such that their longest dimensions are parallel or normal to the magnetic-field direction. The facets of the particles scatter light preferentially throughout a broad angle, centered on 45° to the magnetic-field direction. The peaks occur midway between asbestos fiber peaks, and therefore, their effect could be subtracted from the initial signal to leave the peaks due to fibers.

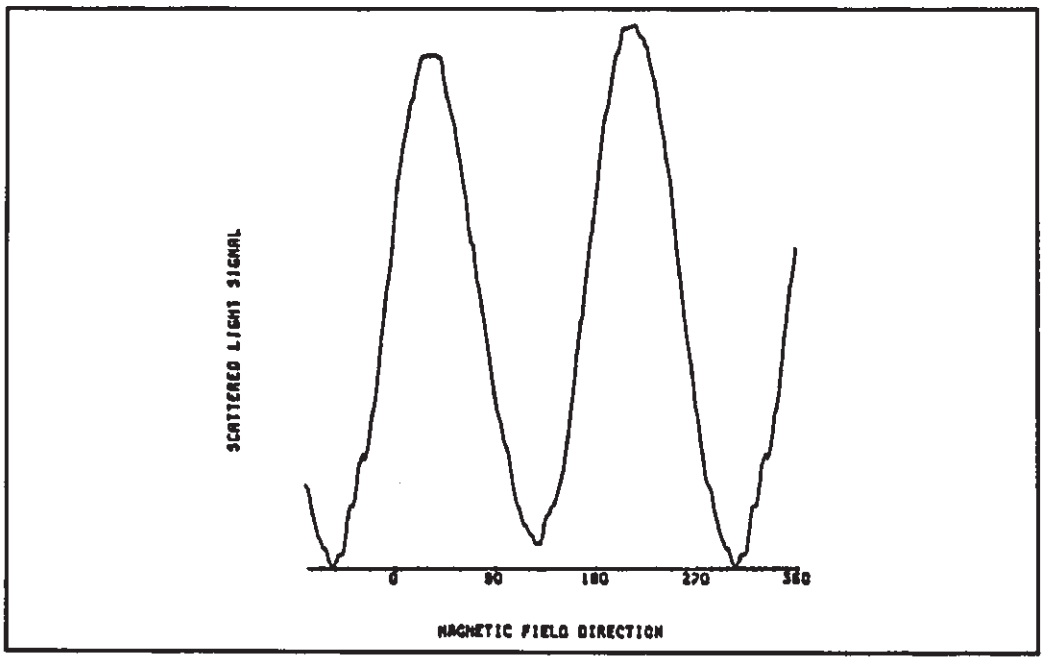

Figure 6.11 Scattered-light profile of borosilicate-glass particle suspension.

6.3.4 Viscous Drag

The scattered-light profile changes shape when the rotation-rate of the magnetic field is varied. Figure 6.12 illustrates this effect. An increase in the rotation rate causes a decrease in the peak height. In addition, a phase lag of the scattered-light peaks is visible at the higher rotation rates. These effects were thought to be due to viscous drag as the fibers rotate in the fluid and led to the investigation described in Chapter 4. Increased drag would lead to increased phase lags. Fibers, for which the drag-torque was greater

than the magnetic torque, would no longer be able to maintain their alignment. These fibers would no longer contribute to the scattered-light peaks, leading to the shrinking of the scattered-light profile at higher rotation-rates.

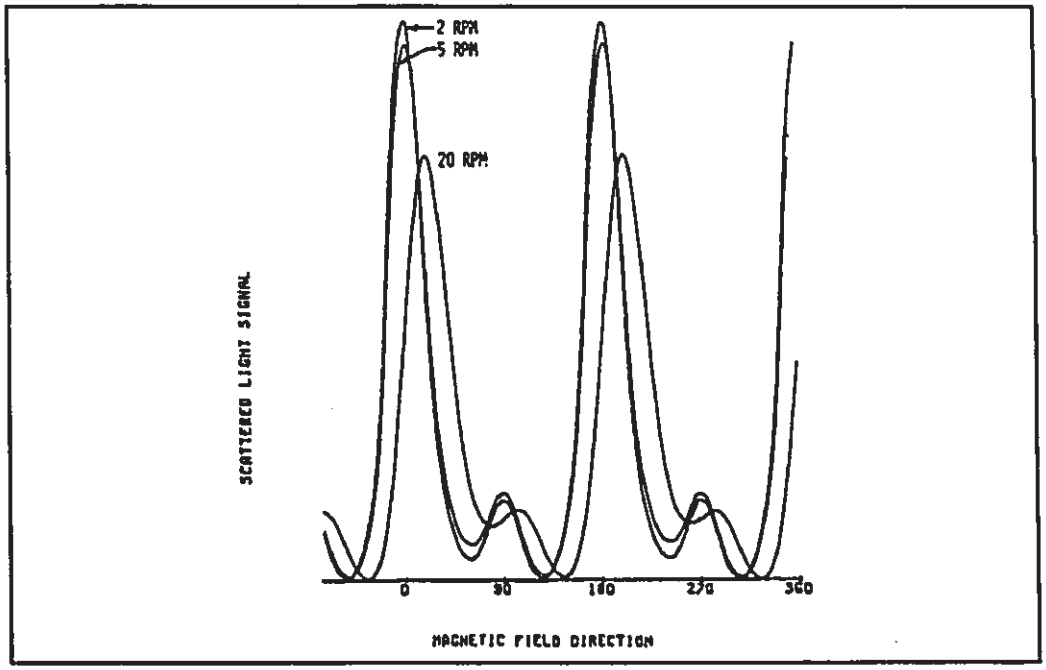

Figure 6.12 Variation of the scattered-light profile with magnetic field rotation-rate.

6.4 Evaluation of the Technique

Chapter 5 described the fixed-particle technique. It was ultimately abandoned in favour of the dynamic-particle technique. A detailed comparison of the two techniques justifying this decision is given below.

6.4.1 Measured Detection Limits

6.4.1.1 Fixed-Particle Method

The detection limit of the fixed-particle method was determined by using aqueous dispersions of asbestos with known concentrations, which were determined by TEM (transmission electron-microscope) analysis. Differing volumes were magnetically

filtered, and samples were prepared and subsequently examined. The results of such studies are shown in Figs. 5.12 and 5.15 for crocidolite and chrysotile, respectively. For crocidolite, the detection limit is approximately 300 fib/mm^2 (0.1 ng/mm^2). At concentrations below this, samples having the same particle loading produced scattering peaks that ranged over a factor of 8. The chrysotile results are particularly interesting. The detection limit is approximately 100,000 fib/mm^2 (1.0 ng/mm^2). At levels below this, chrysotile-type peaks are observed that are unrelated to the chrysotile filter-loading. Measurements on blank filters indicate that low-level chrysotile-type peaks result from the filter structure. These blank filter peaks therefore set the detection limit for this method.

6.4.1.2 Dynamic-Particle Method

Studies of the scattered-light signal as a function of fiber concentration for crocidolite and chrysotile are shown in Figs. 6.9, and 6.10, respectively. The detection limit of the system was 0.5 mfl (million fibers per liter) for crocidolite and 5 mfl for chrysotile. These correspond to mass concentrations of 180 ng/l and 30 ng/l respectively. Fiber detection below these levels was limited by system noise.

6.4.2 Comparing Detection Limits

For use as an analytical technique, the measurements must relate directly to the actual fiber concentration present in the initial aqueous dispersion. The filter-loading of the fixed-particle method can be found using the filter collection-area and the filtration volume (typically 25 ml). A comparison of values calculated for the fixed-particle method with those measured for the dynamic-particle method is given in Table 6.1.

Both tables clearly indicate that the dynamic-particle method has significantly better sensitivity than the fixed-particle method. The primary reason is that the fibers in the fixed-particle technique are partially imbedded in the filter membrane. An additional influence on sensitivity is the residual structure of filters, which leads to erroneous peaks at low scattering-intensities.

Table 6.1 Detection limits based on volume concentrations.

method	crocidolite		chrysotile	
	fiber conc.	mass conc.	fiber conc.	mass conc.
fixed-particle	2.2 mfl	750 ng/l	750 mfl	7.5 μg/l
dynamic-particle	0.5 mfl	180 ng/l	5 mfl	30 ng/l

It is also useful to compare the number of fibers per cross-sectional area of the incident beam. This comparison is presented in Table 6.2.

Table 6.2 Detection limits based on particle concentration illuminated by the laser beam.

method	crocidolite		chrysotile	
	fiber conc.	mass conc.	fiber conc.	mass conc.
fixed-particle	300 fib/mm^2	0.1 ng/mm^2	10^5 fib/mm^2	1.0 ng/mm^2
dynamic-particle	10 fib/mm^2	3.6 pg/mm^2	100 fib/mm^2	0.6 pg/mm^2

Chrysotile fibers often have diameters that are less than the 0.22 μm pore-size of the filters used. This means that chrysotile fibers may become deeply embedded in the filter medium and upon collapsing would be surrounded by the filter medium instead of air, as illustrated in Fig. 6.13. The significance of fibers becoming embedded in the filter can be appreciated by inspection of the Rayleigh equation for light scattered by spheres. The Rayleigh scattering cross-section of a sphere is

$$C_{scat} = \frac{24\pi^3 V^2}{\lambda^4}\left(\frac{n^2-1}{n^2+2}\right)^2 , \qquad 6.1$$

where V is the volume of the sphere, λ is the wavelength of light, and n is the refractive index of the particle relative to the surrounding medium [Kerker 1968]. The term of interest in this equation is

$$\left(\frac{n^2-1}{n^2+2}\right)^2 . \qquad 6.2$$

For a particle with n=1.56 (chrysotile) surrounded by air, Eq. 6.2 has a value of 0.105. For the same particle, surrounded by a filter medium whose refractive index is 1.44, Eq. 6.2 has a value of 0.00299. Consequently, the scattering intensity is reduced by a factor of 35 when the particle becomes embedded in the filter. The reduction for a particle with a refractive index equal to that of crocidolite is a factor of 12.

Note that Rayleigh scattering calculations are valid only for particles smaller than approximately one tenth of a wavelength. Therefore values given above only provide a qualitative explanation as to why chrysotile, whose fibers embed easily in the filter, is difficult to detect at low concentrations using the fixed-particle technique.

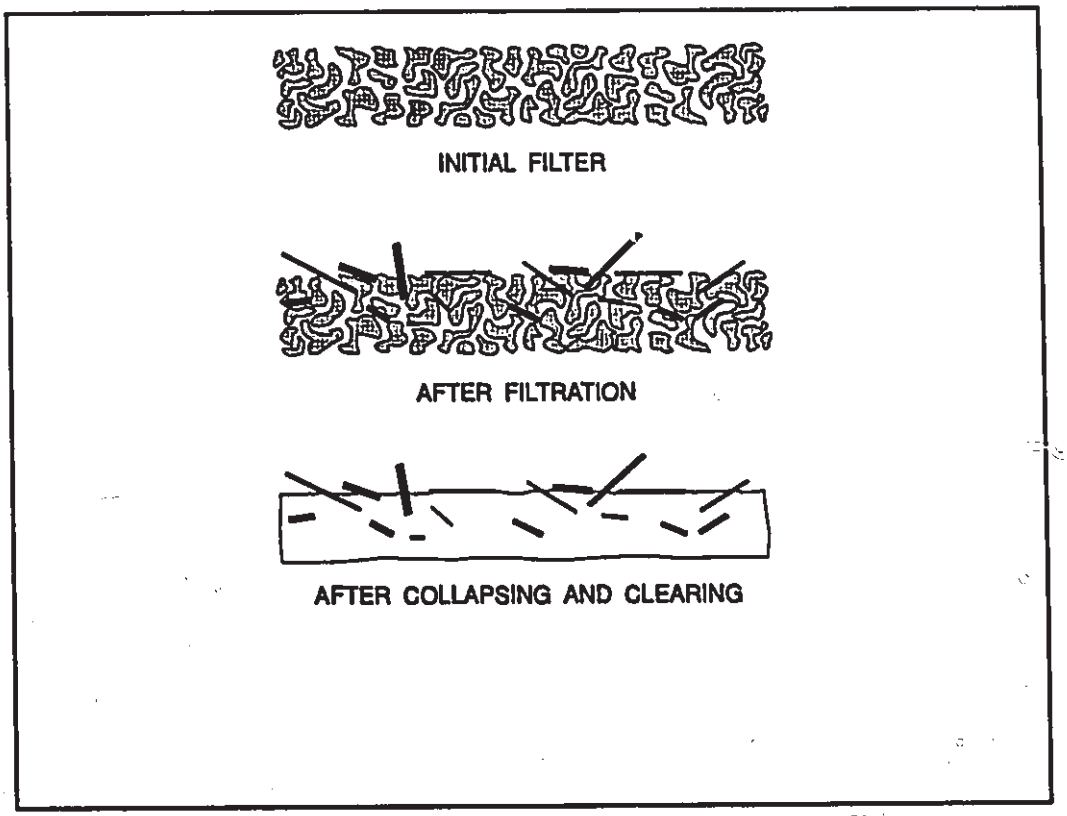

Figure 6.13 Fibers becoming embedded in the filter medium.

6.4.3 Discussion

The main advantage of the fixed-particle method is the relative simplicity of the instrumentation, composed of readily-available commercial components. Beyond this, the advantages start to disappear. The major disadvantage of the dynamic-particle method is the use of a custom-made rotating-magnet assembly. However the numerous advantages include the following:

1) Sample preparation is not required. The aqueous dispersions are placed directly into a spectrophotometer cell.

2) There is no filtration and consequently filter-clearing techniques are unnecessary.

3) Particles in suspension are free to move under motion. This allows scattering from randomly-moving particles to be averaged out over a number of full revolutions, improving the signal-to-noise ratio.

4) The viscous drag effects in the dynamic-particle technique provide information about fiber size that is unavailable with the fixed-particle technique.

Chapter 7
Investigating Viscous-Drag

Earlier measurements, using the dynamic-particle technique, demonstrated a phase-lag of the fibers as they rotated maintaining alignment with the magnetic field. As the rotation rate of the field increased, the phase-lag of the fibers increased. This effect had to be investigated further because it could prove to be a vital key in determining the size of asbestos fibers. A model was developed which confirmed that the phase-lag was a real effect which was related to the dimensions of the fiber. The next step was to test the accuracy of the model.

The only reliable way to test the model is to measure the phase-lag of individual fibers at different magnetic-field rotation-rates. The apparatus used in the dynamic-particle technique was designed for measuring the scattered-light from a collection of particles, and therefore is unsuitable. It became necessary to build a cost-effective experimental system. Chrysotile has a much-weaker magnetic-susceptibility than amphibole asbestos, and is generally of a smaller diameter. The substantially higher cost to make a system capable of observing chrysotile behavior, made it impractical to include chrysotile in this phase of the research.

The description of the experimental system built for this investigation is presented in Section 7.1. Experimental results are presented in Section 7.2 along with a discussion relating the results to the theoretical model described in Chapter 4.

7.1 Experimental System

The experimental system is depicted schematically in Fig. 7.1. The data acquisition system employs a video-cassette tape which permanently records the behavior of individual asbestos

fibers as seen through an optical microscope. In addition, each frame of the video recording has the magnetic-field position and the rotation-rate recorded as a number across the top of the frame.

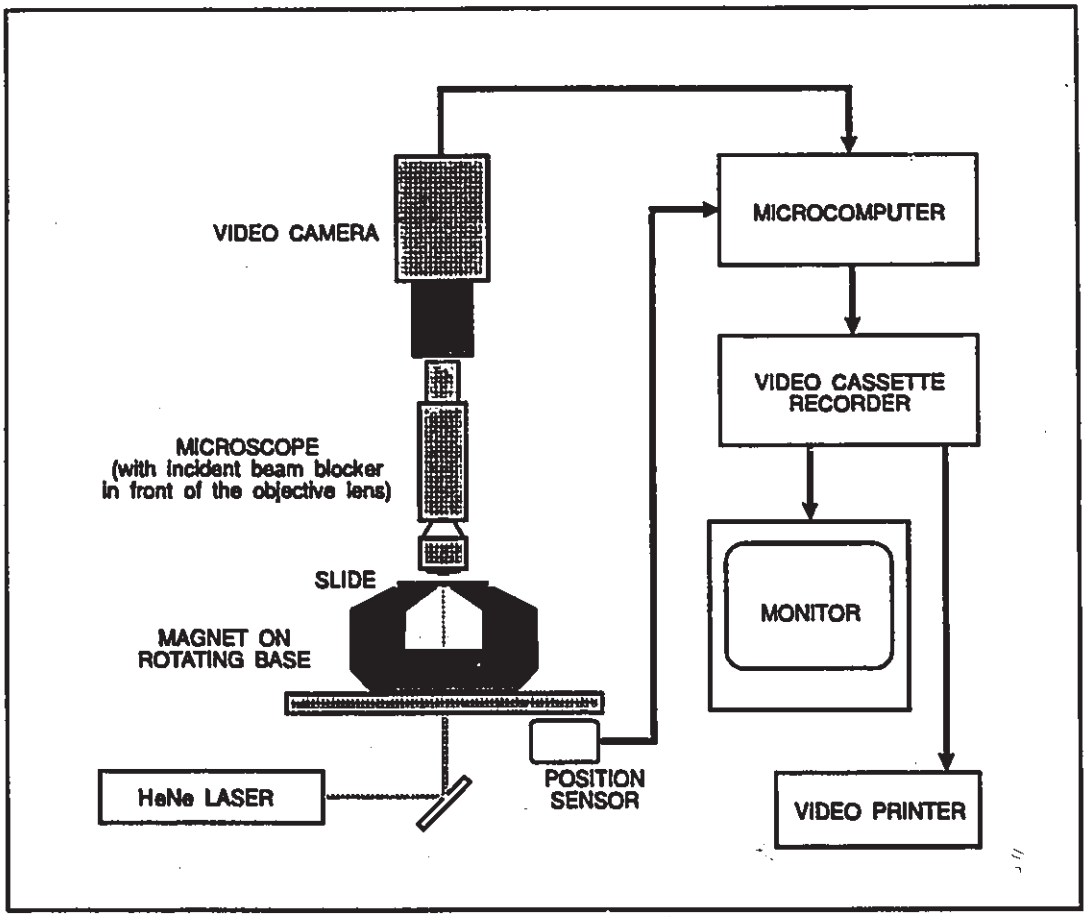

Figure 7.1 Schematic of system used for studying the behavior of individual asbestos fibers in rotating magnetic fields.

Figure 7.2 is a photograph showing the rotating-magnet and optical-microscope assembly. The HeNe laser is at the bottom left of the picture. A mirror under the assembly reflects the beam up along the optic axis of the microscope. The magnet and rotating base have independent adjustments allowing them to be positioned so that the center of the magnet rotates about the center of the optic axis. Each component of the system is discussed separately below.

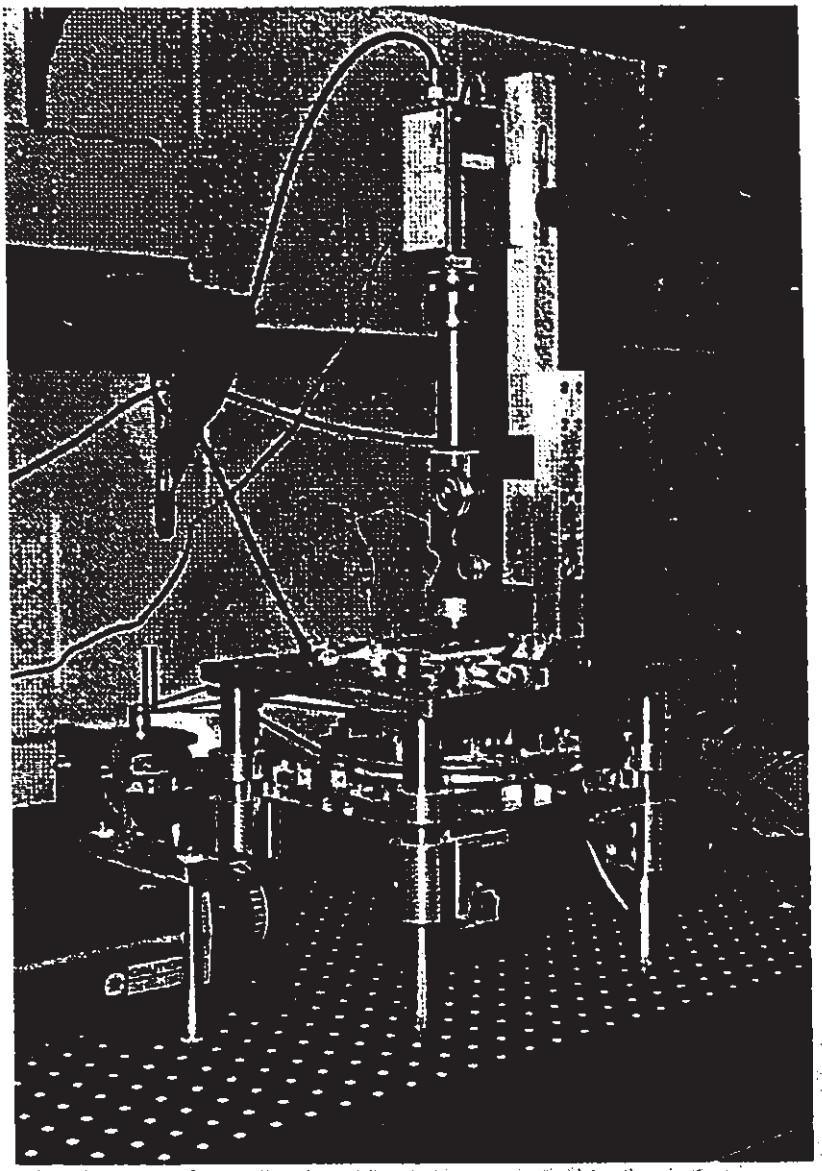

Figure 7.2 System used for studying the behavior of individual asbestos fibers in rotating magnetic fields.

The Light Source

The light source consisted of a 2 mW Helium-Neon laser operating at 633 nm. A variable attenuator in the beam path allowed the beam intensity to be adjusted.

The Optical Microscope

The optical microscope was constructed from various components. The coarse- and fine-focussing mechanisms were salvaged from an old microscope. A single 40x long-working-distance objective was used in conjunction with a 10x eyepiece. The use of a single high-power objective meant that initial focussing was tedious, but once done, focusing between samples could be accomplished using just the fine-focus adjustment. A small mirror was located in front of the objective, along the optic axis. This beam-blocker prevented the direct laser-beam from entering the microscope. In essence, the instrument was a dark-field microscope with bright images against a dark background, formed from scattered light from the objects.

Slide holder

Microscope-slides (50 mm by 75 mm) containing samples were placed on placed on an x-y positioner that had micrometer adjustments. This permitted scanning of the sample to find specific fibers to study.

The Rotating Magnet

The magnet was a permanent magnet with wedge-shaped poles located directly under the microscope slide. The pole tips, which were 4 mm wide and had a pole gap of 4 mm, provided a field of 0.47 T at the sample location. Variation of the magnetic-field strength along the optic/rotation axis is shown in Fig. 7.3. A Hall-effect probe, having a nominal sensor diameter of 1.8 mm, was used to measure the field. The sample is located in a region where the field-strength is an essentially linear function of distance. Therefore, deconvolution, of the smoothing effect caused by the probe-size, will produce the same answer as the measured value at the sample location.

The magnet was mounted on a turntable located under the microscope. The turntable was belt-driven by a variable speed motor. Adjustments were made to the magnet and turntable so that the center of the pole-gap remained on the optic axis while the magnet rotated.

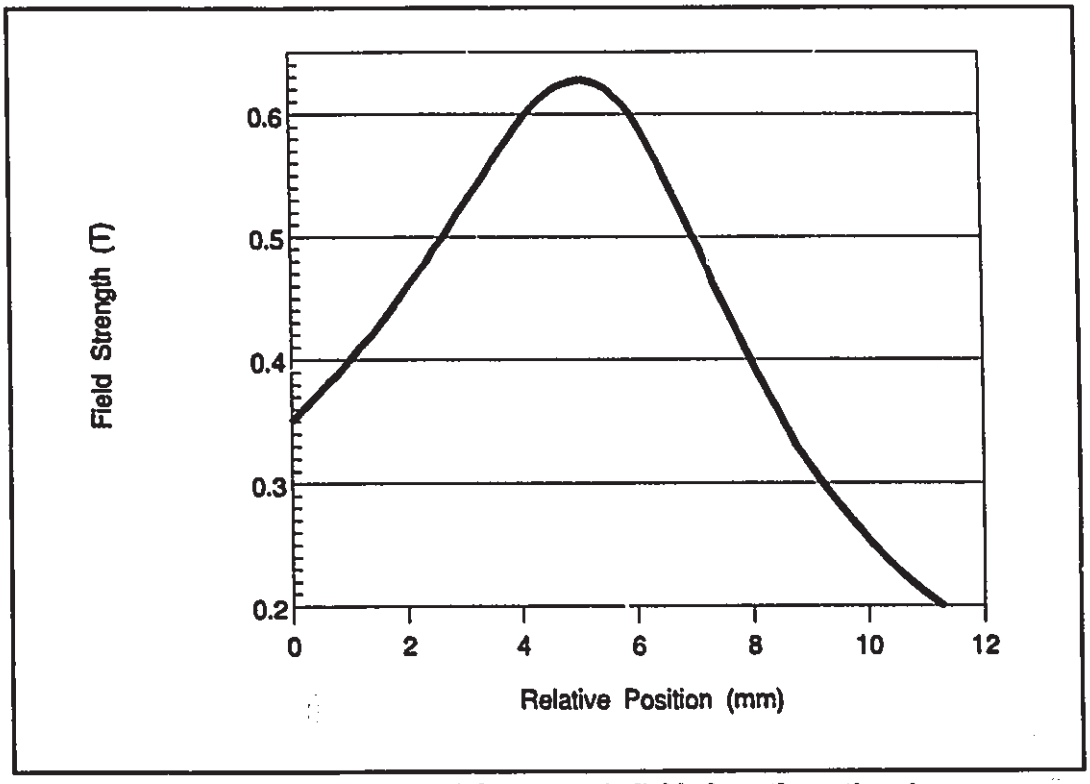

Figure 7.3 Variation of the magnetic field along the optic axis.

The Position Sensor

Two reflective-type optical sensors are used to detect reflective patterns on the underside of the turntable. The one sensor detects the start of a revolution; the other, the relative position of the magnet. Both sensors are interfaced to a microcomputer.

The Video Camera

The use of a video-camera (NEC TI-22A) permitted permanent recordings of fiber behavior to be made. Subsequent analysis of the recordings made the data-collection process a simple task.

The Microcomputer

The function of the microcomputer was to superimpose the magnetic field position and rotation rate on the video camera image. These parameters are determined using the signal from the optical sensors mounted under the magnet turntable. A position

accuracy of 1 deg. and a rotation-rate accuracy of 0.5 deg./s were achieved. The information was superimposed onto the video-camera image using a Bio-Electronics EGAOL^{R} circuit board mated with an EGA video card (in an IBM compatible microcomputer). This modified video-signal was then recorded.

The Video Cassette Recorder (VCR)

All experimental data was recorded on tape with a VCR (Sony model SL-HF900) and analyzed later. An extremely useful feature of the VCR was its ability to step through individual video frames. The VCR field rate (60/s) limits the rotation-speed at which fibers can be analyzed.

The Video Monitor

All viewing was done on the monitor. Initially, the slide samples were scanned to identify specific fibers for investigation. The same monitor was used to observe the recorded data and to measure the phase-lags from the VCR.

The Video Printer

The video printer (Tektronix HC01) prints individual video fields. These images are particularly important for making phase-lag measurements, and for determining fiber dimension. Figures 7.5 to 7.9 are examples of the printer output.

7.1.1 Procedure

The major effort in this phase of the research was the construction of the experimental system. The experimental procedure is straightforward, although it is somewhat tedious to scan across a sample to locate fibers suitable for study. The details of the procedure are as follows.

1) A drop of the aqueous asbestos dispersion is placed on the center of a clean 50 mm by 75 mm microscope slide.

2) A coverslip is placed over the sample and the slide is positioned on the microscope stage.

3) The image is focussed, and then a visual scan is made across the sample to locate fibers rotating in the magnetic-field freely.

4) Once a suitable fiber has been found, VCR recording is begun. The rotation-rate is adjusted to a range of different speeds, allowing sufficient time to reach equilibrium at each speed. Sufficient data is recorded at equilibrium speed for later phase-lag measurements.

5) The VCR recorded data is analyzed to determine phase-lag at the different rotation rates.

7.2 Results and Discussion

Viscous-drag behavior for a crocidolite fiber is shown in Fig. 7.4. The data points are phase-lag measurements obtained from the video recording. This fiber is the long, thin fiber in Fig. 7.5. At high magnetic-field rotation-rates, the fiber experiences a substantial phase-lag; the shorter, thicker fibers remain essentially parallel to the magnetic field.

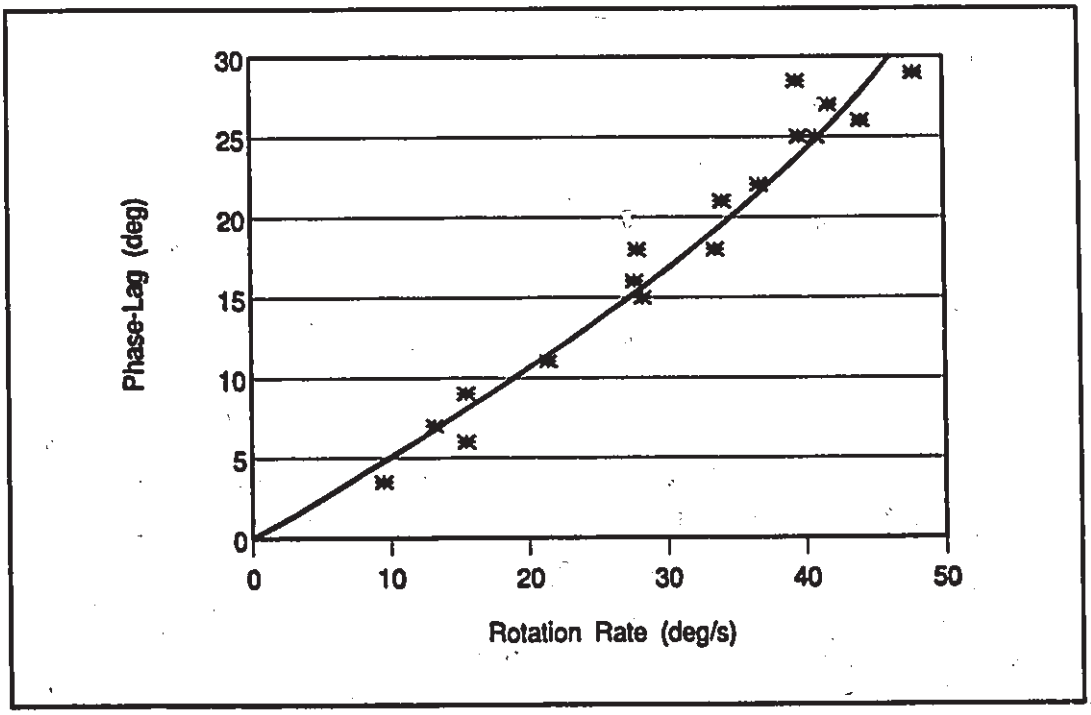

Figure 7.4 Phase-lag for the thin fiber in Fig. 7.5.

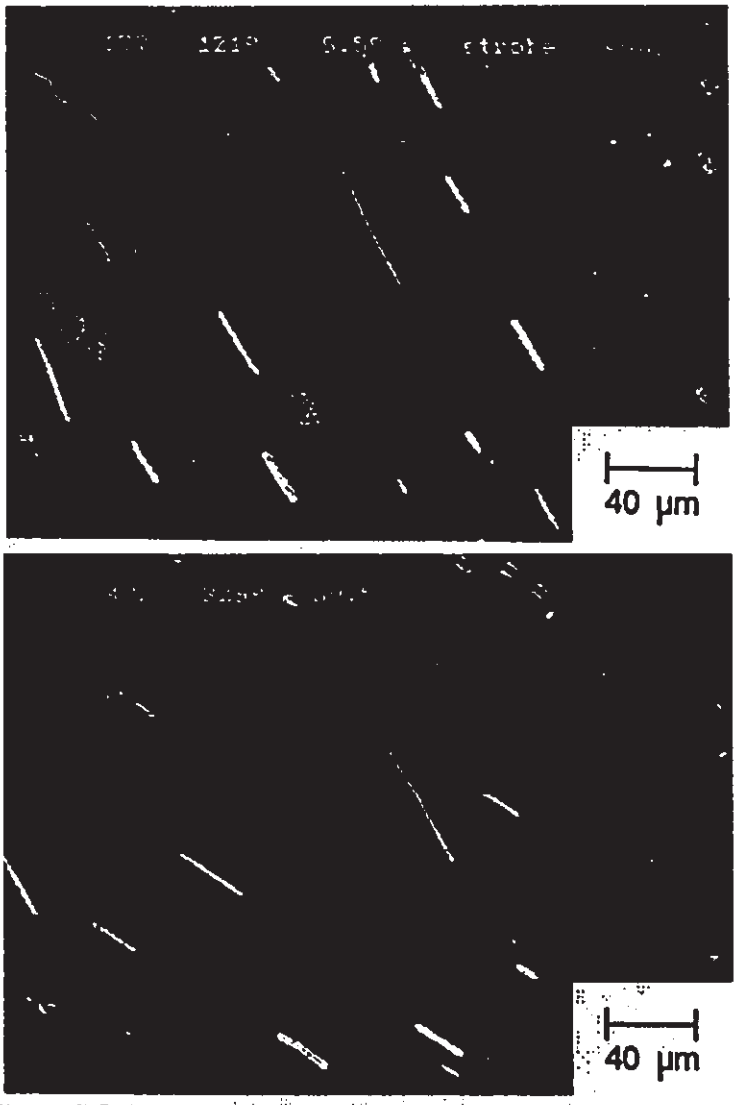

Figure 7.5 Video images of crocidolite fibers at relatively slow and fast magnetic-field rotation-rates.

Video images for several fibers, and the corresponding phase-lag measurements, are given in Figs. 7.6 to 7.9. In all cases, the 0° reference line is parallel to the bottom of the images. The rotation of the magnetic field is counter-clockwise. The orientation of small fibers is difficult to measure precisely, which leads to greater spread in the experimental data.

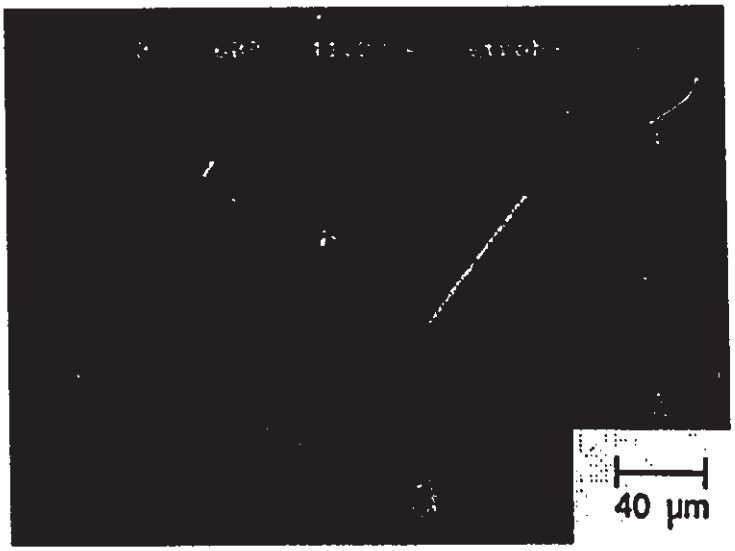

Figure 7.6 a) Video image of crocidolite fibers.

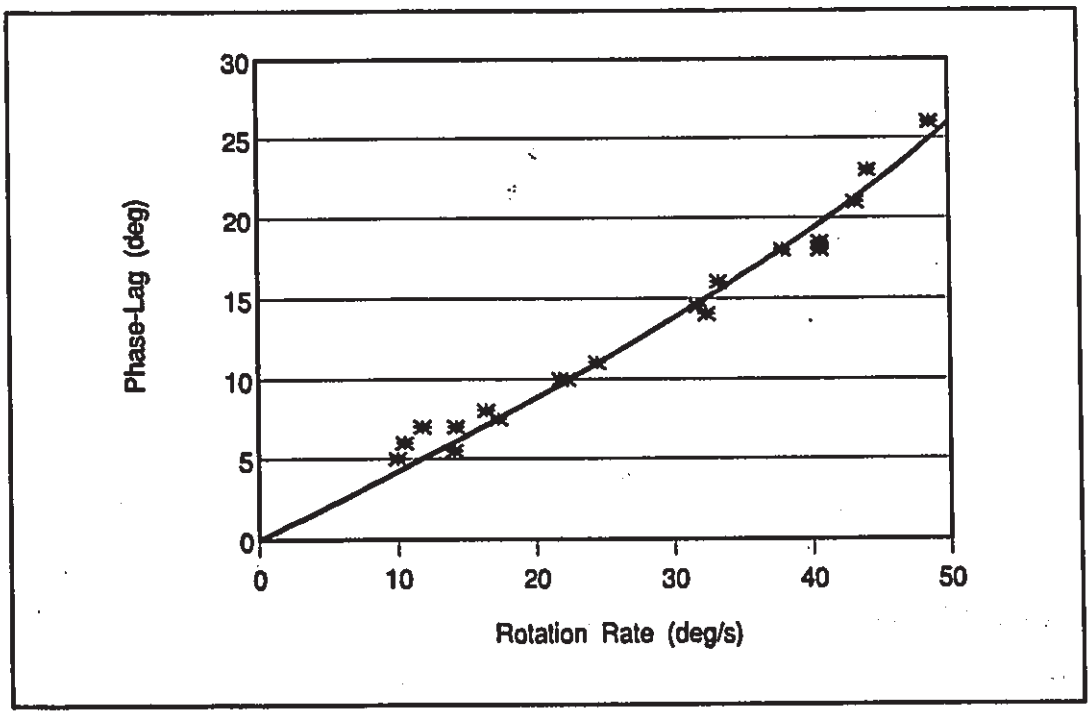

Figure 7.6 b) Phase-lag for the above long, thin fiber.

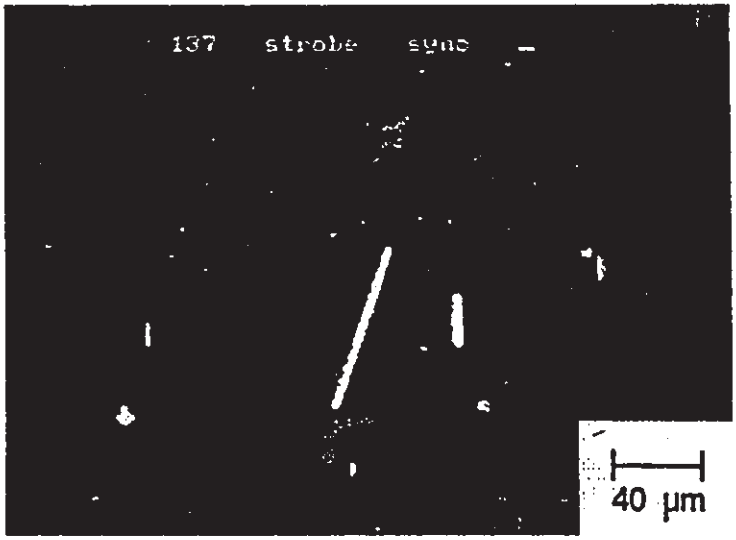

Figure 7.7 a) Video image of crocidolite fibers.

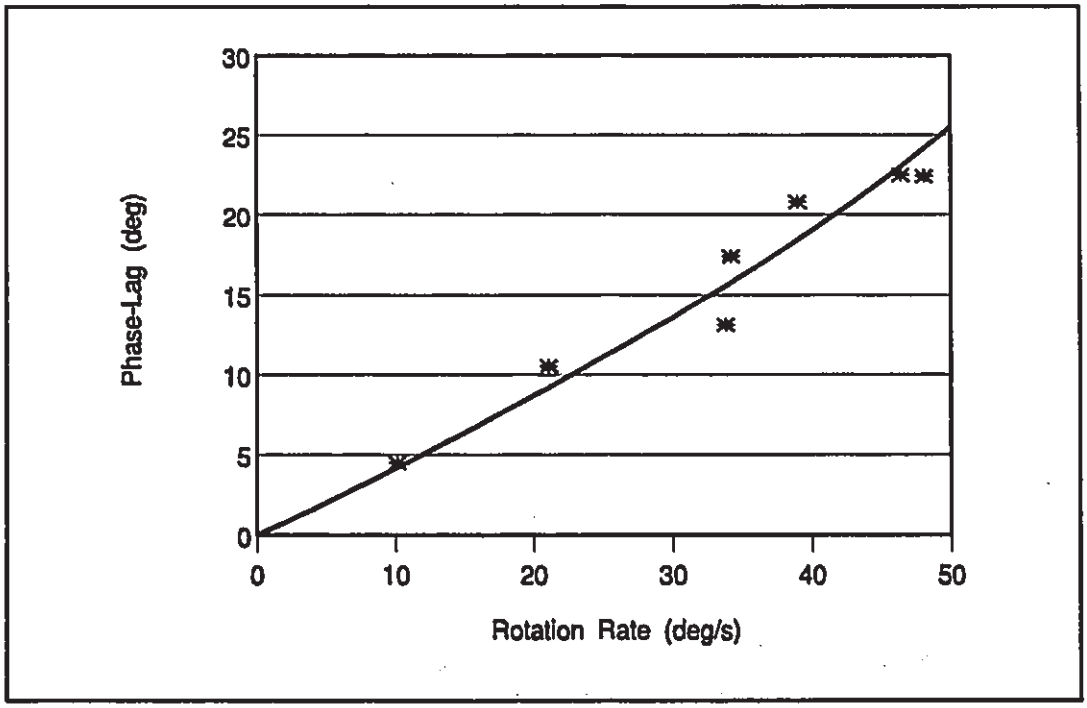

Figure 7.7 b) Phase-lag for the above long fiber.

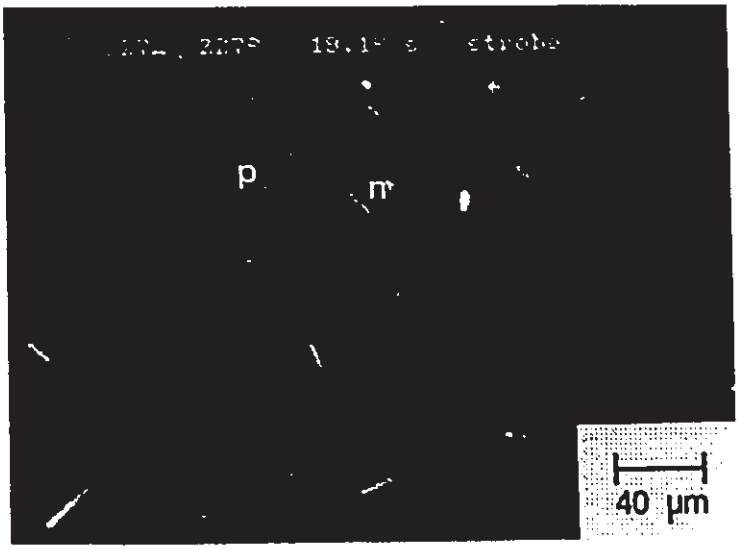

Figure 7.8 a) Video image of amosite fibers.

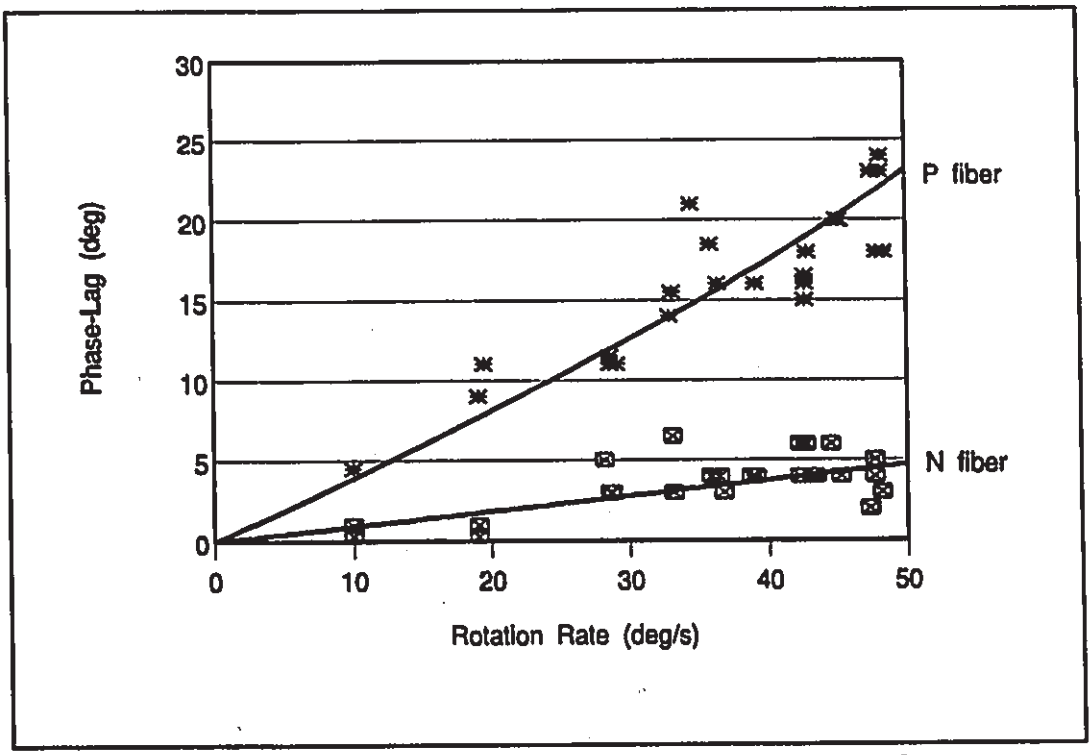

Figure 7.8 b) Phase-lag for the labelled P- and N-type fibers above.

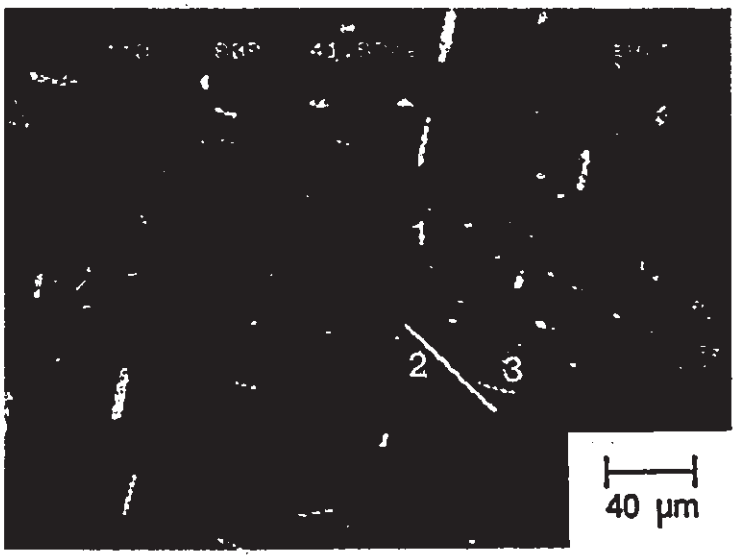

Figure 7.9 a) Video image of the amosite fibers.

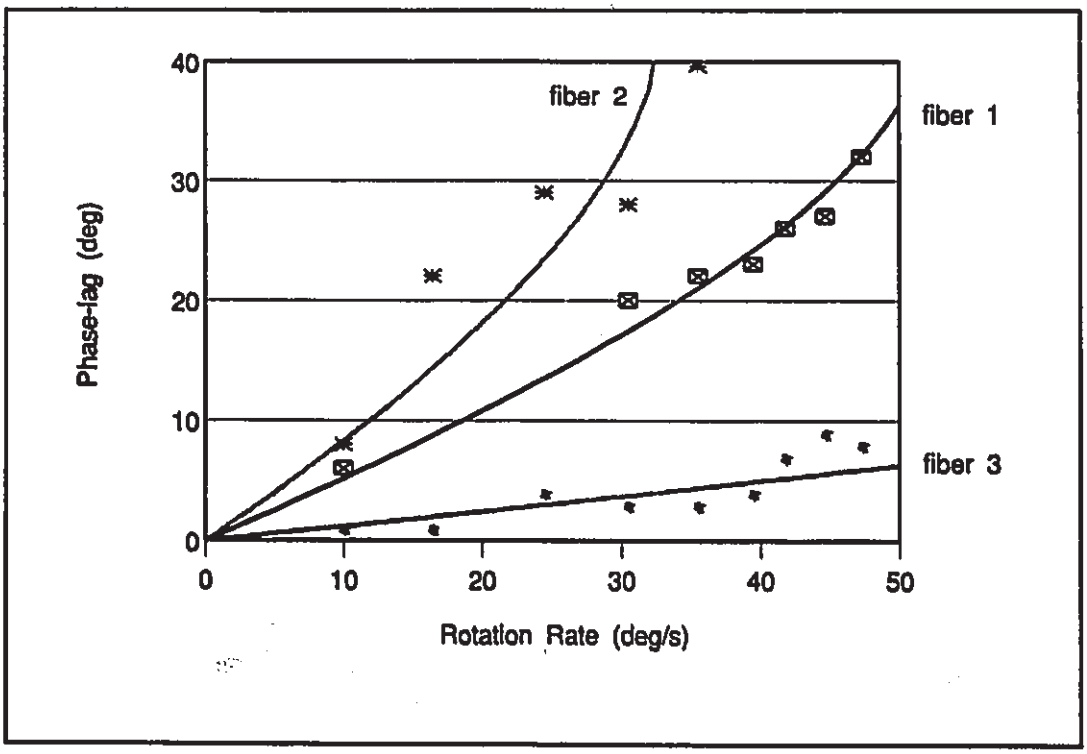

Figure 7.9 b) Phase-lag for the labelled fibers above.

Theoretical curves, fitted to the data, are also provided in Figs. 7.4, 7.6b, 7,7b, 7.8b, and 7.9b. These curves are calculated with the model developed in Chapter 4, using an iterative

procedure in which the diameter was modified to fit the data. The best-fit calculated diameters are given in Table 7.1, together with the corresponding measured values. Measured data is limited to an accuracy of 0.7 μm, the resolving power of the microscope.

Table 7.1 Experimental results versus calculated cylinder diameters

Fiber	Measured Length (μm)	Measured Diameter (μm)	Calculated Diameter (μm)
Crocidolite P-fiber in Fig. 7.4	59.5	2.0	0.80
Crocidolite P-fiber in Fig. 7.6	74.8	2.4	1.15
Crocidolite P-fiber in Fig. 7.7	79.0	3.1	1.22
Amosite P-fiber in Fig. 7.8	35.7	2.0	.57
Amosite N-fiber in Fig. 7.8	15.0	2.4	.60
Amosite N-fiber #1 in Fig. 7.9	24.8	1.0	.33
Amosite N-fiber #2 in Fig. 7.9	59.5	2.0	.60
Amosite N-fiber #3 in Fig. 7.9	18.7	1.7	.60

The theoretical model predicts smaller diameters in all instances. These results are sufficiently close, however, to suggest that the model is basically correct. In fact, the model may provide the most accurate method of determining the actual diameter, at present. One or more of the following factors may contribute to the larger observed diameters.

a) Limited optical resolution.

b) Small fiber dimensions, approaching the limits of continuum mechanics.

c) Fiber cross-section.

Determining the significance of each of these factors, which are discussed separately below, would require further research.

7.2.1 Optical Resolution

The resolving power of the microscope employed is 0.7 μm. This leads to an observed broadening of the actual fiber diameter. In principle deconvolution would remove this effect. However, Mie scattering intensity, and the intensity response of the video-camera, would also have to be taken into consideration.

7.2.2 Limitation of Small Dimensions

Relationships used in the model are based on continuum mechanics. The fiber diameters are approximately 1 μm, which is 2000 times larger than a water molecule. This size difference should be suitably large to allow the use of continuum mechanics. However, there is the possibility that the interaction between individual molecules and the fiber surface needs to be considered.

7.2.3 Fiber Cross-Section

The calculated values are for fibers with circular cross-sections. Amphibole minerals (which includes crocidolite and amosite asbestos) have a characteristic cleavage angle of 55° [Whittaker 1979]. This suggests that the simplest fiber cross-section is a parallelogram with an angle of 55°. A fiber with this cross-section rotates with the narrow edge slicing through the water, while the broad side faces the observer as illustrated in Fig. 7.10. The observed diameter is actually the long diagonal of the parallelogram, which has an area less than the circle enclosing it. When the 55° parallelogram is a rhombus, its area is a maximum, but is only 0.3314 times that of the enclosing circle. The calculated observed-diameters, based on a 55° rhombus cross-section, are tabulated in Table 7.2. These values are in much closer agreement with the measured values. A study of actual fiber cross-sections would be necessary in order to verify this effect on observed diameters. As an additional factor, fragmentation may occur along the length of the fiber, which would lead to a non-uniform cross-section for individual fibers.

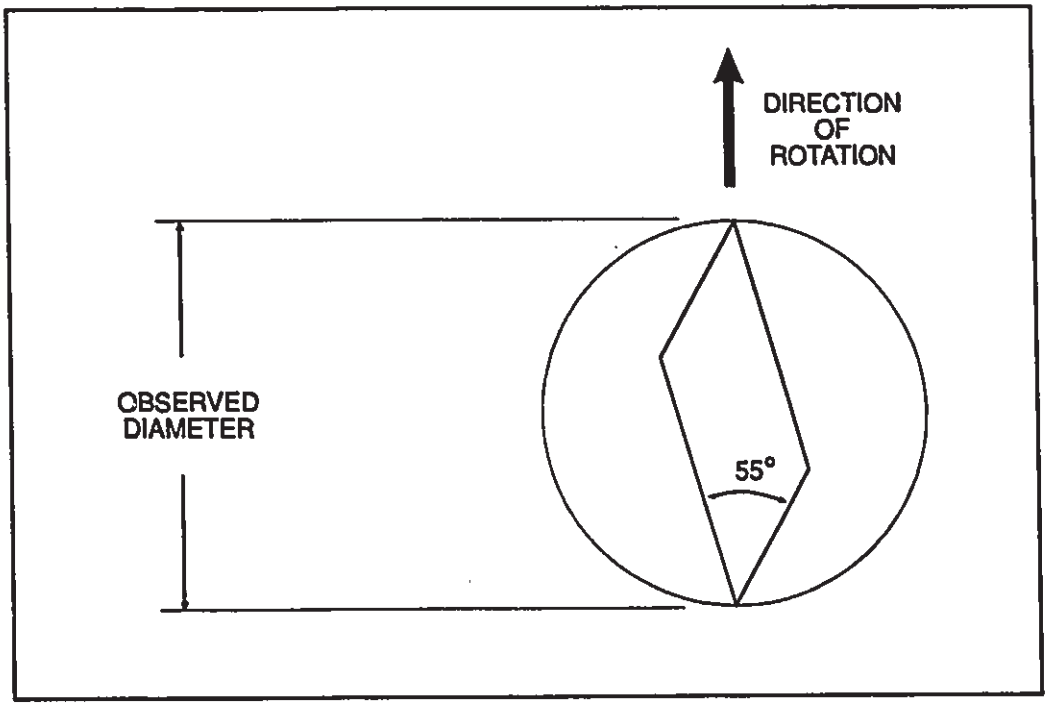

Figure 7.10 Observed diameter for a parallelogram-shaped cross-section.

Table 7.2 Experimental results versus calculated "observed diameters" for a rhombus cross-section.

Fiber	Measured length (μm)	Measured diameter (μm)	Calculated cylinder diameter (μm)	Calculated 55° rhombus "diameter" (μm)
Crocidolite P-fiber in Fig. 7.4	59.5	2.0	0.80	1.60
Crocidolite P-fiber in Fig. 7.6	74.8	2.4	1.15	2.30
Crocidolite P-fiber in Fig. 7.7	79.0	3.1	1.22	2.45
Amosite P-fiber in Fig. 7.8	35.7	2.0	.57	1.20
Amosite N-fiber in Fig. 7.8	15.0	2.4	.60	1.40
Amosite N-fiber #1 in Fig. 7.9	24.8	1.0	.33	0.65
Amosite N-fiber #2 in Fig. 7.9	59.5	2.0	.60	1.30
Amosite N-fiber #3 in Fig. 7.9	18.7	1.7	.60	1.40

Chapter 8

Magnetic-Alignment of Other Minerals

The magnetic alignment properties of crocidolite, amosite and chrysotile were described in Chapter 3. Other minerals were investigated for magnetic-field alignment in order that,

(a) potential interference with the measurement of an asbestos-fiber dispersion can be specified, and,

(b) the alignment properties, if different, can be used to distinguish other minerals from asbestos.

Aqueous dispersions of a range of minerals (fibrous and non-fibrous) were analyzed using the dynamic-particle method. Scattered-light profiles are shown in Figures 8.1 to 8.48, which are located at the end of the chapter. It is important to recognize that these profiles are qualitative, and indicate only the possibility of interference. Some materials, such as halloysite, appear not to undergo strong alignment. On an equivalent mass basis, they may not cause interference with measurement of other alignable, fibrous, material. In some cases, the scattered-light profiles contain contributions from other particulate, having scattered-light profiles similar to borosilicate glass particles. Such undesirable contributions could be removed using a profile subtraction technique.

Some general conclusions can be made from the scattered light-profiles of the minerals selected for observation.

(a) All varieties of chrysotile display broad P-type peaks, which lag behind the magnetic field.

(b) Chrysotile can be discriminated from antigorite, which displays relatively-sharp N-type peaks.

(c) Brucite and lizardite can be mistaken for chrysotile, since both display broad P-type peaks.

(d) All tremolite samples, and the actinolite sample, display only sharp N-type peaks.

(e) Cummingtonite generally displays sharp P-type peaks. An exception is the Mikanui sample, which aligns at about 15° in the T-type mode.

(f) The grunerite sample displays sharp N-type peaks.

(g) The crocidolite samples display sharp P-type peaks.

(h) Anthophyllite displays broad P-type peaks similar to those of chrysotile.

(i) Wollastonite displays broad P-type peaks similar to those of chrysotile.

(j) The amosite samples display sharp P-type and N-type peaks.

It is evident that, if the primary purpose of the technique is the detection of asbestos, there is the potential for interference by fibrous non-asbestos species. Broad peaks also occur from platy minerals such as phlogopite, which have cleavage fragments with high aspect-ratios. If the purpose is to determine if any fibrous mineral species are present, then the technique is highly successful, extremely sensitive, and capable of some discrimination between species.

At first, it was thought that general non-fibrous particulate would contribute only to the base-line level, and not yield peaks. As discussed in Section 6.3.3, this is not the case. The peaks at 45° and 225°, from randomly-shaped particulate, seriously overlap those at 0° and 180° from chrysotile, and may also distort the peaks from low concentrations of amphibole. Where there are large interference peaks, measurements of low fiber concentrations would require the use of profile subtraction techniques.

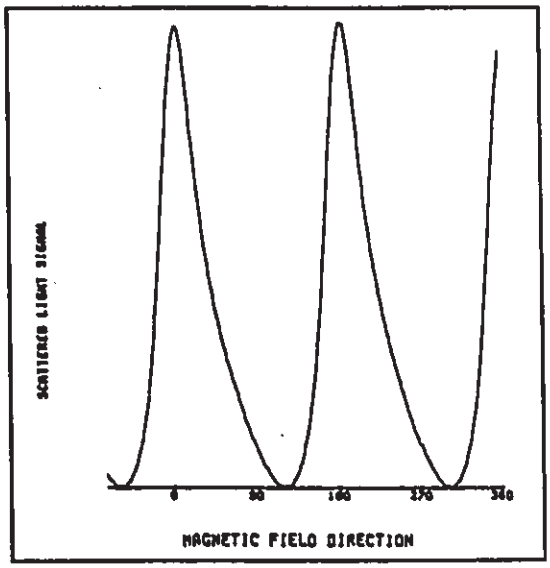

Figure 8.1 Chrysotile (UICC Canadian)

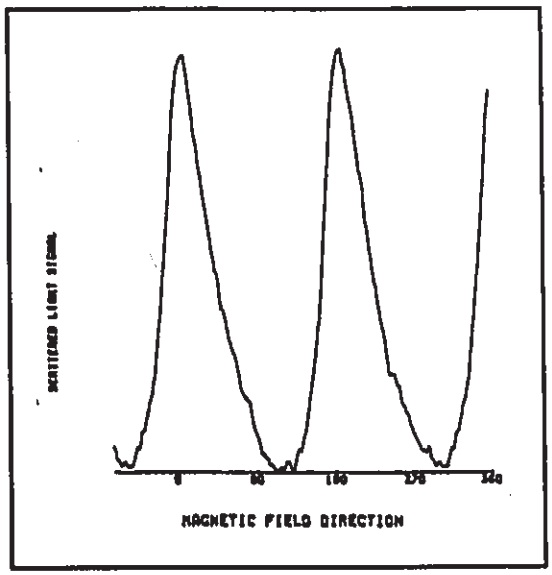

Figure 8.2 Chrysotile (UICC Rhodesian)

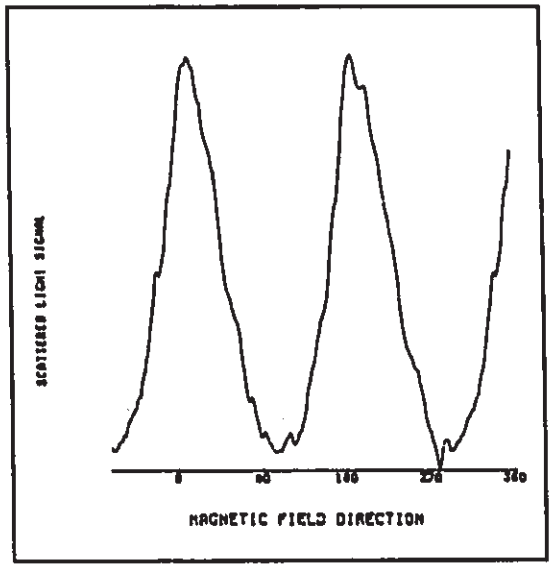

Figure 8.3 Chrysotile (Thetford, Quebec)

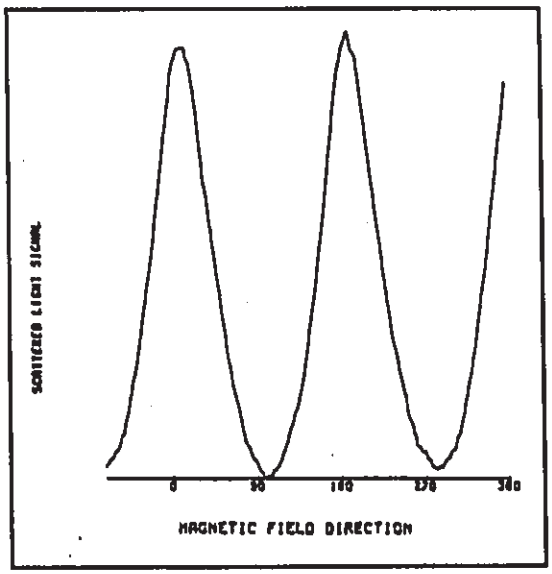

Figure 8.4 Chrysotile (Union-Carbide)

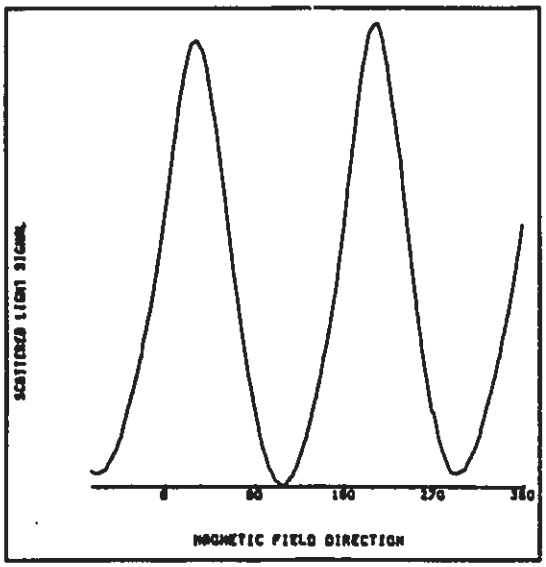

Figure 8.5 Lizardite ("Owen's Pit", Ontario)

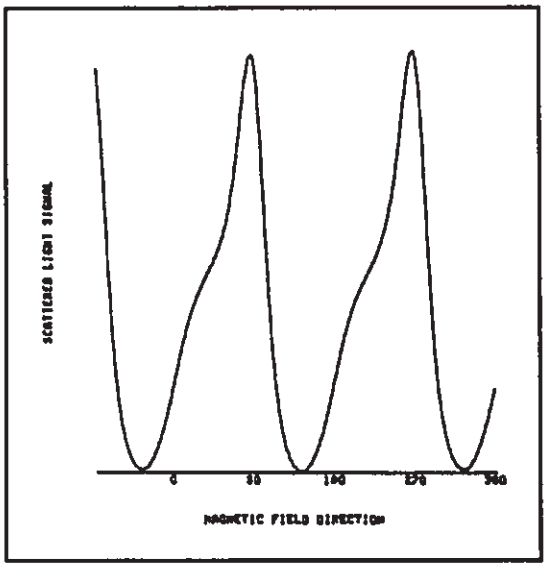

Figure 8.7 Antigorite (East Broughton, Quebec)

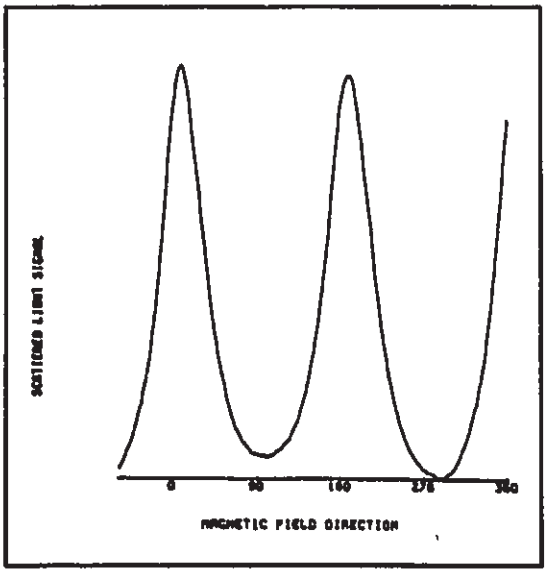

Figure 8.6 Picrolite (Broughton, Quebec)

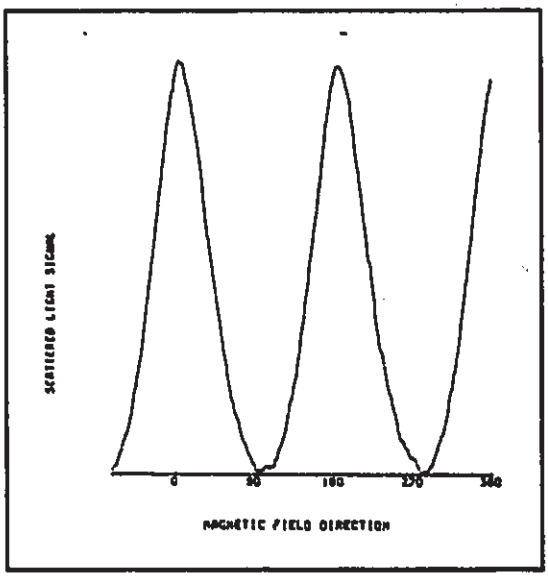

Figure 8.8 Talc (Broughton, Quebec)

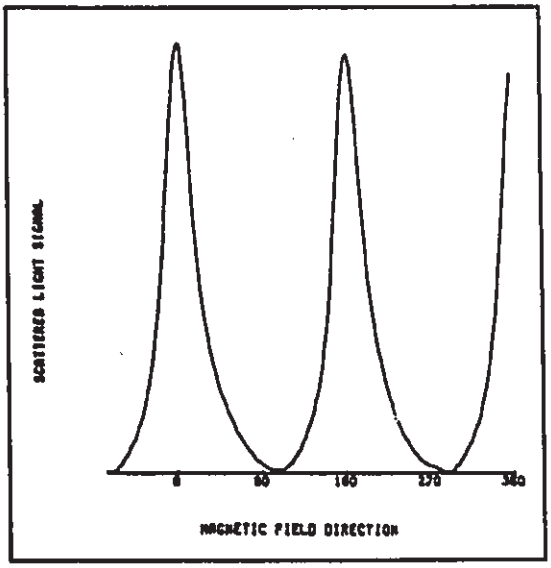

Figure 8.9 Nemalite (Asbestos, Quebec)

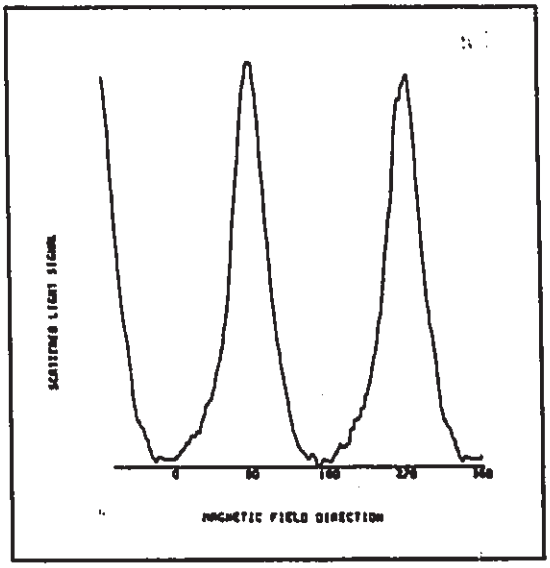

Figure 8.11 Tremolite (Elzivir, Ont.)

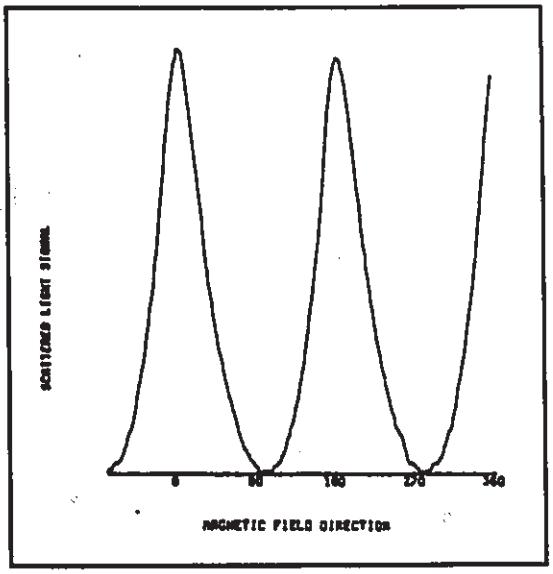

Figure 8.10 Bruceite (Asbestos, Que.)

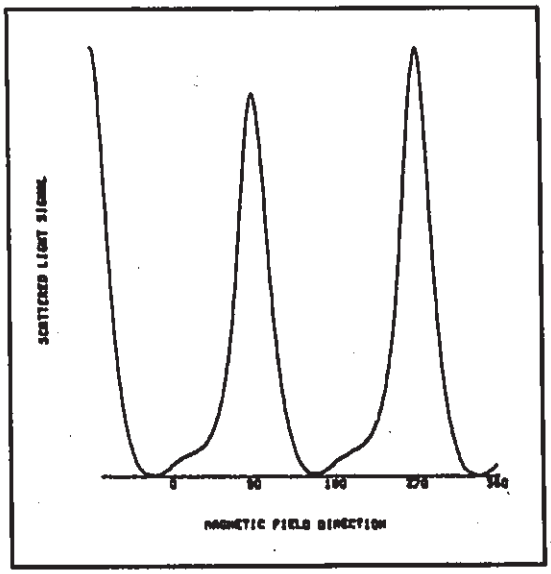

Figure 8.12 Tremolite (Clarendon, Ont.)

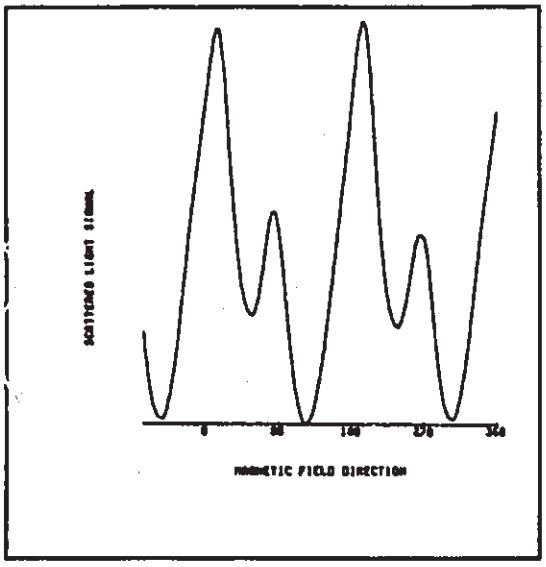

Figure 8.13 Tremolite (Arctic)

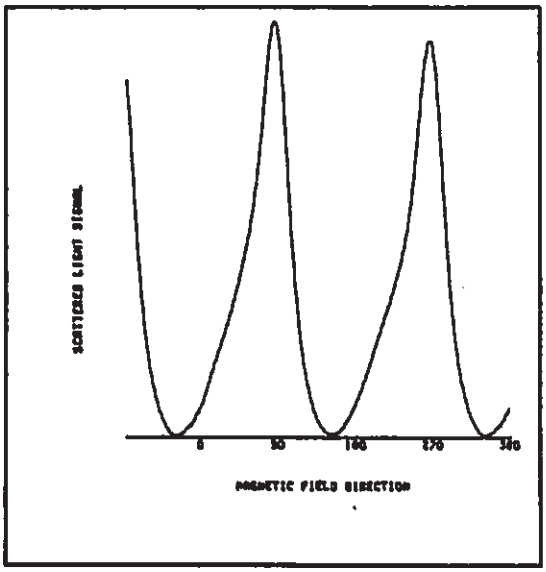

Figure 8.14 Tremolite (Inyo County, Cal.)

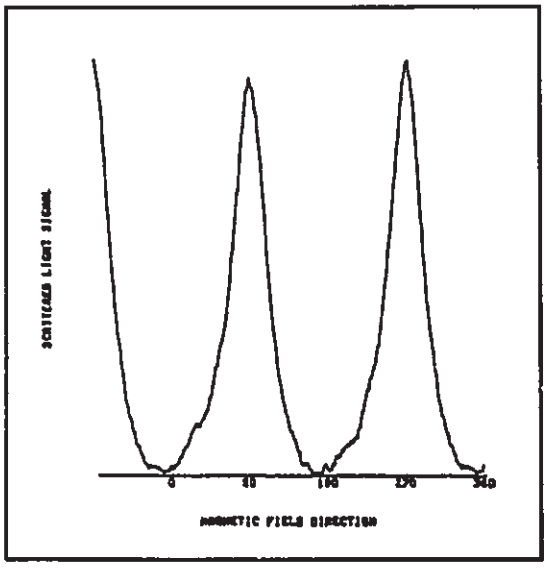

Figure 8.15 Tremolite (Transvaal, RSA)

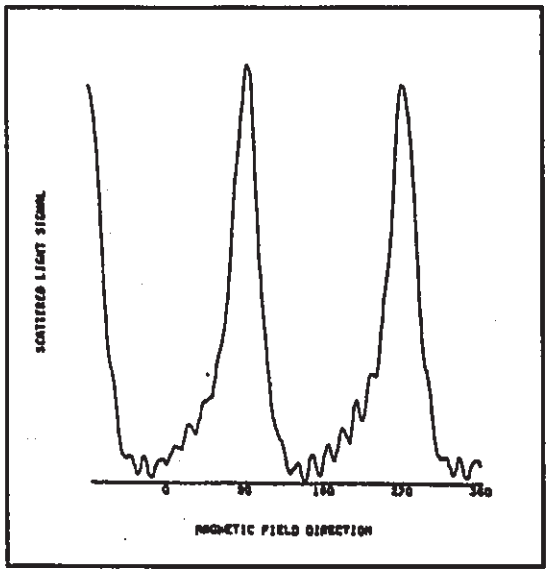

Figure 8.16 Tremolite (Yakutya, USSR)

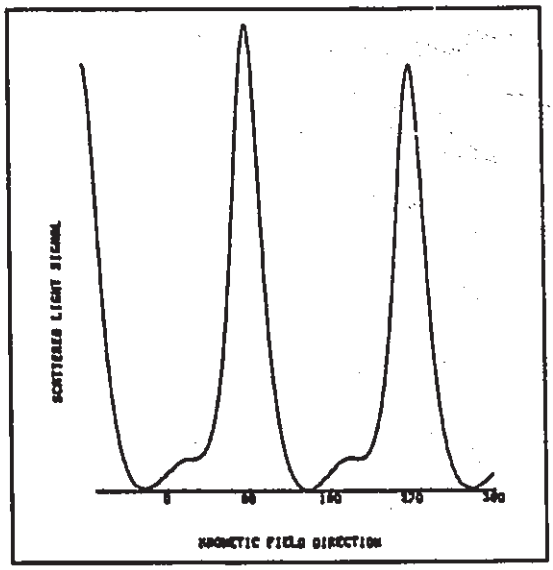

Figure 8.17 Actinolite (Marbridge, Quebec)

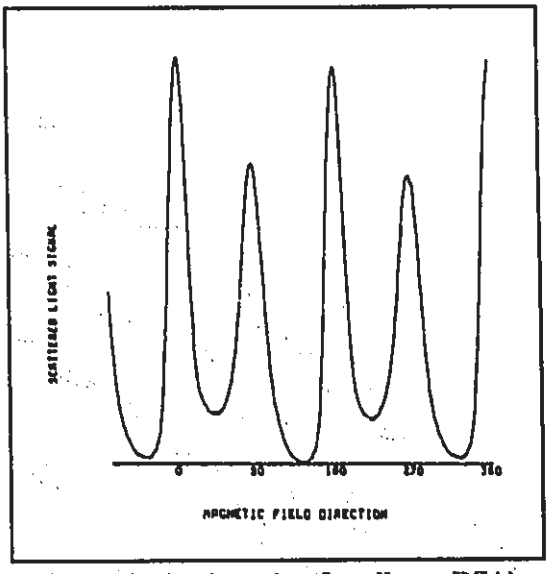

Figure 8.19 Amosite (Lyndberg, RSA)

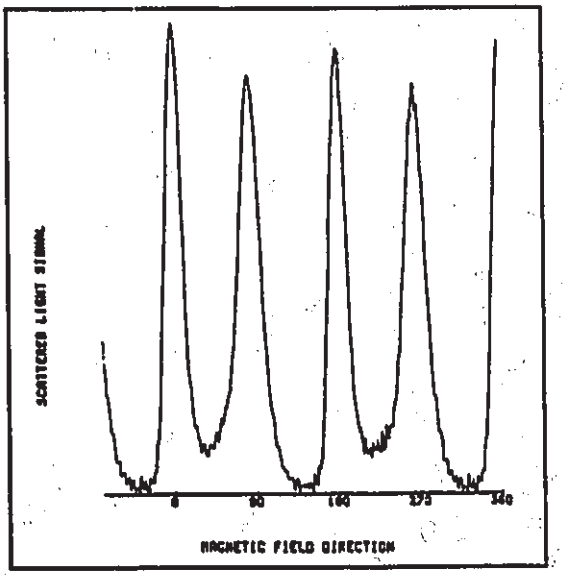

Figure 8.18 Amosite UICC

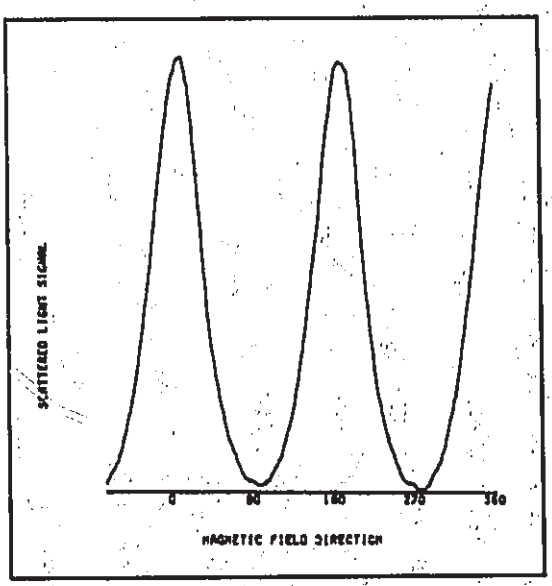

Figure 8.20 Cummingtonite (Soutpansberg, RSA)

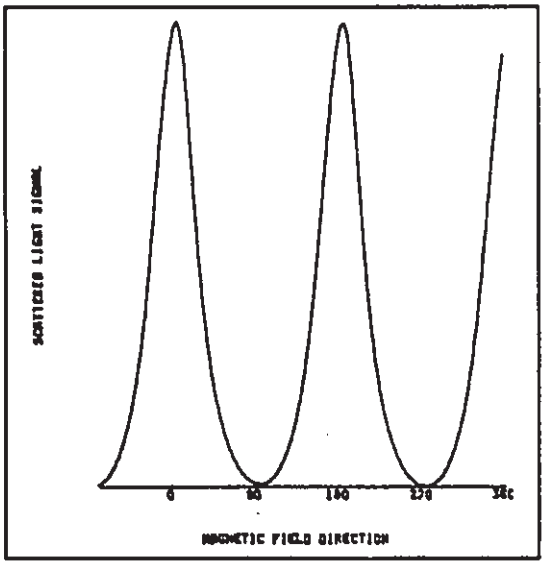

Figure 8.21 Cummingtonite (Mikanui, New Zea.)

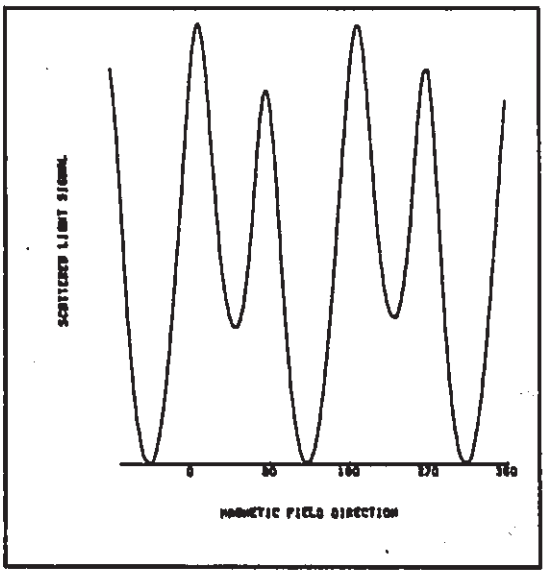

Figure 8.22 Cummingtonite (South Dakota)

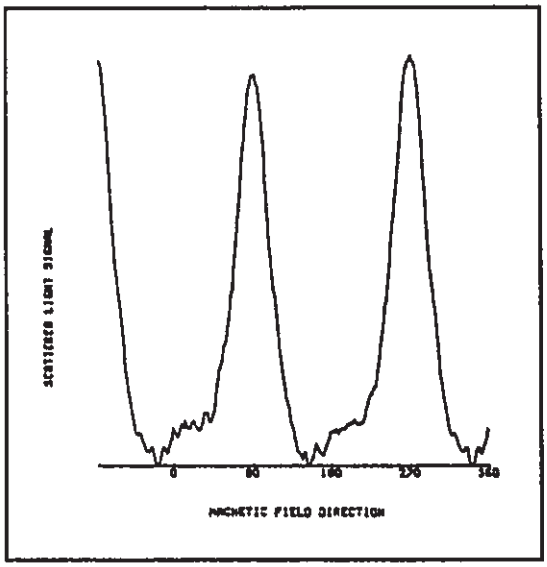

Figure 8.23 Grunerite (Health Lake, Ont.)

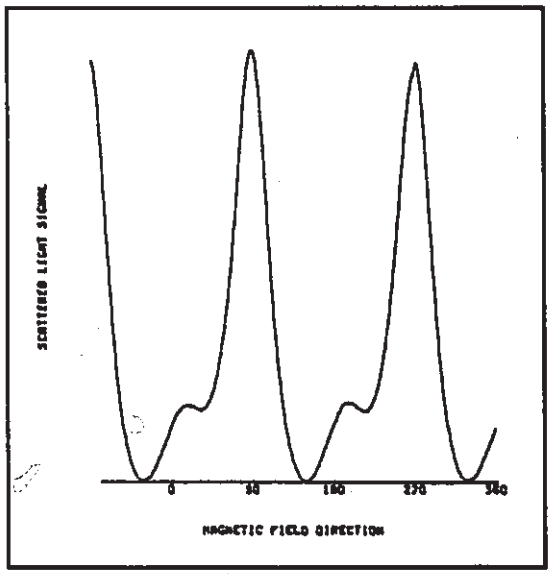

Figure 8.24 Grunerite (Humbolt, Mich.)

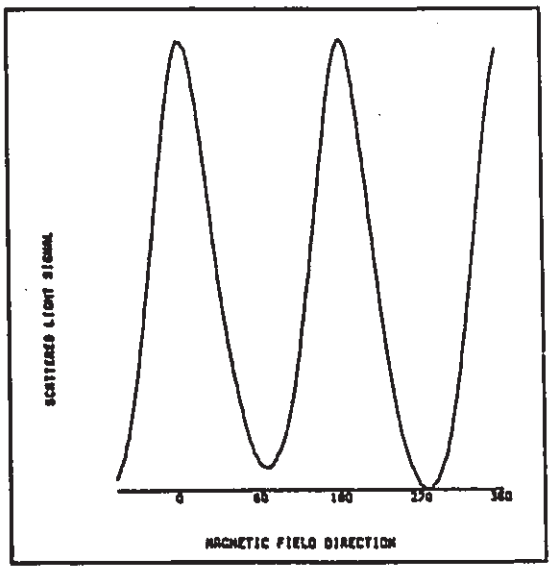

Figure 8.25 Minnesotaite (Mesabi, Minnesota)

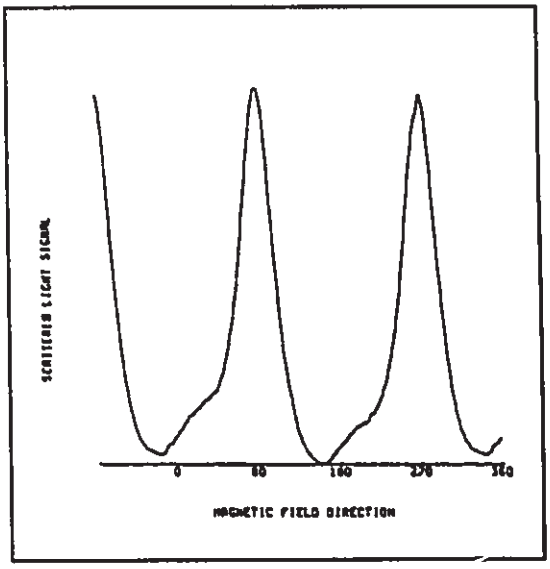

Figure 8.27 Hornblende (Ross, Ont.)

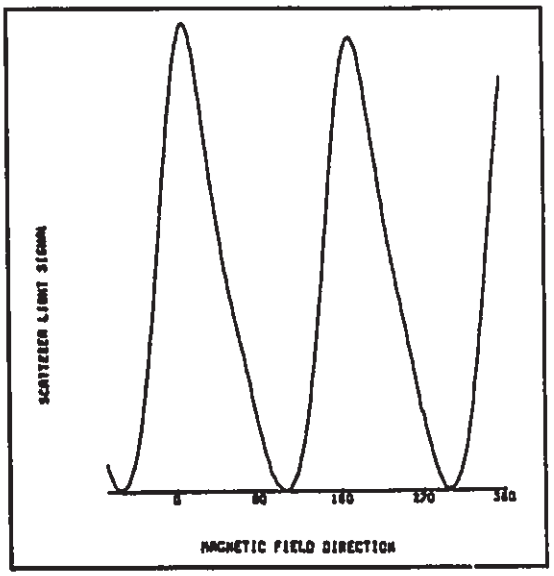

Figure 8.26 Stilpnomelane (French River, N.Z.)

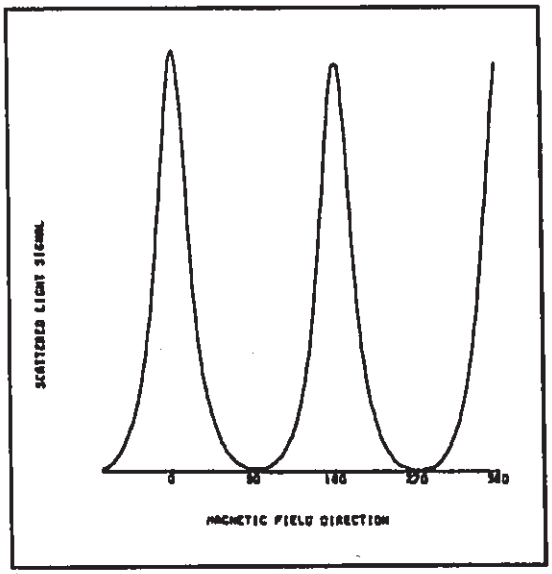

Figure 8.28 Suspected omphacite (Frontenac Co. Ont.)

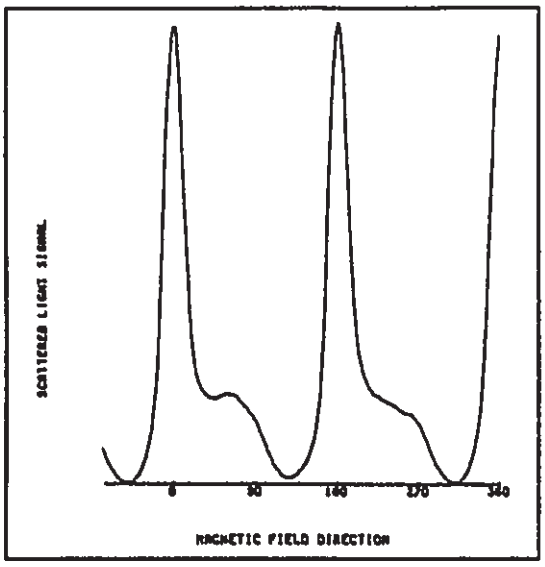

Figure 8.29 Crocidolite (UICC)

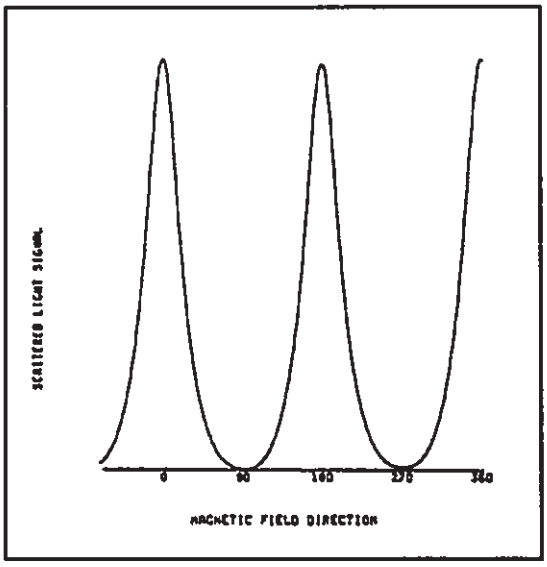

Figure 8.31 Riebeckite (St. Peter's Dome, Col.)

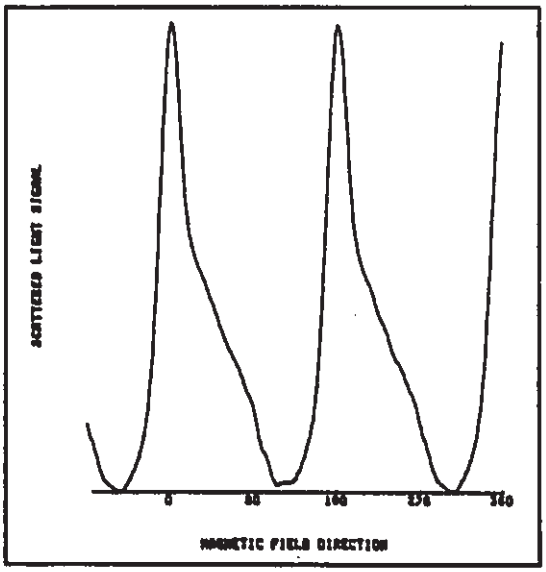

Figure 8.30 Crocidolite (Prieska, RSA)

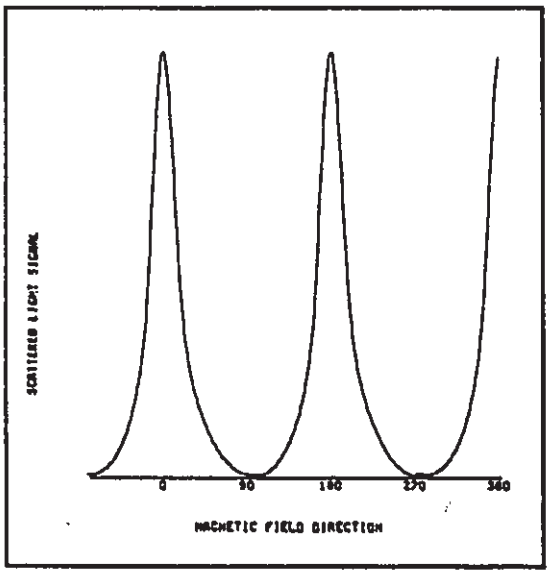

Figure 8.32 Anthophyllite (UICC)

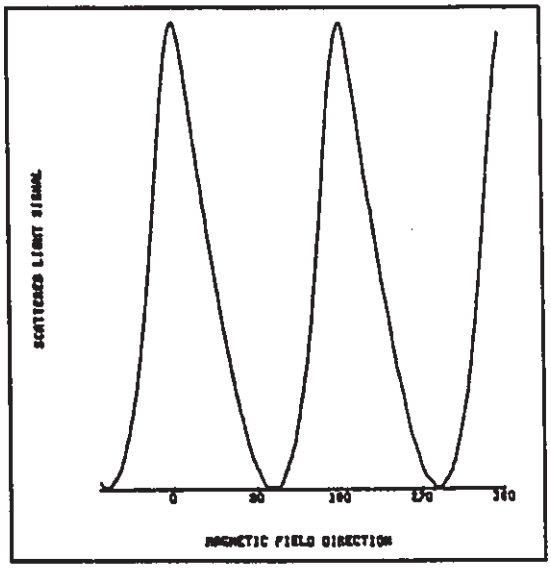

Figure 8.33 Anthophyllite (Montaubun, Que.)

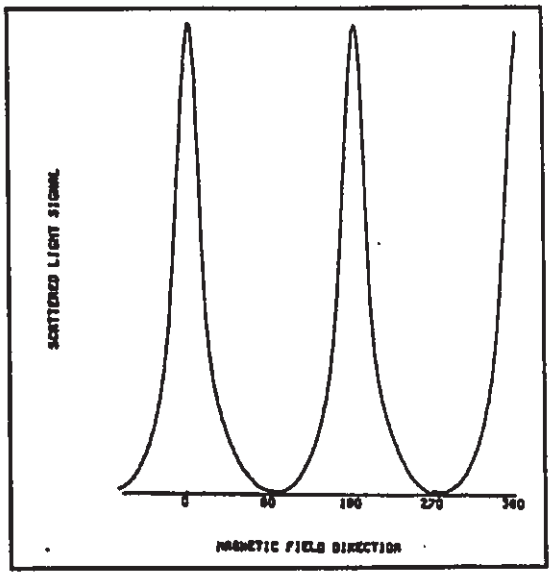

Figure 8.34 Anthophyllite (Salt Mountain, Georgia)

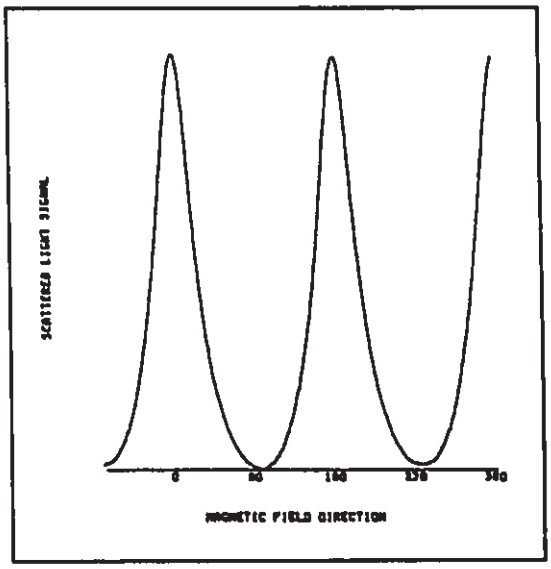

Figure 8.35 Gedrite (Telemark, Norway)

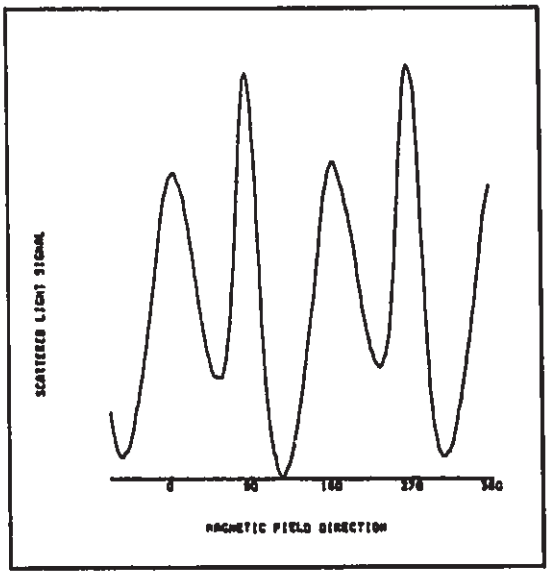

Figure 8.36 Howieite (Laytonville, Cal.)

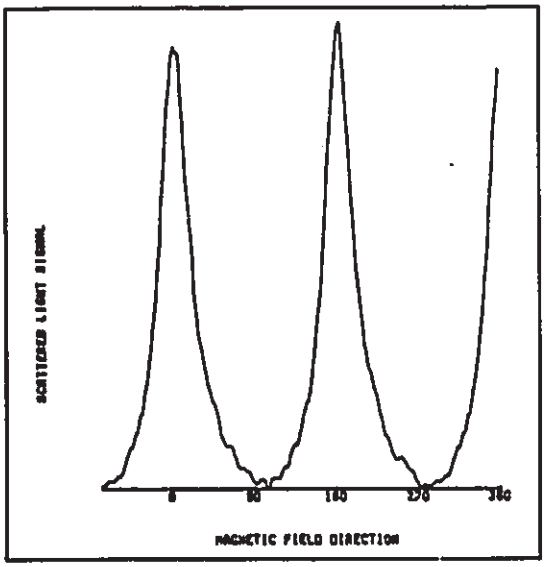

Figure 8.37 Wollastonite (Asbestos, Que.)

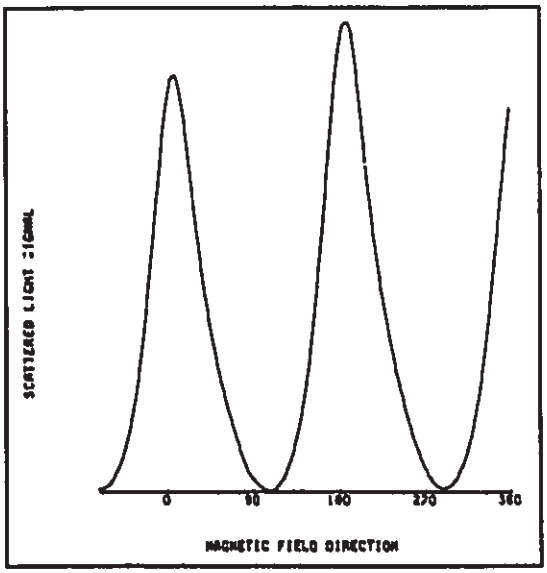

Figure 8.38 Wollastonite (Meldon, Que.)

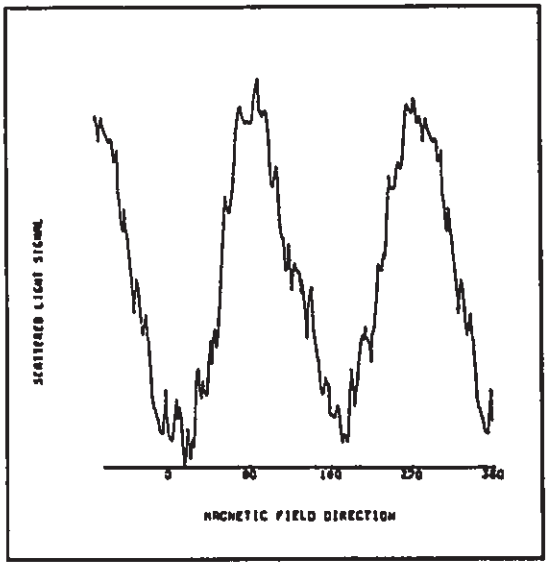

Figure 8.39 Halloysite (Eureka, Utah)

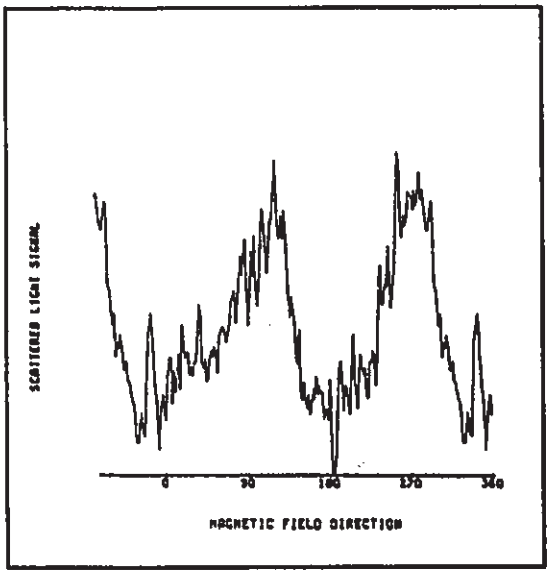

Figure 8.40 Halloysite (Delta, Utah)

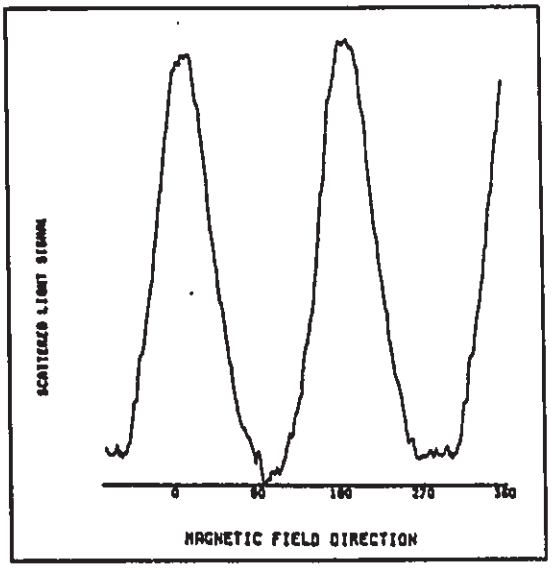

Figure 8.41 Palygorskite (Metaline Falls, Wash.)

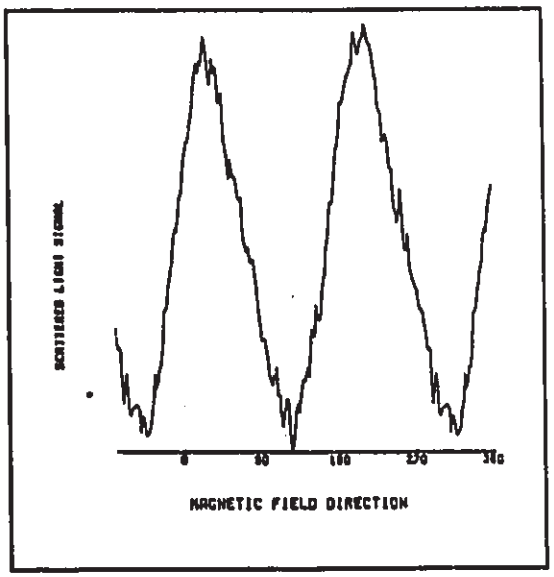

Figure 8.42 Palygorskite (Pormona, Cal.)

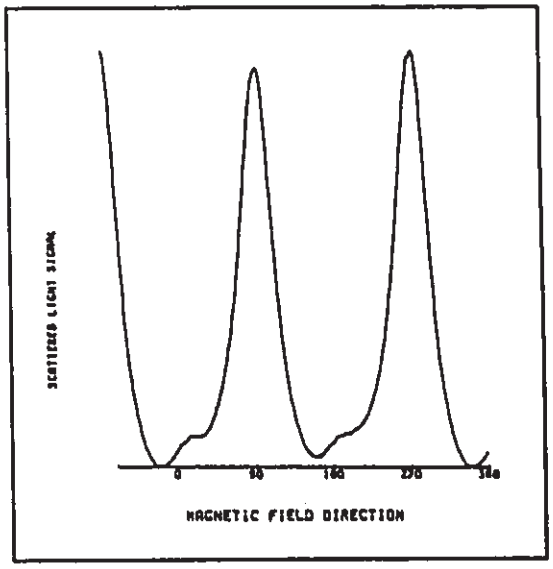

Figure 8.43 Xonotlite (Asbestos, Que.)

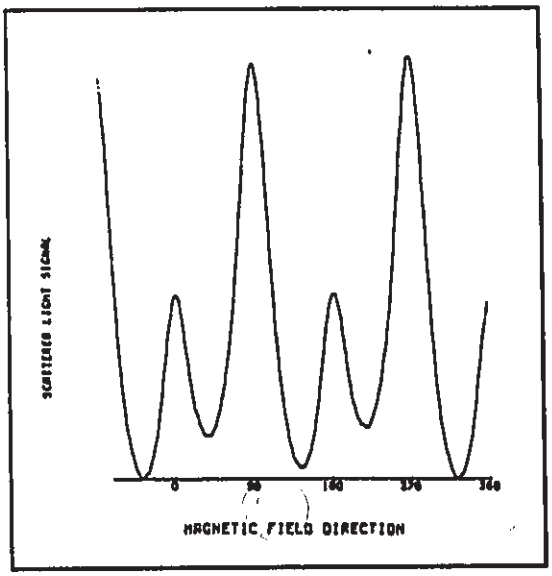

Figure 8.44 Xonotlite (Wakefield, Que.)

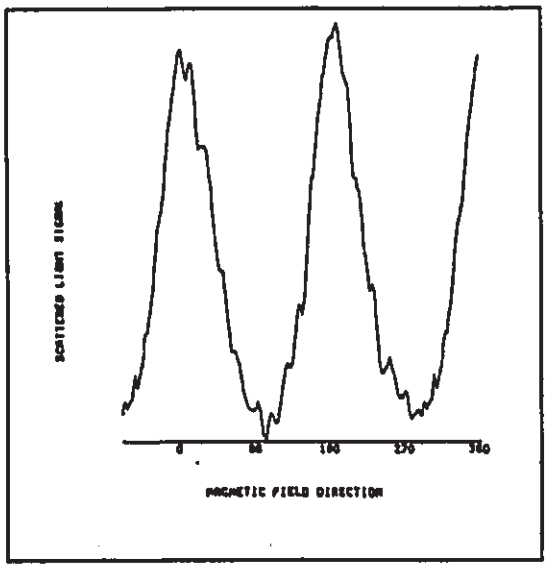

Figure 8.45 Phlogopite (Phalaborwa, RSA)

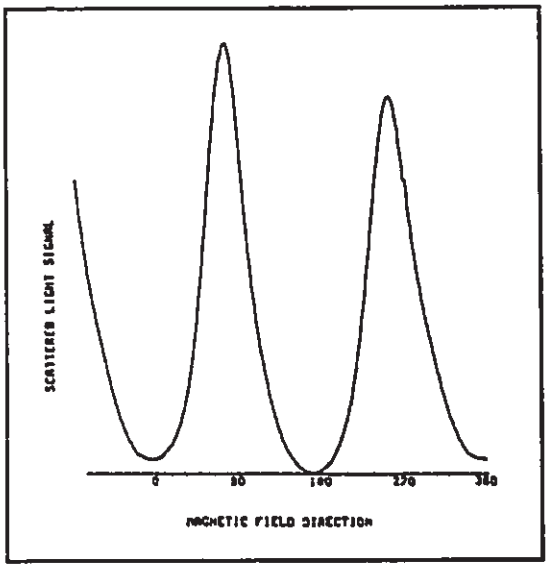

Figure 8.47 Pectolite (Japan)

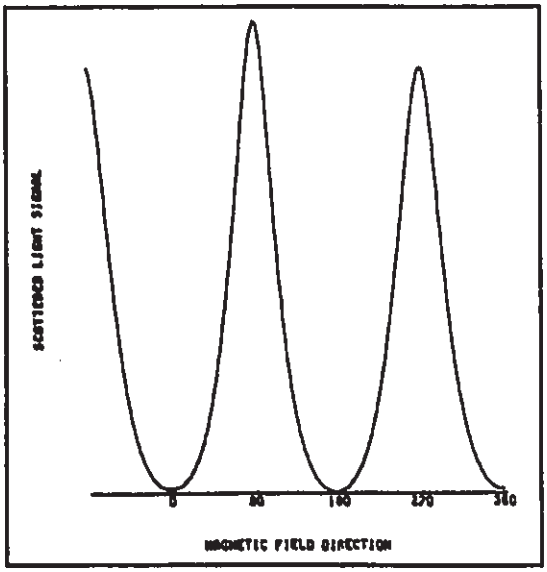

Figure 8.46 Pectolite (Thetford, Que.)

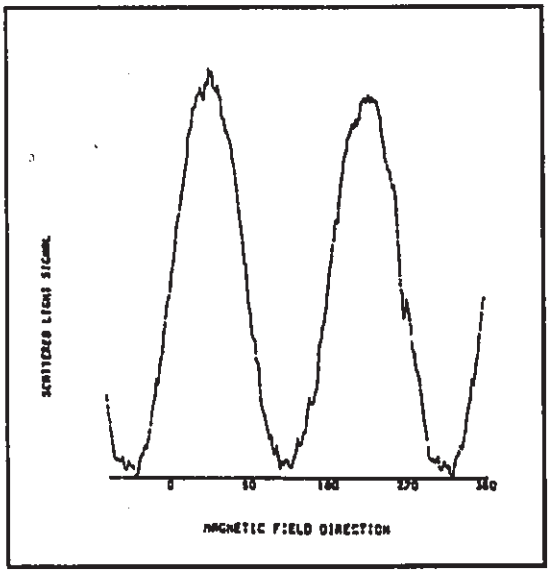

Figure 8.48 Diatomaceous Earth (Seitz supra EKS filter)

Chapter 9
Summary

This research was initiated in response to the need for an automated instrument for measuring asbestos particulate. Timbrell had discovered the magnetic-alignment behavior of asbestos fibers and had done some preliminary light-scattering measurements on aligned-fiber samples. This early work indicated great potential for application to automated instrumentation.

Two techniques were developed. In the first, the fixed-particle technique, an aqueous sample is filtered in a one Tesla magnetic field. The resulting filter contains permanently aligned particulate. The filter is made transparent and then scattered-light measurements are made of the resulting membrane. Initially, the technique looked very promising because the procedure was straightforward and the equipment was simple. However, the sensitivity was low, particularly for chrysotile, for which the residual filter structure can produce erroneous peaks that appear similar to chrysotile peaks. Several attempts were made to improve the sensitivity of the technique. These had limited success and the fixed-particle technique was abandoned in favour of the dynamic-particle technique.

The dynamic-particle technique employed a sample in which the particulate was suspended in water. The sample was located between the poles of a rotating permanent-magnet assembly. As the magnetic field rotated, the particles were free to follow the field. Scattered-light measurements, made directly on the liquid sample, eliminated the problem of filter artifacts encountered in the fixed-particle technique. In addition, the refractive index difference (between the fiber and the surrounding medium) was greater for fibers suspended in water than fibers embedded in a collapsed filter. This results in a higher scattered-light intensity. The result

is that the dynamic-particle technique can detect less than 0.5 mfl (million fibers per liter) of crocidolite, in comparison with 2.2 mfl using the fixed-particle technique. For chrysotile the results are even more dramatic, where the corresponding values are 5 mfl and 750 mfl, respectively. The dynamic-particle technique has been proven to be the method of choice.

Other mineral samples were examined and were also found to align in a magnetic field. If the purpose of the instrumentation is to detect only what is specifically defined as asbestos, then this is a serious complication. However, if these other mineral types are capable of causing serious health problems, it is essential that the technique detect these as well. Because these materials are not used commercially, studies are limited and the magnitude of the hazard is not known. The potential health hazard could be as great as with asbestos.

All reported fiber concentrations in this thesis rely on sample analysis using an electron microscope. Ideally it would be advantageous not to rely on manual counting to calibrate an automated instrument, but to have an instrument that can determine directly the asbestos-fiber dimensions and concentration. This should be possible using the dynamic-particle technique. A signal is produced which varies with the rotation rate of the magnetic field. As the rotation rate increases, the phase-lag of the scattered-light peaks also increase. This variation is due to viscous-drag effects as the fibers attempt to remain aligned with the field. A theoretical model was developed which related these effects to the dimensions fo a fiber. The starting point for the model was the established relationships of fluid dynamics applied to a rotating cylinder. At equilibrium, the torque on a cylindrical fiber, due to the magnetic field, is equal to the torque caused by viscous drag. Equating the expressions for both torques determines the phase-lag. The model revealed that the dominant parameter for the magnetic torque is the fiber volume, and therefore the fiber radius. The torque due to viscous drag is dependent primarily upon the length of the fiber. This means that fibers of the same length, but with differing diameters, will experience similar drag-torques. However, the one with the smaller diameter will experience substantially less magnetic-torque. With less magnetic-torque, there is less force to maintain alignment with the magnetic field. Therefore, the smaller diameter fiber lags the magnetic field by a larger angle.

The model also shows that cylinders having the same length-to-diameter ratio (aspect ratio) will experience very similar phase-lags. Although the aspect ratio of an unknown cylinder can easily be determined from phase-lag data, the actual dimensions require very precise measurements.

The phase-lag of individual asbestos-fibers were measured. The torques were small, of the order of 10^{-18} Nm. These measurements were in excellent agreement with the theoretical model. The fibers cannot be assumed to be cylindrical; their actual cross-sectional shape must be considered. For example, amphiboles are characterized by a 55° cleavage angle, which implies that the cross-section of an amphibole asbestos-fiber is a parallelogram with an inside angle of 55°. Using accurately measured diameters with the model, can yield the actual cross-section size and shape of individual fibers.

Obtaining separate information about the length or diameter, would allow the viscous-drag to determine the actual fiber dimensions. Measurement of the variation of the scattered light intensity with scattering angle (all normal to the length of the fiber) allows the diameter of the fiber to be determined. Therefore, viscous drag behavior combined with simultaneous measurement of scattered light at several angles, has the potential of allowing direct determination of asbestos fiber size. Further research and development based on the research presented in this thesis, would result in significantly improved instrumentation and techniques to monitor asbestos and help ensure a safer environment.

References

Abramowitz, M., and Stegon, I.A., 1970. *Handbook of Mathematical Functions,* Dover Publ. Inc., New York, NY.

Anderson, C.H. and Long, J.M., 1980. Interim method for determining asbestos in water, *U.S. Environmental Protection Agency,* Report No. EPA-600/4-80-005, National Technical Information Service, Springfield, Virginia.

Asbestos International Association, 1979. Reference method for the determination of airborne ssbestos fibre concentrations at workplaces by light microscopy (membrane filter method), *Asbestos International Association,* 68 Gloucester Place, London, W1H 3HL, England.

Birks, L.S., Fatemi, M., Gilfrich, J.V., and Johnson, E.T., 1975. Quantitative analysis of airborne asbestos by x-ray diffraction: final report on feasibility study, *U.S. Environmental Protection Agency*, EPA-650/2-75-004, Research Triangle Park, North Carolina.

Brown, W.F., 1962. *Magnetostatic Principles in Ferromagnetism,* North-Holland Pub. Co. Amsterdam.

CGA Corporation/Precision Scientific Group, 1977. Fibrous Aerosol Monitor, Model FAM, Brochure 11-77-CP-2M.

Char, B.W., Geddes, K.U., Gonnet, G.H., and Monagan, M.B., 1988. *Maple Users Guide, 5th ed.,* Watcom Publ. Ltd., Waterloo, Ont.

Chatfield, E.J., 1984. New methods for monitoring of asbestos fiber concentrations in workplaces and ambient atmospheres, *Proceedings of the Fifth Colloquim on Dust Measuring Technique and Strategy,* Asbestos International Association, Johannesburg, RSA, p. 297-317.

Chatfield E.J., 1979. Measurement of asbestos fibres in the workplace and in the general environment. *Mineralogical Association of Canada, Short Course,* 4 111-163.

Cressey, B.A., 1980. Magnetic orientation of amphibole fibres. Private communication.

Earnshaw, A., 1968. *Introduction to Magnetochemistry,* Academic Press, New York, NY.

Gibbs, G.W., 1979. Techniques of asbestos determination -- research perspective, *Mineralogical Association of Canada, Short Course Handbook,* 4, 253-278.

Heidermanns, G., 1979. Determination of asbestos fine dust according to mass concentration, *Mineralogical Association of Canada, Short Course Handbook,* 4, 165-196.

Kerker, M., 1969. *The Scattering of Light and other electromagnetic radiation,* Academic Press, New York, NY.

Landau, L.D., and Lifshitz, E.M., 1959. *Fluid Mexhanics,* Pergamon Press, Oxford, Eng.

Lilienfeld, P., 1987. Light Scattering from Oscillating Fibers at Normal Incidence, *Jour. of Aerosol Science,* 18-4, 389-400.

Melton, C.W., Anderson, S.J., Dye, C.F., Chase, W.E. and Heffelfinger, R.E., 1978. Development of a rapid analytical method for determining asbestos in water, *U.S. Environmental Protection Agency,* Report No. EPA-600/4-78-066 Athens, Georgia.

Nagata, T., 1961. *Rock Magnetism,* Maruzen Co. Ltd. Tokyo, Japan.

National Bureau of Standards, 1977. A report on the fiber content of 80 industrial talc samples obtained from and using the procedures of the Occupational Health and Safety Administration. *Analytical Chemistry Division, Institute for Materials Research,* No. 20234, National Bureau of Standards, Wachington D.C.

NIOSH, 1979. *Membrane Filter Method for Evaluating Airborne Asbestos Fibers,* National Institute for Occupational Safety and Health, U.S. Dept. of Health, Education and Welfare, Washington, D.C.

Ortiz, L.W., and Isom, B.L., 1974. Transfer technique for electron microscopy of membrane filter samples, *American Indust. Hygiene Assoc.* 35 No. 7, 423-425.

Riis, P., and Chatfield, E.J., 1982. Development of a rapid survey technique for the detection of asbestos fibers, *U.S. National Bureau of Standards,* Special publ. no. 619, Washington, U.S.A. 108-120.

Riis, P., and Chatfield, E.J., 1983. Rapid screening technique for the detection of asbestos fibers in water samples. *U.S. National Technical Information Service,* order no. PB 83-262 915, Springfield, VA.

Stroink, G., 1980. The evaluation and development of new techniques to determine the asbestos content in human lungs, *Final Report, National Research Council Division of Biological Sciences,* Report No. OSU79-00054, Ottawa, Canada.

Stroink G., 1984. The Magnetic Properties of Respirable Asbestos in Airborn Dust and in Lungs of Asbestos Workers, *National Research Council,* Report for Contract No. OST83-00068, Ottawa, Canada

Stroink G., Dunlap, R. A., and Hutt, D., 1981. Room temperature measurements of some Canadian chrysotiles and UICC asbestos samples, *Can. Mineral.,* 19, 519-524.

Timbrell, V., 1972. Alignment of amphibole asbestos by magnetic fields, *Microscope,* 20, 365-368

Timbrell, V., 1975. Alignment of respirable asbestos fibres by magnetic fields. *Annals of Occupational Hygiene,* 18, p. 299-311.

Timbrell, V., 1977. Magnetic separation of respirable asbestos fibers, *Filtration and Separation,* 14, No. 3, 241-242.

Trudeau, M., 1979. Methods for the evaluation of asbestos dust concentration at the workplace, *Mineralogical Association of Canada, Short Course Handbook*, 4, 213-252.

Vickers Instruments, 1979. Private communication from R.W. Gale, Environmental Products Manager.

Vickers Instruments, 1980. Vickers M88 Rapid Fibre Counter, Brochure VM88/1 5/80/NW/10.

Whittaker, E.J.W., 1979. Mineralology, chemistry and chrystallography of chrysotile asbestos, *Mineralogical Association of Canada, Short Course Handbook*, 4, 1-34.

Wicks, F.J., 1979. Mineralology, chemistry and chrystallography of chrysotile asbestos, *Mineralogical Association of Canada, Short Course Handbook*, 4, 35-78.